

A Global Spectral Study of Black Hole X-ray Binaries

R. J. H. Dunn^{1,2*†}, R. P. Fender², E. G. Körding^{2,3}, T. Belloni⁴ and C. Cabanac²

¹Excellence Cluster Universe, Technische Universität München, Garching, 85748, Germany

²School of Physics and Astronomy, Southampton, University of Southampton, SO17 1BJ, UK,

³AIM - Unité Mixte de Recherche CEA - CNRS - Université Paris VII - UMR 7158, CEA-Saclay, Service d'Astrophysique, F-91191 Gif-sur-Yvette Cedex, France

⁴INAF-Osservatorio Astronomico di Brera, Via E. Bianchi 46, I-23807 Merate (LC), Italy

28 August 2018

ABSTRACT

We report on a consistent and comprehensive spectral analysis of the X-ray emission of 25 Black Hole X-ray Binaries. All publicly available observations of the black hole binaries in the *RXTE* archive were analysed. Three different types of model were fitted to investigate the spectral changes occurring during an outburst. For the population, as well as each binary and each outburst from each binary, we construct two diagnostic diagrams. The Hardness Intensity/Luminosity Diagram (HID/HLD), the X-ray colour against the flux/luminosity of the binary is most useful when studying a single binary. However, to compare between different binary systems, the Disc Fraction Luminosity diagram (DFLD) is more useful. The DFLD uses the luminosities of the disc and powerlaw components to calculate the ratio of the disc luminosity to the total luminosity, resulting in a more physical value, which is analogous to the X-ray colour calculated for X-ray binaries. The tracks of the outbursts populate the DFLD more evenly than the HLD. We discuss the limitations of both diagnostic diagrams for the study of the X-ray binary outbursts, and we clearly illustrate how the two diagrams map onto each other for real outburst data. The similarity of the X-ray colour and Disc Fraction behaviour over time during an outburst originally seen in GX 339-4 data is seen in other sources' outbursts. We extract the peak luminosities in a single outburst, as well as the luminosities at the transitions away from- and returning to the powerlaw dominated state for each outburst. The distribution of the luminosities at the transition from the powerlaw to the disc dominated state peaks at around $0.3L_{\text{Edd}}$, the same as the peak of the distribution of the peak luminosities in an outburst. Using the disc fraction to calculate the transition luminosities shows that the distributions of the luminosities for the transitions away from- and return to the powerlaw dominated state are both broad and appear to overlap. Using the change in Disc Fraction to calculate the date a transition occurred is not drastically different from the dates obtained from changes in the timing behaviour of the X-ray binary. In addition, we calculate the rate of motion of an X-ray binary through the DFLD during an outburst, a diagnostic which has the potential to be used as a comparison with populations of active galactic nuclei. The fastest rate of motion is on the egress and ingress from the powerlaw dominated state. A further region of increased speed through the diagram occurs in the disc dominated state on the return to the powerlaw dominated state. Finally we compare the measured X-ray luminosities with a small number of contemporaneous radio measurements. Overall this is the most comprehensive and uniform global study of black hole X-ray binaries to date.

Key words: accretion, accretion discs - binaries: general - ISM: jets and outflows - X-rays: binaries

1 INTRODUCTION

Galactic X-ray binaries (XRBs) are the sites of some of the most energetic and exotic phenomena in the local universe, and may provide us with insights into the action of supermassive black holes in active galactic nuclei. Their energetic influence on their sur-

* E-mail: robert.dunn@ph.tum.de

† Alexander von Humboldt Fellow

roundings and the galaxy as a whole are only just becoming clear (Gallo et al. 2004; Heinz et al. 2008).

Many black hole X-ray binaries (BHXRBS) spend most of their time in a quiescent state where both the X-ray (assumed to arise in the accretion flow) and radio (assumed to arise in a jet-like outflow) emission are at a very low level. Most binaries are discovered when they go through an outburst phase. As described in detail in Fender et al. (2004) but see also Nowak (1995); Done & Gierliński (2003); Homan & Belloni (2005); Remillard & McClintock (2006); Done et al. (2007); Belloni (2009), the outburst starts in the “low-hard” state. The state is described as “low-hard” because the BHXRBS is faint and the X-ray emission is characterised by a hard powerlaw of $\Gamma \sim 1.5$. The term is commonly used to indicate the time during which the X-ray spectrum is hard, regardless of the BHXRBS brightness. The radio emission in the low-hard state is characteristic of a steady jet emitting synchrotron radiation. During the early rise of the outburst, the X-ray and radio luminosities both increase, but the X-ray colour of the spectrum remains hard (Corbel et al. 2000, 2003). As the outburst progresses the thermal emission from the accretion disc rapidly becomes more prominent, until it dominates the X-ray emission. This softening of the X-ray spectrum takes place quickly compared to the rise up from quiescence. The state when the disc dominates the spectrum is called the “high-soft” state. There are two intermediate states between the low-hard and high-soft states (hard-intermediate and soft-intermediate). Not all BHXRBS have been observed to go through both these states during their outbursts. Some BHXRBS are not observed to do a transition and remain in the low-hard state until they return to quiescence (Brocksopp et al. 2004; Capitanio et al. 2009).

The short timescale variability characteristics of the X-ray emission from the BHXRBS also change during the outbursts. The level of the root-mean-square (rms) noise and the appearance and frequency of quasi-periodical oscillations (QPOs) are useful for denoting a more accurate date of transition between states (see e.g. Homan & Belloni 2005; van der Klis 2006; Remillard & McClintock 2006; Belloni 2009). The change in spectral information between two neighbouring states can sometimes be very slight, with no clear distinction between the two.

During the transition to the high-soft state the radio emission has been observed to flare in some BHXRBS (Fender et al. 2004, 2009). Even if the flare is unobserved (be this the consequence of no suitable radio observations, or no radio detection during the transition), the radio emission is quenched on the transition to the high-soft state Fender et al. (1999). The disc gradually fades in the soft state and the non-thermal emission recovers. The source then undergoes the return transition to the low-hard state at a lower luminosity than the transition from the hard to the high-soft state. During this period the radio emission is observed to recover. The brightness of the BHXRBS continues to decrease as it returns to quiescence. See Fender et al. (2009) for a detailed study of the radio emission during BHXRBS outbursts and Corbel et al. (2000, 2003) for the details of the radio-X-ray correlation in the hard state.

Over the past few years the importance of BHXRBS for the evolution of the galaxy has become apparent. The discovery of a jet blown bubble from Cyg X-1 (Gallo et al. 2004) allowed the estimation of the kinetic energy injection into the inter-stellar medium (Heinz & Grimm 2005; Heinz et al. 2008). Searches have been done for other jet-blown bubbles, so far with out clear success (Russell et al. 2006). However, it is reasonable to assume that when exhibiting a steady radio jet, all BHXRBS inject (mechanical) energy into their surroundings. This would have significant effect

on the evolution of the galaxy. The radiative emission from X-ray binaries, of all types, usually dominates the X-ray emission from non-active galaxies. The level of this X-ray binary emission has been used as a proxy for the star formation rate of the galaxy (e.g. Grimm et al. 2003) as well as the stellar mass (e.g. Gilfanov 2004). The global properties of BHXRBS are also useful in fully understanding the links between black holes on all mass scales; in particular studying the coupling between accretion and feedback (both radiative and kinetic), can help us to understand the broader picture of how black holes affect their surroundings (see e.g. Merloni et al. 2003, 2005; Körding et al. 2006, 2008; Merloni & Heinz 2008).

For recent reviews on BHXRBS see Belloni (2009); Gilfanov (2009); Markoff (2009); Fender (2009); Gallo (2009).

Therefore the understanding of the processes which occur during the life of a BHXRBS are important in a wider context. As the radio power, and perhaps the energy injection rate, of the jet increases dramatically during the early stages of an outburst, understanding the outbursts of the population of BHXRBS is one way of refining our knowledge of their impact on their surroundings.

For the study of the X-ray emission from BHXRBS, the *RXTE* satellite has created an extensive archive of data on a wide variety of these objects since its launch in December 1995. This makes a comprehensive and easily comparable study possible, as the same instruments (though with changes in calibration over time) have taken all the observations. The over 13 year baseline of observations means that a number of sources have been observed going through outbursts multiple times. This allows comparison within as well as between sources.

We present an analysis of a sample of 25 BHXRBS which have been observed by the *RXTE* satellite. The sample was not chosen in any statistical way. The binaries were selected from well known BHXRBS (or candidates) as well as those which have been well observed by *RXTE*. We outline the data reduction scheme and model selection in Sections 2 and 3. Our initial comparisons between the binaries using the standard diagnostic diagrams are presented in Section 5. Sections 6 and 7 discuss the outbursts themselves and the properties of the transitions. The radio properties of the binaries during their outbursts are a useful probe of the jet activity. The radio observations which are sufficiently coincident with the X-ray observations are presented in Section 8.

2 DATA SELECTION AND ANALYSIS

The data reduction scheme is very similar to that used for GX 339-4 in Dunn et al. (2008). We briefly recap the method below and highlight any changes from that scheme.

We used all observations of the binaries we selected which were publicly available in the *RXTE* archive¹. This gave around 12 Ms of raw *PCA* exposure over an 13 year period. Not all objects we selected had similar time coverage, some having large volumes of observations over all 13 years, whereas others had few.

All the data were reprocessed so that all observations had the same version of the data reduction scripts applied. Apart from the *PCA* data, we also analysed the *HEXTE* data to constrain the powerlaw slope at high energy which allows for more detailed fitting at low energies. We use the data reduction tools from HEASOFT² version 6.6.2. The data reduction and model fitting were automated so that each observation was treated in exactly the same way.

¹ The cut-off date used to find public observations was 4 August 2009.

² <http://heasarc.gsfc.nasa.gov/lheasoft/>

2.1 PCA & HEXTE Data Reduction

The *PCA* and *HEXTE* data were reduced according to the procedure in the *RXTE* Cookbook³, and only a quick summary is given here.

We used only data from *PCA* PCU-2 as it has always been switched on throughout the mission, and so can be used over the entire archive of data. It is also the best calibrated of the PCUs on *RXTE*. Background spectra were obtained using PCABACKEST from new filter files created using XTEFILT, from which updated GTI files were also created. We use only the bright model for the background. Our aim is to perform a single data reduction routine for all sources, and switching between the faint and bright models may have introduced jumps into our light curves. We also ignored the ELECTRON2 selection criterion when using MAKETIME to create the GTI files. As our analysis concentrates on the outbursts (bright periods) of the X-ray binaries, we do not believe that this will bias our results. However, low flux/counts data were therefore treated with caution. The spectra were extracted and the customary systematic error of 1 per cent was added to all spectra using GRPPHA.

In order that the model fitting in XSPEC was reliable and relatively quick, we only fitted spectra which had more than 1000 background-subtracted *PCA* counts. The excluded observations occur throughout the light curves of the objects, with a concentration in the low flux periods. Our analysis concentrates on the outbursts of the X-ray binaries rather than the quiescent periods. Therefore excluding these low count observations, even if most were taken during quiescence, is unlikely to bias our conclusions about the outbursts.

Where possible, we used both *HEXTE* Cluster A and Cluster B data. Background spectra were obtained using HXTBACK. Spectra were extracted using the routine appropriate to the data-type (Event or Archive). Dead-time was then calculated using HXTDEAD. All spectra for a given ObsID were then summed using SUMPHA, and the appropriate responses and ancillary files were added in as header key words using GRPPHA. In order to accurately determine the slope of the high energy power-law we require *HEXTE* data to be present when fitting a model. There have to be at least 2000 background-subtracted counts in one of the *HEXTE* clusters, with the other having a positive number of counts⁴. As our analysis concentrates on the outbursts of the binaries, we also require *PCA* data to be present to fit the soft energies, where the emission from the accretion disc is found. We bin the *HEXTE* data up to match the binning found in the Standard-2 *HEXTE* data products.

3 MODEL FITTING

The spectra were fitted in XSPEC (v12.5.0an, Arnaud 1996). This latest version of XSPEC does not allow parameters to be extracted if there are unconstrained model components present within the fit (an unnecessary line or disc component for example). We have used this to our advantage by stopping fits where a model component is not necessary (a line component for example) as these would cost time if the code attempted to extract errors for them, as the parameters in these cases are usually poorly determined.

Our analysis focuses on the outbursts of the X-ray binaries. It was therefore necessary to accurately determine the disc properties

during the outburst, requiring that we analyse the spectra down to the lowest possible energies. The energy boundaries corresponding to channel numbers have changed during the lifetime of the *RXTE* mission. The calibration of channel numbers ≤ 6 is uncertain, and we therefore ignore all *PCA* channels ≤ 6 (which corresponds to ~ 3 keV), which allows a consistent lower bound to the spectra, extending them to the lowest possible energies and maintaining calibration. All *PCA* data greater than 25 keV were also ignored. The *HEXTE* data were fitted between 25 and 250 keV. To investigate the evolution of the thermal and non-thermal components during an outburst, three types of models were fitted: Powerlaw (POWER), Broken Powerlaw (BKNPOWER) and Powerlaw + Disc (POWER+DISCBB). This allowed us to study the evolution of the disc and powerlaw over the outburst. As an iron line has been detected in a number of X-ray binaries, for each of these three models, a version including a Gaussian line fixed at 6.4 keV was also fitted. This gave a total of six models which were fitted to each spectrum.

The powerlaws had a soft upper limit of 3 keV and a hard upper limit of 5 keV. The break energy was left free throughout the sensitivity range of *RXTE*, though this does allow it to mimic a low luminosity disc (see Section 5.3). We decided on this approach, rather than having a higher low-energy bound for the break energy as this is more flexible in later stages of the analysis. For the work presented here we use the method in Section 3.1.

Noticeable variations of the hydrogen column density value during state transitions may be observed in BHs (see e.g. Cabanac et al. 2009; Oosterbroek et al. 1996 in GS 2023+338 (V404-Cyg)). However, as *RXTE/PCA* response falls under 2 keV, a systematic study of such variations with this instrument appears to be difficult. Hence we decided to fix its value to the commonly accepted value for binaries (see Table 1). Galactic absorption was modelled using the WABS photoelectric absorption code, with values fixed to the accepted values for the binaries (see Table 1). To obtain fluxes outside of the *RXTE* observing band, for the disc for example, dummy responses were created within XSPEC.

Although GX 339-4 had a correction applied for the galactic ridge emission (GRE) in Dunn et al. (2008), we do not apply any such correction to any of the sources analysed here. We did investigate whether it was possible to determine the level of any such correction from the *RXTE* data itself. In some cases (4U 1543-47, XTE J1550-564, XTE J1650-500, GX339-4 and H 1743-322) this was indeed possible - in some cases even being able to constrain the line parameters. However in all the other sources, there did not appear to be any *RXTE* observations in periods of quiescence where the source was not detectable over the background (in terms of background subtracted counts per second per PCU). Rather than applying the GRE correction to only those sources where it was possible to determine the level of correction from the *RXTE* data, or even those where measures using other observatories have been published, we decided to not apply any correction at all. The level of the GRE during an outburst of an BHXR is very low. Comparing our results from GX 339-4 in this analysis to that presented in Dunn et al. (2008) the average flux difference is 2.27 per cent, with 95 per cent of the observations having a flux difference of less than 5 per cent. Therefore our decision to standardise the spectral fitting across all objects by not applying a GRE correction should not affect any conclusions drawn about the outbursts of the BHXR. Any future work on the decays of the outbursts will need to take the GRE into account, and as such any correction will be applied then.

³ http://rxte.gsfc.nasa.gov/docs/xte/recipes/cook_book.html We encountered some difficulty in fitting discs reliably, especially when the sources are in the intermediate states. The response of *RXTE* is only reliable down to ~ 3 keV, whereas the discs we are

⁴ The background subtraction on some observations resulted in a negative number of *HEXTE* counts in one of the clusters.

trying to measure have temperatures of around 1 keV or less. We set the minimum disc temperature to $k_{\text{B}}T = 0.1$ keV in XSPEC to prevent discs from being fit at very low temperatures. It is likely that in cases where this occurred, the disc was being fit to take into account of any curvature in the powerlaw slope rather than to a true disc component. Before selecting the best fitting model we penalised the χ^2 of disc models which had $k_{\text{B}}T < 0.4$ keV as in early results from the fitting procedure indicated that few discs are detected in *RXTE* data with temperatures lower than $k_{\text{B}}T < 0.4$ keV. In doing this we note that we are likely to have excluded a few disc fits that were reliable.

Although a more complicated model, COMPTT for example, would give more information on the state of the accretion disc and its surroundings there are difficulties with using these models. The models used in this analysis are simple, and so can be fit to observations with low numbers of counts. More complicated models require more counts to enable a complete fit to be made. In our analysis of GX 339-4 we find that although COMPTT does fit well to the high luminosity hard-state observations with the highest number of counts (Dunn et al. 2008). But in the soft state, even the observations with the highest number of counts are unable to constrain all the parameters. To use more complicated models restrict the numbers of observations we could use in our analysis, and so the picture arising from this work would be less complete.

The DISKBB model is a comparatively simplistic model and does not include effects on the disc spectrum from the gravitational potential or from the disc atmosphere. In the *PCA* pass-band, when the discs are at low temperatures, this is unlikely to be of concern. However for higher temperature and brighter, more dominant discs, the resulting distortion of the disc emission may not be well fit by the DISKBB model. But, for the reasons noted above, we still use the DISKBB model rather than adding in further model parameters.

3.1 Selecting the best fitting model

Our best-fitting model-selection routine has changed subtly from that outlined in Dunn et al. (2008). We show the flowchart used in Fig. 1 and outline the procedure here. We still initially select the model with the lowest reduced χ^2 . If this is the simple powerlaw (SP), then that is the best fitting model, as it is also the simplest. If it is the simple powerlaw + gaussian line (SPG) then we test whether the gaussian component is an accurate description of a true iron line in the data. The scheme for this “line test” is identical to that described in Dunn et al. (2008)⁵.

If this best fitting model is a broken powerlaw (BP) or a disc+powerlaw model (DP), we test whether using this more complex continuum model is a significant enough an improvement over a simple unbroken powerlaw, by performing an F -test. If the F -statistic probability $\mathcal{P} < 0.001$ then we select the more complex continuum model.

However, if the best fitting model is BP (or DP) and contains a gaussian (BPG or DPG respectively), then the following is done.

If the χ^2 of the BP (or DP) without the line is less than that of the SP, then these continuum models are tested against each other to see if the more complicated model is necessary. Then subsequently

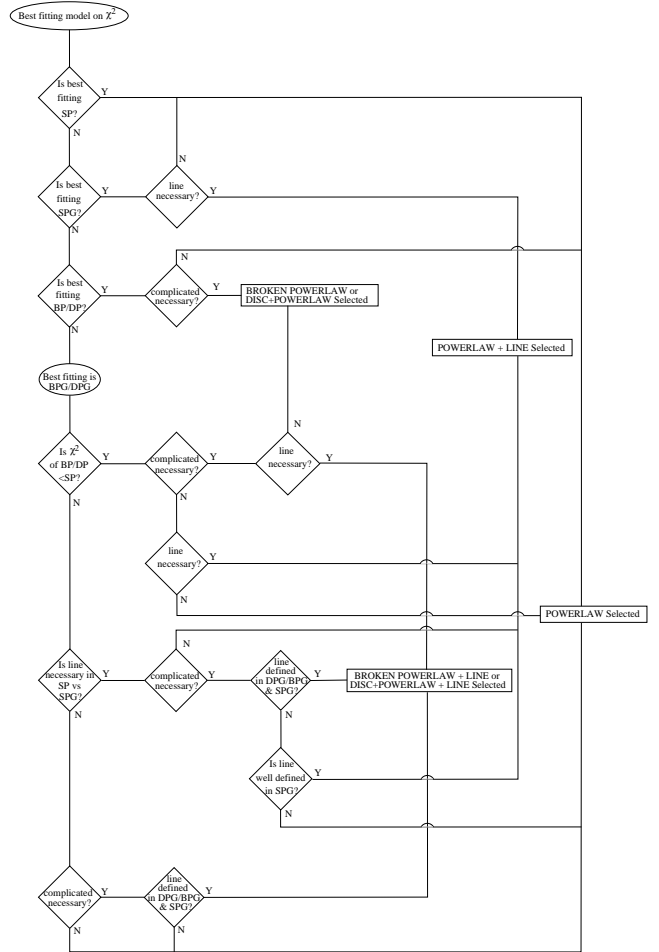


Figure 1. Decision Tree for selecting the best model.

the addition of the line component is tested on the result of the model testing.

If, however, the χ^2 of BP (or DP) is greater than that of the SP, then firstly the existence of the line is tested between SP and SPG. Then if the line is necessary in SPG, the BPG (or DPG) are tested against SPG. If SPG is the best fitting model, then we use the SPG model fit as the best fitting. If the best fitting model is BPG (or DPG), then if the line is well defined ($\sigma < 2$ keV) in both the complicated (BPG or DPG) and SPG models, then the BPG (or DPG) are chosen. If the line is only well defined in the SPG model, then this is chosen, else the SP model is taken as the best fit.

However, if the line is not necessary in the SP models, then although it is not a fair test, then BPG (or DPG) are tested against SP. If SP is the best fitting model, then this is a reliable result. However, if BPG (or DPG) are the best fitting model, then only if the line is well defined ($\sigma < 2$ keV) in both the BPG (or DPG) and SPG models, then the BPG (or DPG) are chosen. Else the best fitting model is SP. All observations with this final set are noted so they can be investigated at a later stage if necessary.

The new feature of XSPEC where fits are terminated if there are unnecessary model components present, allows us to streamline the model selection procedure. These model “fits” are automatically removed from those available to be selected as they are set to have a very high chi-squared value and so are not selected by the routine as a best fit.

We note that we may be missing non-dominant disc compo-

⁵ An F -test using $\mathcal{P} < 0.001$ as the significance level combined with the normalisation of the line and its uncertainty ($\mathcal{N}_{\text{line}} > 3\sigma_{\mathcal{N}_{\text{line}}}$). Both criteria have to be satisfied for the line to be taken as real. Also, if the line width, $\sigma > 2$ keV then this was taken to mean that the line was not well constrained, and the line deemed to be not real.

nents in, for example, the hard state. Even though we fit all observations with a powerlaw + disc model, the lack of sensitivity of the *RXTE PCA* below ~ 3 keV makes detecting non-dominant discs difficult. Therefore even if no significant disc is detected in our analysis, there may be discs present at a very low level in the hard and intermediate states – absence of evidence does not imply evidence of absence.

We also note that we are attempting to fit a line component with a gaussian at a fixed energy, whereas deeper spectra with higher resolution (from e.g. *Chandra* or *XMM-Newton*) are better fit with relativistically blurred line whose peak energy varies (e.g. Miller et al. 2004). The results from the line parameters will appear in a forthcoming publication. However, we do not select models where the line parameters (usually the line width) are not well constrained⁶, even if these are the best fitting.

Any observation with a 3 – 10 keV flux from the best fitting model of less than 1×10^{-11} erg s⁻¹ was discarded from further analysis, as were ones where the flux was not well determined (the error on the 3 – 10 keV flux was larger than the flux itself). It was noted that in some cases, although the flux was high enough and well determined, some of the model parameters were not, especially in the soft state, where the powerlaw parameters may be difficult to determine if the disc is very strong. We therefore excluded these observations from the analysis presented here, however as the disc was fitted successfully, they may be included in a future paper on the disc properties.

Even after this level of selection some spectra still were not well fit by any of the models. To remove the parameters obtained from these poor fits we cut at $\chi^2 < 5.0$.

This selection procedure resulted in a final list of 3919 observations, corresponding to ~ 10 Ms, with well fitted spectra and high enough fluxes and counts. We extract a range of parameters and fluxes for different energy bands and model components which are presented and analysed further the following sections.

The distribution of the reduced χ^2 from all the observations is shown in Fig. 2. There is a clear peak at $\chi^2 = 1$ with a tail extending to higher values of χ^2 , 60.1 per cent of the model fits have $0.8 \leq \chi^2 \leq 1.2$ and 90.2 per cent between $0.7 \leq \chi^2 \leq 2.0$. Our average number of degrees of freedom per spectrum is 111.4. We show on Fig. 2 the expected distribution for 111 degrees of freedom. Given the automatic nature of the data reduction procedure used in this analysis, this tail to higher values of χ^2 is expected. A manual investigation into some of the models with a high χ^2 showed that these observations are a mix of low counts data and occasions where the automated fitting routine failed to find the best fitting model, leaving a poorly-fit simple powerlaw (+gaussian) as the only model with fitted parameters. However, the fraction of high χ^2 values is reasonably small.

4 SELECTED OBJECTS

In our analysis we primarily aimed to select those objects which appear to have been observed regularly with *RXTE*. However, some of the objects only have a few observations taken with *RXTE*. In some cases, although there are many observations, only few pass the counts, flux and model fitting criteria to be analysed further. This sample of X-ray binaries was not intended to be complete in

⁶ Those observations where the line width is unconstrained or if the value of the line width is greater than 2 keV.

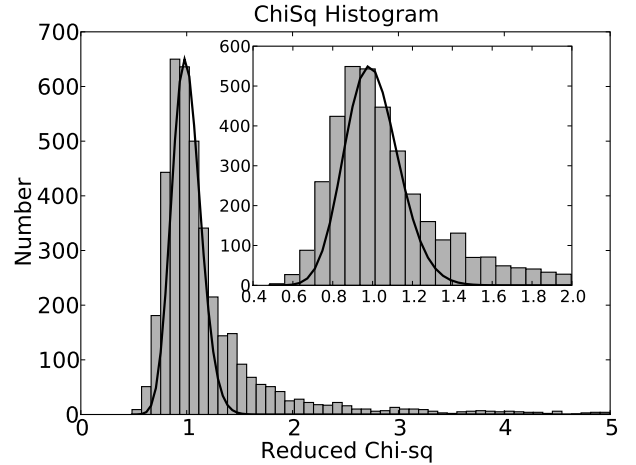


Figure 2. The distribution of reduced χ^2 from all the observations. The inset shows an enlargement around the peak of the distribution. The selection of $\chi^2 < 5.0$ has been applied when creating this plot. We show on top the χ^2 distribution using 111 degrees of freedom.

any way, however, we have attempted to include all BHXRBS with well studied outbursts.

In Table 1 we list the masses, distances, N_H values of the binaries studied in this work. We also summarise the number and total exposure of the X-ray observations used (Table 2). Many of the masses and distances are not well determined, and in these cases we have assumed the distances to be 5 kpc and the masses $10M_\odot$.

The uncertainties in distances and masses affect the calculation of the Eddington Luminosity for these sources. As the majority of relations and diagrams in this work use L_{Edd} to scale the observables, allowing the different binaries to be compared with one another. Without well determined distances and masses then any relation obtained for the ensemble of binaries will be uncertain to some degree.

We note that there is a large range in the number of observations per binary (from almost 700 to less than 10). Therefore in parts of this analysis where the population as a whole is studied, the results will be strongly influenced by those BHXRBS with many observations. However, those BHXRBS with the most observations also tend to be the ones which go through clear outbursts. We also look at the lightcurves to “pre-identify” outbursts, which can then be compared, either to other outbursts from the same source, or to ones from different sources.

The full *PCA* lightcurve of from all the objects over the full 13 years of the *RXTE* mission is shown in Fig. 3. The level of activity from X-ray binaries can easily be seen. Although this plot is in terms of the Eddington ratio, most sources are between 5 and 10 kpc away, so the overall variation in X-ray flux is a factor of four greater. Even with this incomplete sample and the restrictions on which observations are analysed in this work, there are few periods when no BHXRBS is radiating at a significant fraction of L_{Edd} .

5 POPULATION STUDY: GLOBAL PROPERTIES OF BHXRBS

Having analysed this large sample of X-ray binaries we now look at their global properties using well characterised methods.

Table 1. X-RAY BINARY PARAMETERS

Object	M_{BH} M_{\odot}	D kpc	N_{H} $\times 10^{22}$ cm^{-2}	P_{orb} h	M_{*} M_{\odot}
4U 1543-47	9.4 ± 2.0 (1, 2)	7.5 ± 0.5 (3, 4)	0.43 (2, 4)	26.8 (4)	2.45 (1)
4U 1630-47	[10]	10.0 ± 5.0 (5)	> 6 (6)	–	–
4U 1957+115	[10]	[5]	0.15 (7)	9.3 (8)	1.0 (9)
GRO J1655-40	7.0 ± 0.2 (10, 11)	3.2 ± 0.2 (4, 12)	0.8 (13)	62.9 (4)	2.35 (10)
GRS 1737-31	[10]	[5]	6.0 (14)	–	–
GRS 1739-278	[10]	8.5 ± 2.5 (15)	2 (15)	–	–
GRS 1758-258	[10]	[5]	1.50 (16)	18.5 (17)	–
GS 1354-644	> 7.8 = 10.0 ± 2.0 (1)	> 27 = 33 ± 6 (18)	3.72 (18, 19)	61.1 (18)	1.02 (1)
GS 2023+338	10 ± 2 (1)	4.0 ± 2.0 (4)	0.7 (4)	155.3 (4)	0.65 (1)
GX 339-4	5.8 ± 0.5 (20)	8.0 ± 4.0 (21)	0.4 (22)	42.1 (4)	0.52 (20)
H 1743-322	[10]	[5]	2.4 (23)	–	–
XTE J1118+480	6.8 ± 0.4 (1, 24)	1.7 ± 0.05 (25, 26)	0.01 (25)	4.08 (4)	0.28 (1)
XTE J1550-564	10.6 ± 1.0 (3)	5.3 ± 2.3 (4)	0.65 (27)	37.0 (4)	1.30 (3)
XTE J1650-500	< 7.3 = 6 ± 3 (28)	2.6 ± 0.7 (29)	0.7 (30)	7.7 (28)	–
XTE J1720-318	[10] (31)	> 8 = 8 ± 6 (31)	1.24 (31)	–	–
XTE J1748-288	[10]	> 8 = 10 ± 2 (32)	7.5 (33)	–	–
XTE J1755-324	[10]	[5]	0.37 (34)	–	–
XTE J1817-330	< 6 = 4 ± 2 (35)	> 1 = [10] (35)	0.15 (35)	–	–
XTE J1859+226	10 ± 5 (36)	6.3 ± 1.7 (4)	0.34 (36)	9.17 (4)	0.9 (36)
XTE J2012+381	[10]	[5]	1.3 (37)	–	–
LMC X1	10 ± 5 (38)	52 ± 1.0 (39)	0.5 (13)	93.8 (40)	–
LMC X3	10 ± 2 (41)	52 ± 1.0 (39)	0.06 (42)	40.8 (43)	6 (41)
SAX 1711.6-3808	[10]	[5]	2.8 (44)	–	–
SAX 1819.3-2525	10 ± 2 (46)	10 ± 3 (46)	0.1 (47)	67.6 (46)	–
SLX 1746-331	[10]	[5]	0.4 (45)	–	–

Many of the objects do not have well determined distances or masses. In this case we have taken the distances to be 5 kpc and the masses $10 M_{\odot}$, shown in square brackets. A recent critical look at the distance estimates for GRO J1655-40 by Foellmi (2009) indicates a revised estimate of the distance of < 2.0 kpc. (1) Ritter & Kolb (2003), (2) Park et al. (2004), (3) Orosz et al. (2002), (4) Jonker & Nelemans (2004), (5) Augusteijn et al. (2001), (6) Tomsick et al. (2005), (7) Nowak et al. (2008), (8) Thorstensen (1987), (9) Shahbaz et al. (1996), (10) Hynes et al. (1998a), (11) Shahbaz et al. (1999), (12) Hjellming & Rupen (1995), (13) Gierliński et al. (2001), (14) Cui et al. (1997), (15) Greiner et al. (1996), (16) Pottschmidt et al. (2006), (17) Smith et al. (2002), (18) Casares et al. (2004), (19) Kitamoto et al. (1990), (20) Hynes et al. (2003), (21) Zdziarski et al. (2004), (22) Miller et al. (2004), (23) Capitanio et al. (2005), (24) Wagner et al. (2001), (25) Chaty et al. (2003), (26) Gelino et al. (2006), (27) Gierliński & Done (2003), (28) Orosz et al. (2004), (29) Homan et al. (2006), (30) Miniutti et al. (2004), (31) Cadolle Bel et al. (2004), (32) Hjellming et al. (1998b), (33) Kotani et al. (2000), (34) Revnivtsev et al. (1998), (35) Sala et al. (2007), (36) Hynes et al. (2002), (37) Campana et al. (2002), (38) Hutchings et al. (1987), (39) di Benedetto (1997), (40) Orosz et al. (2009), (41) Cowley et al. (1983), (42) Haardt et al. (2001), (43) Hutchings et al. (2003), (44) in’t Zand et al. (2002), (45) Wilson et al. (2003), (46) Orosz et al. (2001), (47) in’t Zand et al. (2000).

5.1 Hardness Luminosity Diagram

The natural first step is to follow e.g. Homan et al. (2001); Belloni (2004); Fender et al. (2004), and plot the X-ray observations in a Hardness-Intensity Diagram (HID) - in this case a Hardness-Luminosity Diagram (HLD) to show the state changes of the BHXRBs during their outbursts. We extract the 3 – 6, 6 – 10 and 3–10 keV luminosities from the spectra. The X-ray colour was calculated from $L_{6-10 \text{ keV}}/L_{3-6 \text{ keV}}$ and plotted against $L_{3-10 \text{ keV}}$ in Fig. 4.

If all the X-ray binaries behave in a similar way during their outbursts, they would be expected to overlap in a well defined region of the diagram. However the overlap is not expected to be perfect (see later in this section). For the Hardness-Intensity diagrams for the individual outbursts from individual sources see Appendix Fig. A.1 and Fig. A.2.

Most of the objects do overlap in the hard-state “stalk” and in the soft-state region. However there are some outliers which fall below the majority of the soft state, and some which appear harder than most of the other hard state observations. The two objects which have soft X-ray colours but are at lower luminosities than most (XTE J1550-564, XTE J1859+226), have two separate expla-

nations. In XTE J1550-564 the X-ray colour softens towards the end of the outburst in 1998 and so the track reappears below the majority of the soft state points. Fainter observations which were cut from our analysis show the XTE J1550 returns to the hard state shortly after our points cease (Homan et al. 2001). For XTE J1859 the peak of the outburst is not far below the rest on Fig. 4, so in this case, the decay in luminosity while in the soft state is just more than in the other binaries.

The two objects which have observations at higher X-ray colours ($\gtrsim 1$) than most others in the sample are 4U 1630-47 and SAX J1819.3-2525. SAX J1819.3-2525 is known to be a peculiar source with strong and rapid variability with a possible shrouding of the black hole (Maitra & Bailyn 2006). 4U 1630-47 has a high N_{H} , which is a possible cause for its “shift” of the canonical track through the HLD to harder values. In the Appendix, the individual HLDs and curves show that almost all of the individual outbursts are shifted towards harder X-ray colours. However, both GRS J1737-31 and XTE J1748-288 also have high N_{H} values but neither has the equivalent extreme shift in X-ray colours. XTE J1748-288 shows a slight hardening compared to the rest of the binaries on its return to the hard state. There are only a few ob-

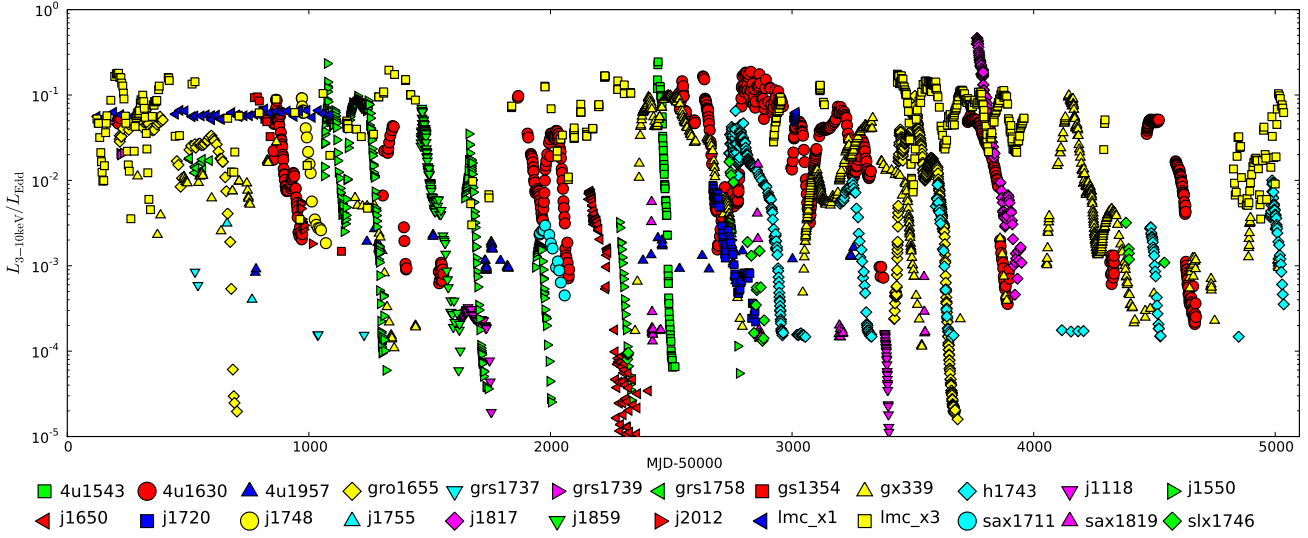


Figure 3. TOP The light curve for all the objects in the sample. Each object has a different symbol. BOTTOM Legend for the different symbols used for the plots showing different objects.

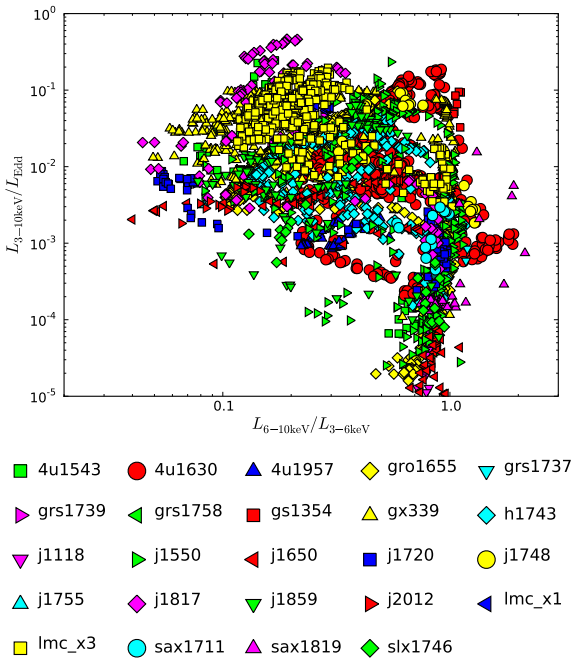


Figure 4. TOP The HLD for all observations of all the objects. Each object has a different symbol. BOTTOM Legend for the different symbols used for the plots showing different objects.

servations of GRS J1737-37 but these are also fractionally harder than the norm. This effect of the values of N_{H} is discussed below.

There are two main problems with the HLD as it has been used in Fig. 4. The main problem is that as the distances of the BHXRBS are uncertain to probably a factor of two, the relative luminosities are not that well constrained. Secondly, as we are using the 3 – 10 keV luminosities in the construction of the HLD, the effects of galactic absorption are different for each object and affect the values of the measured luminosities.

The HLD does well when studying outbursts of individual objects, especially when in combination with X-ray timing and variability information, to determine the state of the XRB. However, as the X-ray colour is used, then with the inability of being able to accurately determine both the disc emission and the effect of any absorption from the spectrum alone limits the usability of the HLD to compare quickly and easily between sources. We therefore turn to another diagnostic diagram for the study of the evolution of the outbursts of XRBs.

We do note, however, that when using a wide band luminosity (e.g. 0.1 – 100 keV) rather than just 3 – 10 keV there is better agreement between the soft states of the binaries as this a more accurate measure of the total luminosity of the source. However, this cannot account for the effects of absorption on the X-ray colour.

5.2 Disc Fraction Luminosity Diagram

The HLD compares the soft X-ray luminosity to the hard X-ray luminosity to give a rough characteristic of the spectral state. The soft X-ray band is dominated by the disc when in the soft state, and the hard X-ray band comes mainly from the non-thermal X-ray emission which has been suggested comes from a corona. The X-ray colour is therefore a proxy for the extent to which the thermal component is dominating the X-ray emission from the binary.

We therefore construct a diagram to compare the relative strengths of the disc and the powerlaw components. Previous studies which have used the relative strengths of the disc and powerlaw components to study the outburst properties include (Kalemci 2002; Kalemci et al. 2004; Tomsick et al. 2005; Kalemci et al. 2006; Körding et al. 2006; Dunn et al. 2008). Körding et al. (2006) formulated the “Disc Fraction Luminosity Diagram” (DFLD) for AGN, as an HLD from the X-ray spectrum alone does not work as the disc emission peaks in the UV. The soft X-rays give information on warm absorbers rather than the accretion disc. They therefore calculated the disc and powerlaw luminosities, and combined

Table 2. OBSERVATION NUMBERS AND TIMES

Object	Total Obs	Exposure Ms	Selected Obs*	Exposure Ms
4U 1543-47	101	0.210	61	0.147
4U 1630-47	868	1.629	704	1.371
4U 1957+115	98	0.458	59	0.260
GRO J1655-40	572	2.254	484	1.829
GRS 1737-31	5	0.045	5	0.045
GRS 1739-278	10	0.022	6	0.017
GRS 1758-258	10	0.007	9	0.007
GS 1354-644	9	0.049	8	0.049
GS 2023+338	4	0.005	0	0.000
GX 339-4	971	1.954	709	1.682
H 1743-322	364	1.030	346	0.998
XTE J1118+480	97	0.186	81	0.170
XTE J1550-564	397	0.868	365	0.833
XTE J1650-500	175	0.271	108	0.191
XTE J1720-318	97	0.247	63	0.125
XTE J1748-288	23	0.092	21	0.074
XTE J1755-324	2	0.006	2	0.006
XTE J1817-330	154	0.383	123	0.329
XTE J1859+226	127	0.300	121	0.292
XTE J2012+381	25	0.045	15	0.036
LMC X1	72	0.351	69	0.349
LMC X3	684	1.607	471	1.048
SAX 1711.6-3808	17	0.040	13	0.029
SAX 1819.3-2525	58	0.132	48	0.114
SLX 1746-331	58	0.153	28	0.091
Totals	4998	12.34	3919	10.09

Differences between the exposure stated here for GX 339-4 and in Dunn et al. (2008) arise from the use of the true exposure rather than the difference in start and stop times of the observation. * After removing high χ^2 observations, low flux observations et cetera.

them in a way to emulate the HLD:

$$\text{Powerlaw Fraction} = \text{PLF} = \frac{L_{1-100 \text{ keV, PL}}}{L_{0.001-100 \text{ keV, Disc}} + L_{1-100 \text{ keV, PL}}}$$

$$\text{Disc Fraction} = \text{DF} = \frac{L_{0.001-100 \text{ keV, Disc}}}{L_{0.001-100 \text{ keV, Disc}} + L_{1-100 \text{ keV, PL}}$$

We use the unabsorbed powerlaw luminosity, but only determine the flux down to 1 keV to prevent the low energy end from being overly dominant. We are unable to determine both the absorption and the low-energy cut-off of the powerlaw from the *RXTE* data, and so use a fixed value of N_{H} for the fitting, and a standard low energy bound to the powerlaw flux for all objects. Although this may introduce excess powerlaw luminosity into our calculations, it is standard across all objects, as the true low energy behaviour of the powerlaw cannot be determined from the *RXTE* spectra. The disc luminosity is also the unabsorbed luminosity to full capture the radiative output of the disc. The energy range used is purposefully large to ensure we cover as much of the disc emission as possible. This diagnostic diagram is therefore less sensitive to the effects of N_{H} (the powerlaw luminosity still includes the effects of N_{H} instead of a low energy cut off), as in the outbursts, the low energy emission is dominated by the unabsorbed disc emission.

We show in Fig. 5 the relation between the disc fraction and the X-ray colour of the observation. The arrangement of the points shows that the calculated disc fractions are well determined. In fact, for many objects there is a constant relation between the two diagnostic values when the disc fraction is not zero. The approximate

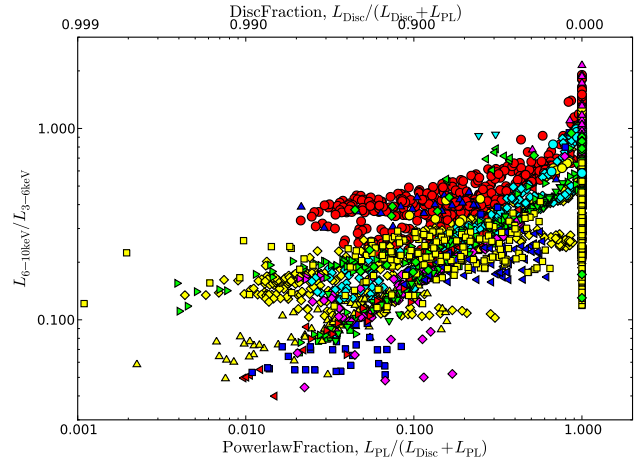


Figure 5. The correlation between the X-ray colour and the disc fraction. See Fig. 4 for the legend to the symbols used.

relation is quadratic, where the powerlaw fraction is proportional to the square of the hardness ratio. There are some which do not appear to lie on the relation. The clearest are 4U 1630-47 and LMC-X3. 4U 1630-47 has a large value for N_{H} , which hardens the spectrum, so moving the soft state to harder X-ray colours. The same can be said, to varying degrees, of H 1743-322 and XTE J1748-288. In LMC-X3, there is very little variation in the X-ray colour for a large range in disc fraction. In this source, the powerlaw is not always well determined underneath a very dominant disc, likely to result from the distance of the source.

GRO J1655-40 and XTE J1550-564 also appear at harder X-ray colours than the majority of the other sources at the same disc fractions. The N_{H} s for these two sources are not particularly high, so this is unlikely to be the reason for their offset. They do both have atypical outbursts, with XTE J1550-564 performing a complete loop in the HLD, and GRO J1655-40 having a very strong very high state. Whether these features also manifest themselves in the relative strengths of the powerlaw and disc components is not clear.

On our Disc Fraction Luminosity diagrams (DFLDs), we plot both the Powerlaw and the Disc Fractions as axes. We retain the powerlaw fraction for the main x -axis for similarity with the HLDs, and use the disc fraction as the secondary (upper) x -axis. We hope that this will minimise confusion when talking about the disc fraction. We note that uncertainties in the luminosity of the observation arising from uncertainties in the masses and distances of the object have not been accounted for in Fig. 6.

Rather than using the canonical state descriptions (hard, soft, intermediate etc.) when discussing the DFLD, we will use disc- and powerlaw-dominated states. The reason for this is that the intermediate and hard states are compressed together. This makes distinguishing the standard states as determined from the X-ray colours difficult on the DFLD. Therefore, we use the two-state description as mentioned above. We define the two states as follows, a powerlaw-dominated state is one where the powerlaw fraction is greater than 0.8 (disc fraction less than 0.2). The disc dominated state is therefore the converse. For the moment we do not consider the observations which are intermediate between the disc dominated and powerlaw dominated states.

Some of the objects (XTE J1817-330 and LMC X-3) appear to have luminosities above the Eddington luminosity. In the case

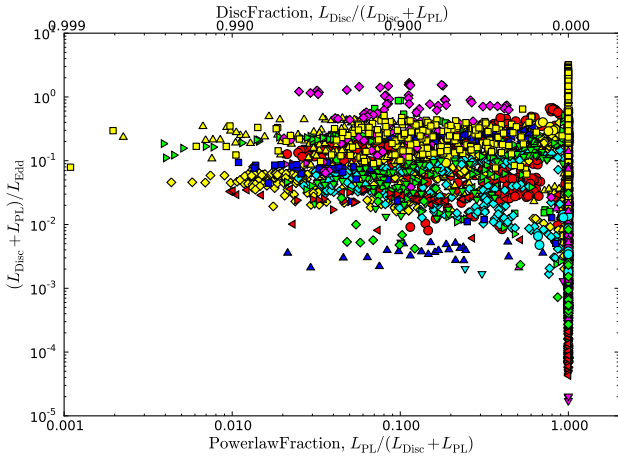


Figure 6. The DFLD for all observations of all the objects. Each object has a different symbol. See Fig. 4 for the legend to the symbols used.

of XTE J1817-330 the distance to the source is not well known and there are large uncertainties on the mass of the compact object. In the assumption that XTE J1817-330 is not a super-Eddington source, we can use the Eddington luminosity to place limits on the distance of the source for different values of the mass of the compact object. We have currently used a value of 10 kpc, which results in a maximum Luminosity of $1.7L_{\text{Edd}}$. Therefore, assuming that the mass of the central object is $\sim 4M_{\odot}$, the upper limit on the distance is ~ 8 kpc. For the upper mass limit of $\sim 6M_{\odot}$, the upper limit on the distance is ~ 10 kpc and for the lower mass limit of $\sim 2M_{\odot} \sim 5.6$ kpc.

For LMC X-3 the situation is less clear. The distance to the source is well known and the mass is also comparatively well determined. The DFLD of LMC X-3 alone is strange. The “stalk” extends well beyond the most luminous disc dominated state. Investigating the individual fits more closely, we found that not all of the best fit results were well fit. Although there are sufficient counts in the *HEXTE* band to pass our selection criteria, they are not sufficient to constrain the powerlaw at high energies. At low energies, in the *PCA* band, the data are dominated by the disc, preventing a powerlaw component to be fitted to the data. As the powerlaw parameters cannot be accurately determined, XSPEC may not extract values for this (disc + powerlaw) model. This model fit is then penalised in the model selection routine, and results in a best fitting model with only a powerlaw component. In some cases, the powerlaw is well-fitted, but has a very steep slope. The steep slope at the low energies, where the powerlaw fits the rise of the disc component results in a high powerlaw normalisation, from which the powerlaw luminosity, and hence total luminosity, is calculated. Fitting only a disc model, although it would allow the study of the disc parameters (and may be done for a future publication) would not allow the calculation of an accurate disc fraction.

The DFLD constructed from the SDSS⁷ by K rding et al. (2006) is shown in their Fig. 10. The DFLD presented in Fig. 6 appears similar in appearance to the expected DFLD simulated for a sample of BHXRBS undergoing outbursts by K rding et al. (2006). There are some outlying points, but most of the observations lie in a swathe between 1 and 50 per cent of L_{Edd} . The outlying points may arise from the uncertainty in the values of the distances and

masses of the XRBS. The radio properties across the DFLD are described in Section 8. We now discuss the properties of the DFLD in more detail.

5.3 Cross mapping of HID and DFLD

The mapping of the HID to the DFLD and vice-versa was not investigated clearly in Dunn et al. (2008). Although we now have more populated diagram, the mapping from HID to DFLD and vice versa is not easily determined for the complete population. This arises because of the problems with the HID outlined in Section 5.1. The effects of absorption on the soft end of the spectrum re-appear when converting Disc Fractions for all the sources back onto the HID. It is therefore easiest to see the mapping for individual objects. As every object, and even every outburst (see Section 6) is different we show the mapping for three representative outbursts in Fig. 7. Correcting for the hardness when used in the HID would more easily allow the comparison between sources (Done & Gierliński 2003).

In Fig. 7 we show the HID and DFLD for GX 339-4, GRO J1655-40 and H 1743-322. To highlight the variation across the diagram, we select a number observations with specific X-ray colours or disc fractions. These have been given a different colour to show the pattern of variation between the two diagnostic measures.

Roughly, the most disc dominated states are the soft states, and the powerlaw dominated states are the hard and intermediate states. However the exact mapping, especially the HID intermediate states, appears to vary from source to source. The state transitions will be easier to map when they can be clearly identified from changes in the timing properties of the sources, rather than from X-ray colours at present. For further discussions on the transitions between states see Section 7.

The apparent lack of points between powerlaw fractions of 1 and ~ 0.3 result from the low energy limitations of the *RXTE PCA*. The discs we are attempting to analyse are $\lesssim 1$ keV whereas the lowest calibrated spectral energy bin is around 3 keV. Therefore as the disc emission strengthens as the source moves into the soft state, the X-ray colour softens. However, our fitting algorithm may take a broken powerlaw over a disc and powerlaw fit for these intermediate states. Only when the curvature of the multicolour disc is clearly evident will a disc and powerlaw be a better fit, by which time the source is almost fully into the soft state. There is very little difference in the χ^2 values of the fits, but as both models have the same number of degrees of freedom, finding out which is the appropriate one to choose is not straightforward. Rather than choosing disc models where they may not have been fitted well, or may not be appropriate, we currently continue to use the model selected on χ^2 terms. This has on a handful of occasions resulted in observations where the best fit is a broken powerlaw, but all the neighbouring observations are disc model fits (see Appendix Fig. A.1 - 4U 1630-47 Outburst 7 & 8). Rather than adjusting these model fits by hand, and therefore possibly biasing our results, we leave these observations as they are, especially as they stand out clearly.

Therefore in some cases the DFLD as determined from *RXTE* compresses some of the intermediate states into the powerlaw dominated state. The extent to which this occurs varies on a source-by-source basis. As can be seen in Fig. 6 the area between disc fractions of 0.3 to 0.9 is fairly well populated whereas in Fig. 7 for GX 339-4, there is a gap, but in GRO J1655-40 there is not. However above a certain X-ray hardness, all the points are compressed on to a single line. The DFLD is therefore not ideally suited to the study of the hard and intermediate states.

The fan-like mapping of lines of constant X-ray colour onto

⁷ Sloan Digital Sky Survey, Adelman-McCarthy et al. (2008)

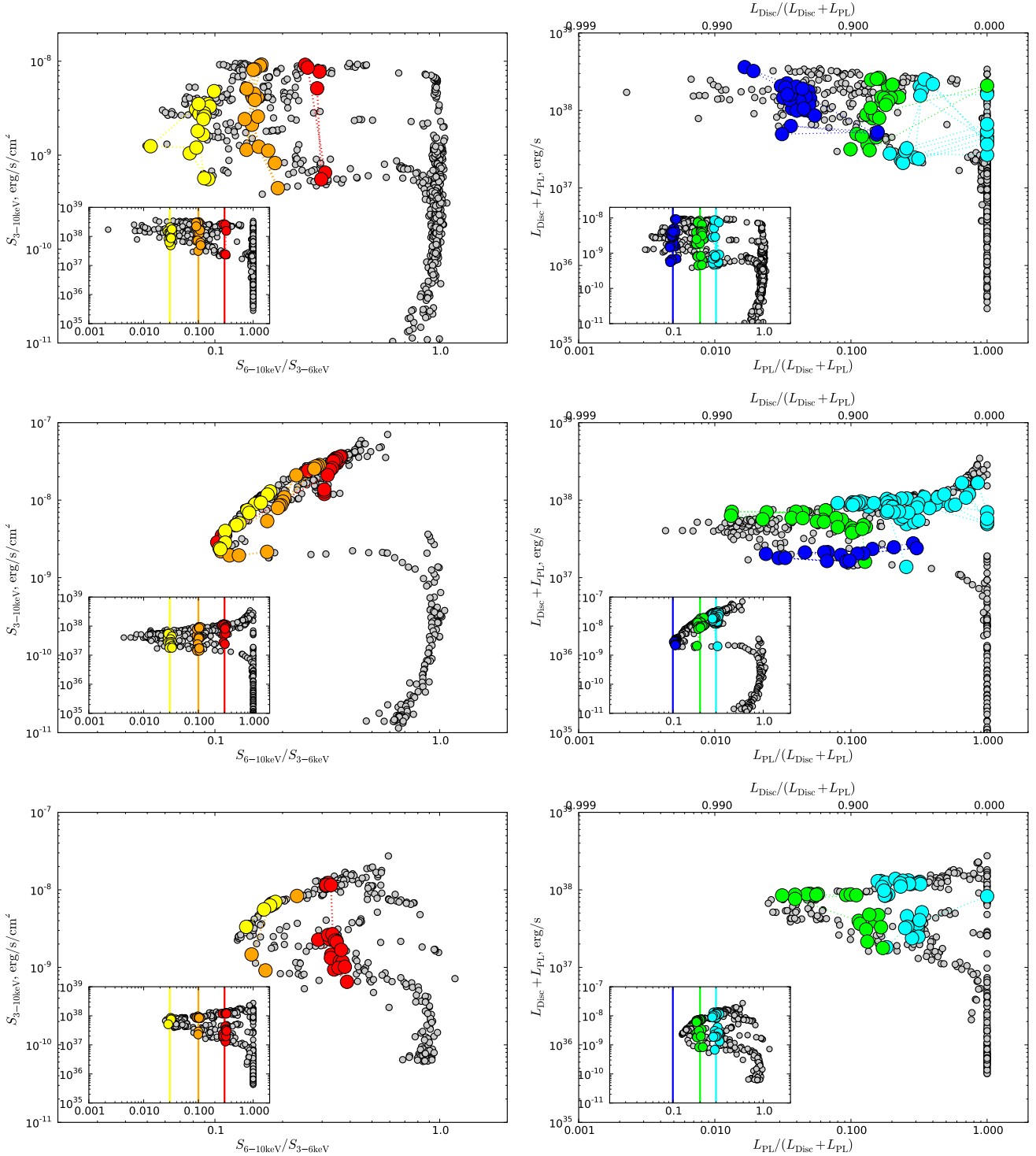


Figure 7. The mapping of one diagram onto the other. LEFT: HID with specific disc fractions highlighted, and RIGHT: DFLD with specific X-ray colours highlighted. The highlighted disc fractions are red 0.3, orange 0.1, yellow 0.03; and the highlighted X-ray colours are cyan 0.3, green 0.2, blue 0.1. TOP: GX 339-4, MIDDLE: GRO 1655-40 and BOTTOM: H 1743-322

the DFLD, indicates that while the source remains in the soft state, the disc begins to cool and decay. Although this can be seen as the total luminosity in the soft state decreases, the level to which this is the disc or the powerlaw is less clear from using the X-ray colour and a 3 – 10 keV luminosity. In the DFLD the level to which the

disc dominates the X-ray emission from the binary is clearly seen to decrease before the source re-enters to the hard state.

This mapping of the X-ray colour onto the Disc Fraction was expected from the simulation of an BHXRB DFLD by Körding et al. (2006) as shown in their Fig. 11. Although also intended to show the positions of AGN classes on the DFLD, the

split into only hard, hard intermediate and soft states is similar to the distribution of the lines of constant X-ray colour (from which the states can usually be determined).

The transition across from the powerlaw to the disc dominated state in the DFLD can be at a single or decreasing luminosity (horizontal or sloping line in Fig. 7), mimicking that what happens in the HID. However, on the return, the HID transition appears to horizontal and rapid, whereas the decline to the powerlaw dominated state in the DFLD shows the disc dominance gradually declining as the luminosity decreases. There are more observations where the return transition has been monitored, only one of which is close to horizontal (XTE J1650-500, see Appendix Fig. A.1).

This comparison between the HID and DFLD shows that for individual outbursts or objects the HID is most suited as the different states are not compressed together. The intermediate, hard and soft states are easily discernable. When using the DFLD, the intermediate states are compressed with the hard states. However, for the reasons outlined in Section 5.1, it is not best suited for comparing outbursts from different objects.

5.4 Speed of motion

We investigated the speed of motion of an BHXRB through the HID and DFLD. Under the assumption that AGN are just scaled-up versions of BHXRBs, then as they are going to evolve much more slowly than BHXRBs, a population study will definitely be required to investigate them. Under the assumption that the temporal evolution of AGN are the same as for BHXRBs, the speed of motion of the BHXRBs through the DFLD shows where AGN are most likely to be found. When the BHXRBs move rapidly through the DFLD, they do not spend long in that area of the diagram, and so are not observed often in that area of the diagram. Hence for a population of AGN, they will be preferentially be observed in the areas of the DFLD where the BHXRBs move more slowly.

To allow the easy comparison of the speed at different points within these diagrams, the relative changes were calculated:

$$\text{Rate} = \left(\frac{x_i - x_{i-1}}{\frac{(x_i + x_{i-1})}{2}} \right) / (t_i - t_{i-1}) \text{ day}^{-1}, \quad (1)$$

where x_i is the quantity whose rate of change we calculate at the observations of interest, x_{i-1} is the value at the previous observation, and t are the dates of the observations. We do not take values for the rates of motion when the two observations are separated by more than five days. This is to remove large values when an outburst is badly sampled on the rise or decline. This process removed around 200 observations from these plots.

We calculate the rates in Disc Fraction and Luminosity separately. From these two rate calculations we calculate the overall rate of motion through the plane using Pythagoras' theorem. However we do not currently calculate the direction of the overall motion. To show the variation of the rate of motion through the plane, we average within the grid squares shown by the dotted lines in Fig. 8. To further clarify the diagrams, we also truncated the colour scales.

It is obvious that the slowest change in disc fraction would be in the powerlaw dominated state (Disc Fraction < 0.2). This slow rate of change of disc fraction can be seen at the base of the "stalk" in the low luminosity part of the diagram. The fastest rate of change of disc fraction might be expected on the transition across to the disc dominated state. This is seen on the transition to- and the transition from- the disc dominated state at all luminosities as the dark band around a disc fraction of ~ 0.4 . There is another

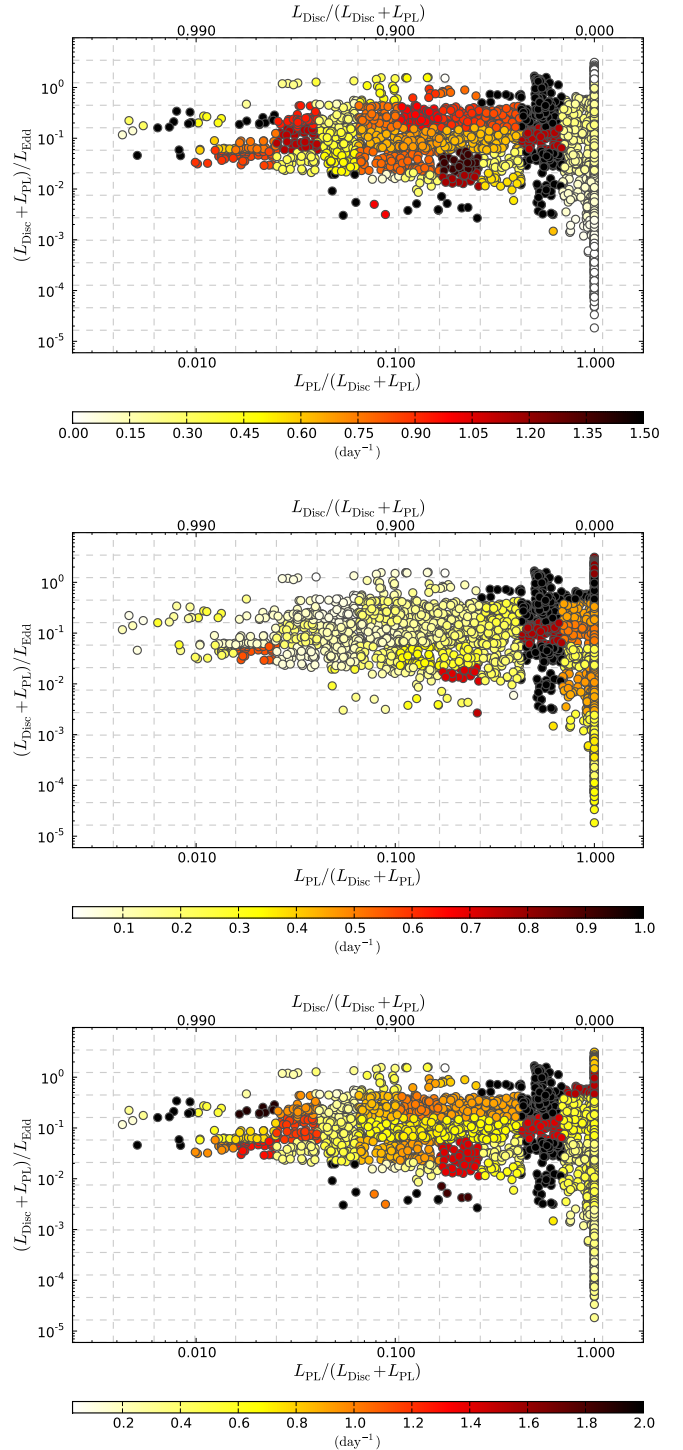


Figure 8. Rate of motion through the DFLD in Disc Fraction (TOP), Luminosity (MIDDLE) and both combined (BOTTOM). The colour scales have been truncated for clarity.

minor rise in rate mid-way through the disc dominated state (disc fractions ~ 0.8) at the lower end of the luminosity range at these disc fractions. This may be an indication of an increase in the rate of motion back towards the powerlaw dominated states. This feature may become clearer once the distances and masses of the BHXRBs

are more certain, and the levels of their transitions, and tracks in the DLFD are more precisely positioned.

The variation in change of rate of the luminosity is much clearer. There is a small peak at the top of the powerlaw dominated state, but the greatest rate of change is found in the same region as for the rate of change of disc fraction - on the departure from and entry to the powerlaw dominated state (disc fractions of ~ 0.4). In the most disc dominated state there is little variation in the luminosity - and the rates of change are uniform across the region. There appears to be a slight increase in the rate during the decline, as the source approaches the powerlaw dominated state.

When combining the rates, the effect of both the disc fraction and the luminosity rate distributions are seen. The disc fraction rates dominate the diagram being much stronger. What is clear, however, is that the rate of motion through the softest, most disc dominated states is comparatively slow. The final brightening of the hard state along with the beginnings of the transition across towards the disc dominated state, as well as the final parts of the decline back to the hard state are the regions where the BHXRBs change their characteristics the fastest.

The region marking the transition from the powerlaw dominated to the disc dominated states with an increased rate of motion may result from our model selection procedure. The differences in χ^2 between the broken powerlaw ($DF = 0$) and disc+powerlaw ($DF \neq 0$) are small, but the differences in disc fraction are large. As the BHXRB rejoins the hard state there is some fluctuation as to which model is chosen. This effect occurs on both transitions, and at a period where a high duty cycle of observations is likely. Therefore it is possible that the sudden change from pure powerlaw to disc + powerlaw, possibly with some oscillation, contributes to this region of increased rate of motion.

Some of the grid squares include very few points. The small numbers of points in these squares some cases leads to extreme rates, usually high. We ignore these grid squares in our interpretation above as the few numbers of points do not reflect the global properties.

6 SIMILARITY OF OUTBURSTS

As noted in Dunn et al. (2008) two outbursts of GX 339-4 were remarkably similar, even though they had different tracks in the HID and were separated by two years. This had been pointed out for the bright part of the outbursts by Belloni et al. (2006). Of the binaries in this sample there are many which do not show much of an outburst. This can result from the fact that no strong outburst has been observed by *RXTE*. However in a number of cases, only the tail end of the outburst has been seen, i.e. after the source has reached the soft state. The brightening of the binary in the hard state was missed. The rise from the soft state is likely to have been monitored by the *ASM* on *RXTE*. However pointed *PCA* observations will only have started after an interval, by which time these sources have already reached the soft state. This allows us to conclude that the rises and transitions of these sources was extremely rapid, occurring over a couple of days or so. Even with this missing information we are still able to extract parameters from the lightcurves and their shape to be compared to those outbursts which have been fully sampled.

In the Appendix in Fig. A.1 we show the outbursts disc fraction curves, as well as the X-ray colour curves, with their luminosity as colour scale. The basic shape is the same as in the two outbursts from GX 339-4 (Dunn et al. 2008). There is a “hardening” (disc becomes less dominant) in the middle of the outbursts

which is associated with an increase in flux.

In some cases the “hardening” occurs without an increase in flux, and in others vice versa. In some cases we do not observe the beginning of the outburst, but still can see some of the spectral and flux variation within the outburst - 4U 1543-47, 4U 1630-47, XTE J1817-330 and XTE J1859+226 all clearly show some of these features. For comparison we also show the same curves using the X-ray colour in the Appendix, Fig. A.1.

Using the All Sky Monitor (*ASM*) on *RXTE* Gierliński & Newton (2006) investigated the behaviour of the transition from the hard to the soft state. They found two categories for the transitions - bright/slow and dark/fast, with separations in the transition luminosities (~ 0.06 vs $< 0.01 L_{\text{Edd}}$ respectively), the duration of the transition and the shape of the transition on the HID. In the BHXRBs’ spectral evolution presented here, as we are using the *PCA*, in many cases the beginning of the outburst has been missed, and we are therefore unable to accurately comment on the type of outburst (e.g. 4U 1543-47). Unsurprisingly we do agree on the classifications from Gierliński & Newton (2006). Only in 4U 1630-47 and GRO J1655-40 can we investigate additional transitions. The outburst sequence in 4U 1630-47 is very complex, and therefore very difficult to classify, and we do not attempt to. GRO J1655-40 is likely to be a bright-slow transition as it takes 100 days to reach its most disc dominated/softest state, makes the transition at around $\sim 0.06 L_{\text{Edd}}$ and has a strong very high state.

6.1 Peak Luminosities

On the curves in Fig A.1 we show the lines used to calculate the transitions between the different states. The vertical lines show the dates where the transition between disc and powerlaw dominated states took place as calculated by the changes in disc fraction. We also show as the two horizontal lines the powerlaw fractions used to determine the date of the transition. The date given is when the source crossed the powerlaw fraction = 0.8 line if this was able to be interpolated reliably. We use a powerlaw fraction = 0.8 when calculating the transitions to make sure that we clearly identify the tracks away from- and return to the powerlaw dominated/hard state. If not, then the first/last disc dominated state is used to estimate the luminosity on the entry to and exit from the disc dominated state (see Section 7 for more complete details of the procedure).

The difficulty of using *RXTE* data in this analysis is apparent in some of the Disc Fraction curves (see Appendix Fig. A.1). There are some points which have a powerlaw fraction of 1.0 even though most of those which surround them are in the disc dominated part of the diagram (e.g. GX 339-4, Outburst 4, and 4U 1630-47). In these cases the disc is not strong enough to be the best fit model given the statistical cuts we have made. These observations are easily identified in the Disc Fraction curves in the Appendix. Using an X-ray observatory which has a better low energy response than *RXTE* would allow the more gradual change from pure powerlaw to powerlaw + disc to be observed in all objects. In some objects this discrete nature is not observed, presumably because either the disc or powerlaw parameters are such that the disc is easily identified at low disc luminosities.

We compare the distribution of peak Luminosities achieved in the outburst with those analysed in Chen et al. (1997). Their best fit to the distribution is a gaussian with a mean of -0.7 and a Full Width Half Maximum (FWHM) of 0.82 in logarithmic

space⁸. Our distribution, see Fig. 9, shows a very similar distribution ($\mu \sim -0.91$, $\sigma \sim 0.71$, the average of the least squares and downhill simplex algorithms). Our distribution has a very similar mean, but is broader. We perform a Kolmogorov-Smirnov (K-S) and a t -test on the two samples, and it is unlikely that they are drawn from different populations and unlikely that they have different means ($P_{K-S} = 0.38$ and $P_t = 0.40$).

The excess at low Eddington fractions is likely to arise from identified outbursts⁹ - periods of emission in the *RXTE* lightcurve - where the source did not reach a true peak in emission. It was either monitored by chance in quiescence for a length of time, the full outburst was not observed by *RXTE* (as in XTE J1118+480) or the outburst was a hard state only outburst. We therefore ignore this tail. This excess was also seen in Chen et al. (1997), who put it down to arising from uncertainties in the masses, distances and spectral shapes of their sources.

As was already noted in Chen et al. (1997) amongst others, the peak of the peak luminosity distribution does not occur at 100 per cent of the Eddington ratio, but at around $0.2L_{\text{Edd}}$. This will be explored further with the study of the transition luminosities in Section 7.

From disc instability models, the peak outburst luminosity is expected to correlate with the orbital size of the binary (King & Ritter 1998; Shahbaz et al. 1998). As shown in Table 1, we have the orbital parameters for about half of our sample of BHXRBs. We extracted the peak luminosities for outbursts which showed a transition (either away from or return to the powerlaw dominated/hard state, see Section 7) and plotted these against the orbital period. There was no clear correlation, neither when using the X-ray colour, nor when using the Disc Fraction when determining the transitions. However, there are significant limitations to our calculations of the transitions (see Section 7) and unmeasured orbital periods, and so unfortunately we cannot conclude anything from the apparent lack of a correlation.

7 TRANSITION LUMINOSITIES

Having produced a large number of HLDs and DFLDs we can extract the luminosity of the BHXRB during the transition between different states. If the BHXRBs behave in a very similar way, then these should occur at very similar fractions of L_{Edd} . Although we calculate the transitions for each outburst where possible, to study their distribution, we only take those where both transitions have been observed.

In those outbursts when only the return to the canonical hard state is observed we do not attempt to interpolate a beginning to the outburst. If the first observation of an outburst is sufficiently soft (X-ray colour or Powerlaw fraction < 0.3) then no attempt is made to find the transition away from the powerlaw dominated state. If the first observation is in the powerlaw dominated state (X-ray colour or Powerlaw fraction > 0.8) then to calculate a transition each observation is stepped through to find the first which has an X-ray colour/Powerlaw Fraction < 0.3 . Then the observations are stepped through in reverse to find the last observation with X-ray colour/Powerlaw Fraction > 0.8 . The observations which bracket

⁸ We fit gaussian profiles to the data from Chen et al. (1997) in order to compare the two distributions statistically. Our best fit values are $\mu \sim -0.81$ and $\sigma \sim 0.36$ in logarithmic space.

⁹ We pre-identify times when the source was bright to make the automatic transition detection easier.

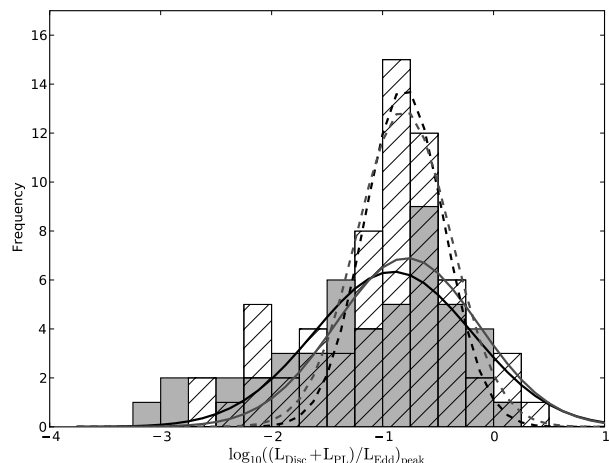


Figure 9. The distribution of the peak luminosities within each outburst for the objects in our study (solid grey) and that from Chen et al. (1997) (“/” hatched). Least squares fitting in grey, the downhill simplex fitting in black lines. The solid curves are the fits to our distribution. We fit the data from Chen et al. (1997) using both the fitting methods, and show the results with the dashed lines.

an X-ray colour/Powerlaw Fraction > 0.8 are used to interpolate when the transition occurred and what luminosity the source was at. If the bracketing observations are more than 10 days apart, then the softer/more disc dominated observations’ date and luminosity are used. This process is reversed to find the return transition. These dates are shown on the curves in Appendix Fig. A.1.

We chose the values of 0.3 and 0.8 to ensure we have a complete transition from the hard to the soft state. In Dunn et al. (2008) we used values of the X-ray colour of 0.22 and 0.87 derived from the timing properties in Belloni et al. (2006) to select purely soft- or hard-state observations. When looking at the HIDs from the BHXRBs in this work, using these values would have been too restrictive, not detecting transitions in sources where the HID looks similar to the canonical HID, but is for some reason truncated or offset (e.g. 4U 1630-47). We therefore chose a more “inclusive” set of values to determine transitions.

The exact value of the Disc/Powerlaw Fraction at the point of transition may vary from source to source. For a few of the sources, we investigate the results of the previous studies on the timing properties of the sources as they make the transition to obtain the true dates. We show in Table 3 a selection of the transition dates for the source which have had them determined from timing properties.

We do not look for transitions including the intermediate states, as these are difficult to determine from spectral information alone. We also excluded those sources where the data although being very sparse, would give a transition date and flux, and those where no clear outbursts are apparent in the light curves, but the spectral variations would have resulted in transitions being detected. This was accomplished using the pre-identification of outburst periods in the lightcurves.

The locations of the dates where transitions occurred are shown in the figures in the Appendix (Fig. A.1). The cross-matching between the *RXTE* observations shown here, and those determined from timing information was done to a tolerance of ± 1 day. In most cases the timing-determined transitions and those from X-ray colour or Disc Fraction values are not wildly dissimilar (see Table 3). Although it would be better to use the transition values as deter-

Table 3. TRANSITIONS FROM TIMING ANALYSES

Object	Timing Date Range		State Transition	X-ray Colour Date MJD	Disc Fraction Date MJD	Ref.
	MJD	MJD				
4U 1543-47	52473.25	52474.17	HSS → IMS			(1)
	52479.74	52480.66	IMS → LHS	52483	52478	(1)
4U 1630-47	50855	50856	LHS → VHS			(2)
	50874	50884	VHS → HSS			(2)
	50888	50890	HSS → LHS			(2)
	50951		HSS → LHS			(3)
	51395		HSS → LHS	51351		(4)
	52057.96	52059.38	HSS → LHS		52049	(4)
GRO J1655-40	50663.7	50674.4	HSS → LHS	50676	50672	(4)
	53440		LHS → HSS	53440	53440	(5)
	53442		LHS → HSS			(6)
	53501		HSS → VHS			(5)
	53506		HSS → IMS			(6)
	53520		VHS → HSS			(5)
	53625		IMS → LHS	53633	53628	(6)
	51200.9	51220.8	HSS → LHS	51201	51201	(4,7)
GX 339-4	52394.4	52398.7	LHS → HIMS	52401	52411	(8)
	52410.5	52411.6	HIMS → SIMS			(8)
	52558.6	52560.4	SIMS → HSS			(8)
	52693.7	52694.9	HSS → HIMS	53734	53719	(8)
	52740.0	52741.7	HIMS → LHS			(8)
	53233		HIMS → SIMS	53228	53234	(9)
	52929.98	52930.90	HSS → IMS			(10)
H 1743-322	52937.51	52938.00	IMS → LHS	52941	52938	(10)
	51305.12	51308.32	HSS → LHS		51290	(4,11)
XTE J1550-564	51661		LHS → IMS	51659	51673	(12)
	51672.4	51673.0	IMS → HSS			(4) ^a
	51673.4	51674.7	HSS → IMS			(4)
	51675.5	51676.4	IMS → LHS			(4)
	51677		IMS → LHS	51683	51664	(12) ^a
	52231	52232	HSS → LHS	52238	52234	(4)
XTE J1720-318	52652		LHS → HSS			(13)
	52715.47	52728.58	HSS → LHS	53735	52735	(14)
XTE J1748-288	50975	50977	VHS → HSS		50975	(15,16)
	51007	51012	HSS → LHS		51006	(15,16)
XTE J1755-324	50661	50758	HSS → LHS			(4)
XTE J1817-330	53885		HSS → IMS	53906	53886	(17)
	53889		IMS → LHS			(17)
XTE J1859+226	51524		HSS → IMS	51613	51597	(4)

LHS - Low Hard State, HSS - High Soft State, SIMS - Soft Intermediate state, HIMS - Hard Intermediate State, IMS - Intermediate State. Where possible we give the two dates which bracket the change in state as determined in the other studies indicated. Where only a single date was given or able to be determined, we give that date. The nomenclature for the states is that of the study in which transition dates are presented, and may not reflect the current view. ^a We note that the two different transition determinations for XTE J1550-564 do not fully coincide. We also show the transition dates obtained in this work, as determined from the X-ray colour and disc fraction changes. Those transitions where no date was obtained from this work are still shown for comparison to Appendix Fig. A.1.

(1) Kalemci et al. (2005), (2) Trudolyubov et al. (2001), (3) Tomsick & Kaaret (2000), (4) Kalemci (2002), (5) Brocksopp et al. (2006), (6) Debnath et al. (2008), (7) Nowak et al. (2002), (8) Belloni et al. (2005), (9) Belloni et al. (2006), (10) Kalemci et al. (2006), (11) Homan et al. (2001), (12) Miller et al. (2001), (13) Remillard et al. (2003), (14) Brocksopp et al. (2005a), (15) Revnivtsev et al. (2000b), (16) Revnivtsev et al. (2000a), (17) Gierliński et al. (2008).

mined from timing information, this is not possible for all sources and all outbursts. We therefore use the method outlined above.

In some sources the accurate determination of the transition date from the observations was not possible from gaps or noise in the light, X-ray colour or Disc Fraction curves (see e.g. 4U 1630-47 Outburst 3 and GX 339-4 Outburst 1). This leads to uncertainties when calculating the distribution of the transition luminosities.

As not all the binaries have well determined masses and distances we estimate the effect of these uncertainties on the transition luminosities in the following way. The uncertainties in the masses

and distances are propagated through to the L/L_{Edd} values. We then do a simple Monte-Carlo simulation on the binning of the transition values. Values for L/L_{Edd} are randomly selected from a gaussian distribution with the 1σ values derived from the error propagation values. These values are then binned into a histogram. We repeat this 1000 times to obtain uncertainties on the values of the bins, which are shown as the lines on the bars in Fig. 10.

As a result of the transient nature of the source, many are only observed by *PCA* after they have already transited into the soft state because of an extremely rapid rise through the hard state. Therefore

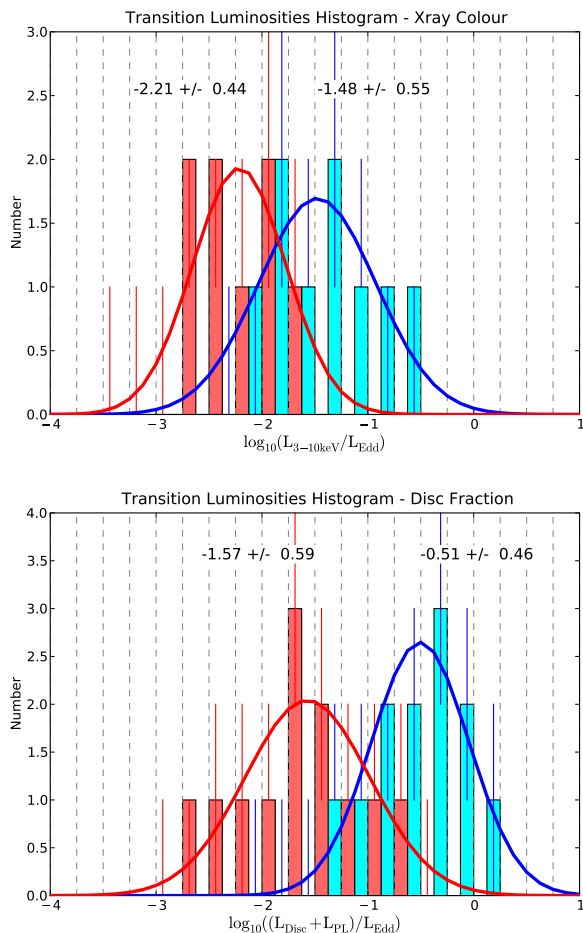


Figure 10. Histograms showing the transition luminosities for the outward (blue) and return (red) transitions in the HLD and DFLDs for the outburst where this can be clearly done. The lines on the bars show the uncertainties in the values of the bars as determined by our Monte Carlo routine. The best fit gaussian distributions are shown on top of the histograms. TOP: transitions from the X-ray colour, BOTTOM: from the disc fraction. Note that the luminosities on the x -axis are calculated in different ways.

the hard-to-soft transition has been missed. In order to fairly compare the distributions of the luminosities where the transitions occur we show the distributions of only those transitions where both the egress from- and ingress back into the hard state are determined.

In Fig. 10 we show the distributions using both the powerlaw fraction and the X-ray colour as a marker of the transitions. We also show the best fit gaussian distributions on top of the histograms. The X-ray colour transitions occur at lower values of L_{Edd} than those for the disc fraction as the former are calculated from the 3 – 10 keV luminosity rather than the total X-ray luminosity. The two distributions of the transition luminosities overlap though the peaks are distinct in both the X-ray colour and disc fraction calculations.

The best fit values to the distributions of the transitions are shown on Fig. 10. Using the disc fraction to determine the transitions shows that most of the transitions from the powerlaw dominated to the disc dominated state occur between 3 and 100 per cent L_{Edd} . The luminosities of the transitions from the disc dominated to the powerlaw dominated states occur between 0.5 and 10 per cent L_{Edd} .

Kalemci (2002) compared their powerlaw ratio (PLR, the ratio of the powerlaw to total flux in 3 – 25 keV band) to changes in the timing behaviour for a number of black hole binaries. The changes in short timescale timing behaviour e.g. the level of the total rms noise, and the frequency of any quasi-periodical oscillations (QPOs) are frequently used to determine an accurate transition date between states (van der Klis 2006). The value for their PLR is around 0.6 at the time of the transition as determined from timing analysis. We construct this PLR for a number of our data points. Comparing the two ratios, a value for the PLR of around 0.6 corresponds to a range in powerlaw fraction of 0.4 to 0.6.

The Powerlaw Fraction presented here has a wider energy band, using values of 0.8 to determine the luminosity at the transition is likely to not be too distant from the true transition point as determined from changes in the timing properties (see above). Depending on the observation rate, there may be a large uncertainty as to whether the luminosity taken as the transition luminosity is close to the true value. When the transition from the hard state into the soft state is not clearly observed, then it is not clear exactly which observations’ luminosity is closest to the one at transition. Given the uncertainties in the masses and distances, the fact that the transitions are not at a constant luminosity in some sources or the poor sampling, both of which result in an inaccurate transition luminosity only contribute to the uncertainties, rather than being the overriding ones. Further analysis is required to determine the disc fraction at state transition, and from these extract the luminosities.

In a study of 10 Neutron and Black Hole X-ray binaries, Maccarone (2003) found that most of the Soft-to-Hard transitions occurred between 1 and 4 per cent of L_{Edd} , with a few source’s transitions occurring at lower luminosities. They also found that the distribution of the Soft-to-Hard transitions was narrower than that of the Hard-to-Soft. In Fig. 10, the Soft-to-Hard transition luminosities calculated using the X-ray colour and also when calculated using the disc fraction have the same width as the Hard-to-Soft transition luminosities. In all cases, the distributions have been equally affected by broadening caused by the uncertainties in the distances and masses of the BHXRBS, so there should still be a difference in the widths of the distributions.

From Figs. 9 and 10 the peak luminosities and the Hard-to-Soft transition luminosities appear to occur at the same Eddington fraction. We show in Fig. 11 the relation between these two luminosities. Only 15 outbursts have a Hard-to-Soft (powerlaw dominated to disc dominated) transitions determined from the method outlined above, and most do seem to track (within a factor of three) the one-to-one relation. Some from 4U 1630+47 are low, but this BHXRBS has a very complex outburst sequence and some of these may not be true outbursts; and also one each from GRO J1655-40 and XTE J1550-564, both of which have strong Very High States. We note that the luminosities that we extract for the transition luminosity may not be the same as that determined using the timing properties of the BHXRBS, but they are reasonably close. There are only a few BHXRBS (8) and they cover only just over an order of magnitude in luminosity but the similarity of the peak and transition luminosities is intriguing. When using the X-ray colour to determine the transitions, the peak luminosity is more likely to occur during the transition itself.

8 RADIO

Some of the BHXRBS studied here have been the subject of intensive radio observations during one or more of their outbursts.

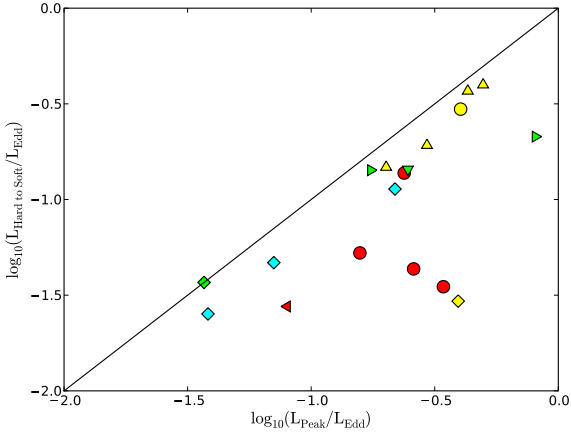


Figure 11. The luminosity at the Hard to Soft transition as a function of the peak luminosity of the outburst. The solid line shows the one-to-one relation.

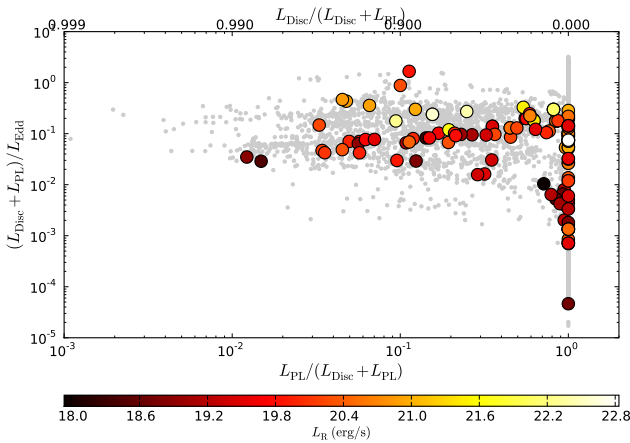


Figure 13. The DLFD with the observations which were coincident with 8.4 GHz radio observations highlighted, showing their radio luminosities.

This data comes from a variety of instruments and at a number of frequencies. A detailed and comprehensive study on the radio emission from the BHXRBs is presented in Fender et al. (2009).

We select coincident radio observations by allowing a difference of up to two days between the X-ray and the radio observation. We also allow for upper limits to be linked to X-ray observations where they are reported. Both detections and upper limits are listed in Table 4. Although there are most observations at 15 GHz (mainly from XTE J1859+226 from Brocksopp et al. 2002), the observations at 8.4 and 5 GHz are more useful as they span a wider number of binaries.

Studies of the radio luminosity of GX 339-4 by Corbel et al. (2000, 2003) showed that in the hard state the radio and the X-ray fluxes are related in a non-linear way. Using a larger sample of black hole X-ray binaries Gallo et al. (2003) showed this relation to apply to essentially all binaries. Shortly thereafter this relation was extended to AGN by Merloni et al. (2003); Falcke et al. (2004) independently. This fundamental plane of black hole activity includes the mass of the black hole as

$$L_{\text{radio}} \propto L_{\text{X-ray}}^{0.6} M^{0.7}.$$

This relation is applicable to BHXRBs in their hard state. Using the disc fraction to restrict which points to plot is in this case problematic. Choosing radio observations taken in the powerlaw dominated state would include hard state observations, but also hard-intermediate states. However, Fender et al. (2004) show that the radio flares tend to occur on the transition between the soft and hard states. We therefore do select the radio observations from the powerlaw dominated state only.

As our sample covers a relatively small range in L_{radio} , $L_{\text{X-ray}}$ and M rather than try and obtain the best fit for the fundamental plane, we plot a projection of the best fit plane parameters as obtained from larger samples across a wide range of black hole masses in Fig. 12. We have plotted points from a number of radio frequencies on the same diagram in the assumption that the spectral index¹⁰, $\alpha = 0.0$. This was done to increase the number of points on the diagram, and the assumption of $\alpha = 0.0$ is reasonable as the jet should be self-absorbed in the powerlaw state. There is a large scatter around the expected relation, however with the uncertainties in the masses and distances of the black holes this is expected. The high radio luminosity points from SAX J1819.3-2525 is that from the exceptional radio flare reported in Rupen et al. (2003b), the like of which has not been observed since from any other system. The radio observations of GX 339-4 clearly follow the fundamental plane relation. For most of the other objects the variation in X-ray and/or radio luminosity is too limited to determine any result. The uncertainties in the masses and distances effect the clarity of any underlying relation across this very small sample.

The development of the fundamental plane built on earlier investigations into a correlation between the radio and X-ray luminosities of the BHXRBs in the hard state. In Fig. 12 we also show the correlation between L_{radio} and $L_{\text{X-ray}}$ as shown for GX 339-4 by e.g. Corbel et al. (2000, 2003)

$$L_{\text{radio}} \propto L_{\text{X-ray}}^{0.7}.$$

As the masses for many objects are not well determined, and are very similar, this correlation is as clear as the fundamental plane, but the error bars are much reduced. In this case the considerable scatter still remains even though there are few parameters which are uncertain.

On first sight, the radio/X-ray correlation of our sources is not very tight. However, this is mainly do to our statistical approach. In Fig. 12 we show all observations, which do have a radio detection and have a powerlaw fraction above 0.9. While this selects mainly hard state observations, it cannot take peculiarities into account. For example, SAX J1819.3-2525 has nearly always a powerlaw fraction of around 1 (see Appendix, Fig. A.2), but the observed radio emission originates in an optically thin flare Rupen et al. (2003a). As the radio emission therefore does not originate in an optically thick compact jet it should not follow the radio/X-ray correlation found for hard state XRBs. Also GRO J1655-40 shows some points far away from the correlation. These points correspond to a time shortly after the state transition, where the compact jet is just restarting. For restarting jets see e.g., Russell et al. (2007); Fender et al. (2009). This explains the 'inverted dependency' (lower X-ray luminosities show higher radio fluxes) of those points. In fact, detailed inspection of most outlying points indicate that the radio emission does not originate in a compact jet. In addition the correlation shown here combines several radio frequencies to obtain enough data-points. The necessary

¹⁰ We define the radio spectral index as $S_\nu \propto \nu^\alpha$.

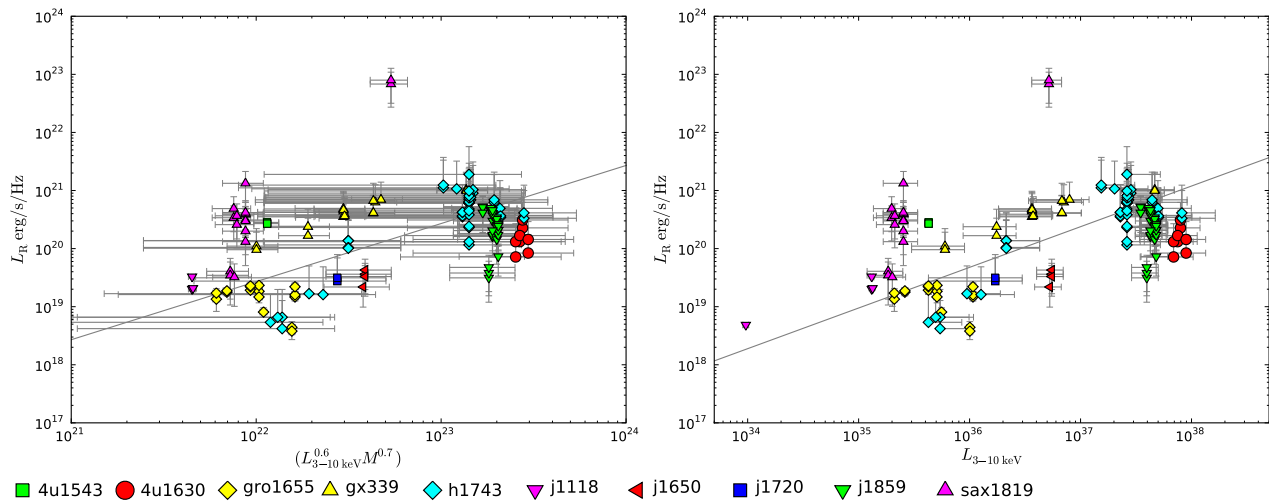


Figure 12. The fundamental plane and radio-X-ray correlation for the radio observations and objects presented in this work at a radio frequencies of 8.4, 5.0 and 1.5 GHz assuming a spectral index, $\alpha = 0.0$. We restrict the observations to those with a Powerlaw Fraction > 0.9 - the powerlaw dominated state. The error bars are derived both from the uncertainties in the fluxes/flux densities measured, as well as in the distances and masses of the black holes themselves. LEFT: We show fundamental plane for the radio observations, including the masses of the black holes, where they are available. The line is not a fit, but to guide the eye as to where the relation would lie from Merloni et al. (2003) indicating where $L_{\text{radio}} \propto L_{\text{X-ray}}^{0.6} M^{0.8}$ would lie. RIGHT: The radio-X-ray luminosity correlation as shown in e.g. Corbel et al. (2003) of $L_{\text{radio}} \propto L_{\text{X-ray}}^{0.7}$. The line is also not a fit, but a guide to the eye as to where the relation would lie.

extrapolation further increases the scatter around the intrinsic correlation. As the radio/X-ray correlation is not a central theme here and one would need careful inspection of each observation, we do not proceed further in this analysis.

We also show the 8.4 GHz radio luminosity as a function of position on the DFLD (Fig. 13). The radio luminosity from an BHXRBB peaks (sometimes with an extremely bright radio flare) during the transition from the powerlaw to the disc dominated state, as seen on an HID. Showing the data on a DFLD compresses the hard-intermediate state onto the powerlaw dominated branch and so the radio flare is expected to be seen at the top of the “stalk” of the DFLD. However, as not every object is observed in the radio, not every radio flare is observed, and, from Section 7, the transitions from the powerlaw dominated to the disc dominated state do not occur at very similar total luminosities, the distribution is not very clear in Fig. 12.

9 DISCUSSION

We have completed a complete and comprehensive analysis of a large fraction of the publicly available data on low mass black hole X-ray binaries present in the *RXTE* archive. Using the best fitting of one of three simple models for the continuum emission we have been able to investigate the global properties of the BHXRBB outbursts.

9.1 Diagnostic Diagrams

In the study of the global properties of the outbursts of BHXRBBs we have presented two diagnostic diagrams, the Hardness-Luminosity Diagram and the Disc Fraction Luminosity Diagram. These two diagrams are both useful when studying BHXRBBs but are best suited to different aspects of the investigations.

The HLD is a simple diagram to construct, requiring in the simplest case only the ratio of the detected counts in two bands. This means that it can be quickly constructed to follow an in-progress outburst, but will also work for short observations or faint sources or states, when the number of counts is low and reliable spectral studies are difficult. However, by only using the detected counts, the X-ray colours determined are affected by any absorption along the line of sight. This makes comparing the behaviour between sources non-trivial, as each BHXRBB has a different N_{H} column.

The DFLD returns more physical information on the parameters of the XRB system, within the limitations of the models fitted. With the simple set of models fitted in our analysis presented in this paper, the behaviour and variation of the powerlaw and the disc throughout the outburst can easily be traced. The result of the analysis, if not the diagram, returns more information than the HLD. However, the requirement to fit spectra and determine model parameters limits the type of observations which can be investigated, ruling out low counts (short or faint) observations.

The limitations of the *RXTE* satellite also restrict the usefulness of the DFLD in the study of the powerlaw and intermediate states (as identified from the HLD). The lack of low energy sensitivity means that the detection of non-dominant discs is not always successful. This compresses a large fraction of the intermediate states on top of the hard states (without any disc). However, as the disc parameters are extracted from the model fits to the spectra, the investigation into the the disc parameters and their behaviour throughout the BHXRBB outbursts is more accurate (to be presented in a forthcoming paper).

As spectral models are fit to the observations, the effects of the absorption column can be removed, allowing for an easier comparison between sources. This allows the variation of the BHXRBB population to be easily studied. However the compression of the intermediate states onto the powerlaw dominated “stalk” means that

Table 4. RADIO DATA

Object	Number of observations					Reference
	15 GHz	8.4 GHz	5 GHz	2.3 GHz	1.5 GHz	
4U 1543-47		2	2		2	(1,2)
4U 1630-47		20	22			(3)
4U 1957+115						-
GRO J1655-40		10	15		3	(4,5,6,7,8,9,10,11,12,13)
GRS 1737-31						-
GRS 1739-278						-
GRS 1758-258						(14)
GS 1354-644						-
GS 2023+338						-
GX 339-4		17	15	1	3	(15,16)
H 1743-322	7	59	44		23	(17,18,19,20,21,22,23,24,25)
XTE J1118+480	30	2	2			(26,27,28,29,30,31,32 ¹)
XTE J1550-564						-
XTE J1650-500		5	5	2	2	(33)
XTE J1720-318		8	9			(34)
XTE J1748-288		8	12	5	6	(35,36,37)
XTE J1755-324						(38)
XTE J1817-330		1	3		1	(39,40)
XTE J1859+226	225	27	21	5	90	(41)
XTE J2012+381	2	1	2		2	(42,43,44)
LMC X1						-
LMC X3		1				(45)
SAX 1711.6-3808						-
SAX 1819.3-2525		11	7			(46,47,48,49,50,51,52)
SLX 1746-331						-
Totals	264	171	160	13	132	

The number of radio observations which were taken within 2 days of an X-ray observation. In some cases radio observations have been found, but none were taken within 2 days of an X-ray observation.

(1) Park et al. (2004), (2) Kalemci et al. (2005), (3) Hjellming et al. (1999), (4) Hunstead & Campbell-Wilson (1996), (5) Rupen et al. (2005e), (6) Rupen et al. (2005l), (7) Rupen et al. (2005i), (8) Rupen et al. (2005a), (9) Rupen et al. (2005j), (10) Rupen et al. (2005h), (11) Rupen et al. (2005f), (12) Rupen et al. (2005d), (13) Brocksopp et al. (2005c), (14) Lin et al. (2000), (15) Corbel et al. (2000), (16) Gallo et al. (2004), (17) McClintock et al. (2007), (18) Rupen et al. (2003c), (19) Rupen et al. (2004a), (20) Rupen et al. (2004e), (21) Rupen et al. (2005k), (22) Corbel & Tzioumis (2008), (23) Rupen et al. (2008a), (24) Kalemci et al. (2008), (25) Rupen et al. (2008b), (26) Pooley (2005), (27) Rupen et al. (2005b), (28) Angelakis & Kraus (2005), (29) Rupen et al. (2005g), (30) Rupen et al. (2005c), (31) McClintock et al. (2001), (32) Pooley (2001), (33) Corbel et al. (2004), (34) Brocksopp et al. (2005b), (35) Brocksopp et al. (2007), (36) Hjellming et al. (1998a), (37) Strohmayer et al. (1998), (38) Ogley et al. (1997), (39) Rupen et al. (2006b), (40) Rupen et al. (2006a), (41) Brocksopp et al. (2002), (42) Pooley (1998), (43) Wagner et al. (1998), (44) Hynes et al. (1998b), (45) Gallo & Tzioumis (2007), (46) Hjellming (2000), (47) Tomsick et al. (2002), (48) Rupen et al. (2003b), (49) Rupen et al. (2003a), (50) Rupen et al. (2004d), (51) Rupen et al. (2004b), (52) Rupen et al. (2004c). ¹ We thank Guy Pooley for providing the radio data on XTE J1118+480.

the HLD is more useful for studying an individual source or outburst, whereas the DFLD is useful for studying the outburst evolution for a population of BHXRBs.

The *RXTE* satellite is currently the only instrument which allows the work done in this study to be carried out. The large archive contains a large number of observations of a wide variety of sources. The coverage at high energies is vital for constraining the slope of the powerlaw emission in the soft state, where the disc emission dominates the signal from the *PCA*. However, the limited low energy coverage is not ideal as it does not allow accurate fitting of the disc properties when the disc does not completely dominate the low-energy spectrum. Also the N_{H} cannot be determined from the observations themselves and we are reliant on values from more detailed studies.

Until an observatory with a greater sensitivity and wider (at least at the low energy end) spectral coverage has created an archive of observations to match those from *RXTE* presented here, the combination of both the Disc Fraction information and the X-ray colour may be necessary to fully determine the state of the BHXRB. AS-

TROSAT¹¹ and MAXI¹² fit these specifications and hopefully over time will build up the archive required. This increase in the low energy sensitivity should allow the disc to be fit in cases where it is not dominant, therefore allowing the intermediate states to be investigated by the DFLD.

The individual DFLDs for the BHXRBs show a great deal of similarity between each other - which is then reflected in the combined DFLD in Section 5.2. All BHXRBs where the outbursts are well sampled and not “messy” show the simultaneous change in disc fraction and luminosity on the return to the hard powerlaw dominated state at the end of an outburst, moving diagonally in the DFLD. Their equivalent motion in the HLD tends to be horizontally during the transition to the hard state.

A number of BHXRBs also show this diagonal motion in the DFLD at the start of their outbursts - GX 339-4 is a notable exception. These two trends indicate that, whereas in most HLDs

¹¹ <http://meghnad.iucaa.ernet.in/~astrosat/>

¹² <http://kibo.jaxa.jp/en/experiment/ef/maxi/>

the transitions to the soft state are at a constant luminosity and very quick, the DFLD compresses these intermediate states into the powerlaw dominated state. Only the softest states exhibit a powerlaw fraction < 1 , and so the decay through the disc dominated state is clearly seen in the DFLD. The most disc dominated states appear mid-way through the outburst, rather than at the highest luminosity disc dominated states. This may result from the limitations of the DISKBB model outlined in Section 3.

9.2 Outbursts

We used an initial version of the results to identify periods when the XRBs were in outburst. Given the range in outburst forms and shapes in the HLD and DFLD this allowed the restriction of the ranges in which to search for transitions and peak luminosities. There are only a few objects which have periods when it is not exceedingly clear where to split up the light curve.

In Fig. A.1, many of the outbursts show a hardening after the first excursion into the disc dominated state, which is sometimes associated with an increase in luminosity (see also Casella et al. 2004; Kubota & Done 2004; Belloni et al. 2005, 2006; Dunn et al. 2008). If the increase in luminosity occurs, then in some cases the track in the DFLD is the same - there is no hysteresis. In others the luminosity does not rise, or even continues to fall during the excursion towards the hard state. The cause of this excursion is not clear.

The relative variation of the luminosities of the powerlaw and disc components determine whether the excursion runs along the same track. In Fig. 14 we show the relative variation of these luminosities. Where the powerlaw and disc luminosities are approximately equal at the beginning of the outburst, the result will be overlapping tracks in the DFLD (GRO J1655-40, H 1743-322 and XTE J1859+226). These all occur before the powerlaw luminosity falls drastically away from the disc luminosity once the BHXRb is fully in the disc dominated state, and therefore are in the transition stage across to the disc dominated state, and possibly indicative of a very high state.

If the powerlaw luminosity increases mid-outburst, with little change in the disc luminosity (4U 1543-47, GX 339-4 and XTE J1859+226) then the behaviour is different. Depending on the rate of decay of the disc, the total luminosity decline slows or even temporarily reverses. The powerlaw fraction increases, but the track of the BHXRb through the DFLD does not lie on the track of the entry into the disc dominated state.

Although distributions of the transition luminosities, as shown in Fig. 10, are easily determined, it is difficult to conclude whether the distribution for one transition is broader than the other or not. When using the X-ray colour to determine the transitions, the Hard-to-Soft transition luminosity distribution is broader than the Soft-to-Hard transition luminosity distribution. However, when using the disc fraction, the two distributions are almost equally broad. There are 8 outbursts in the X-ray colour and 11 outbursts in the disc fraction plots¹³. Given these relatively small numbers of transitions and the fact that differences in the distribution widths are not present in both methods of calculation, we cannot say whether our calculations support the work of Maccarone (2003) or not. Future determinations of the transitions (from e.g. timing analysis) and

improved measurements of the distances and masses will allow a more detailed analysis.

10 CONCLUSIONS

We have performed a consistent spectral analysis on a large sample of well known black hole X-ray binaries. Using a set of simple models we fit the spectra to study the evolution of the outbursts. Two standard diagnostic diagrams show that the level of similarity between the outbursts is very high. Further improvements in the overlap and the comparison of the sources will result with more accurately determined distances and masses. A critical analysis of the two diagrams shows that for individual sources or outbursts, the HLD is best suited, being able to separate the different states (even if not being able to identify them). The DFLD, being independent from the effect of N_H and a more physical description of the characteristics of the system, is more useful when studying the population as a whole. However, currently the spectral limitations of the *RXTE* satellite restrict the diagnostic ability of the DFLD to the soft state. The overlap in the DFLD is very striking, indicating that in at least the states where the disc is strongest, the BHXRb behave in a very similar way.

The rates of motion through the DFLD show surprising uniformity, however currently this only reflects the motion through the soft state, rather than at the true transition periods. There is a region of increased rate of motion on the transition between the disc dominated and the powerlaw dominated states, and another on the lower luminosity part of the disc dominated states. Using the change in the disc fraction, as well as the X-ray colour, we determine the dates and luminosities of the transitions to- and from the soft or disc dominated states. The distributions of these luminosities are both broad and overlap. However, the uncertainty in the masses and especially distances comes through to this analysis and we are not able to clearly say whether one distribution is significantly broader than the other, especially as there are only a comparatively small number of outbursts which show both transitions.

We investigate the location of the radio emission on top of the global DFLD. However, the very different observation rate make it difficult to determine if there is any pattern from this analysis alone. The small range in black hole masses also limits our ability to study the $L_X - L_R$ correlation.

ACKNOWLEDGEMENTS

RJHD acknowledges support from the Alexander von Humboldt Foundation. EGK acknowledges funding from a Marie Curie Intra-European fellowship under contract Nr. MEIF-CT-2006-024668. TMB acknowledges support ASI via contract I/088/06/0 and thanks the International Space Science Institute (ISSI). This research was supported by the DFG cluster of excellence Origin and Structure of the Universe (www.universe-cluster.de). We thank the anonymous referee and Andrea Merloni for suggestions which improved this manuscript and Guy Pooley for the radio data for XTE J1118+480. This research has made use of data obtained through the High Energy Astrophysics Science Archive Research Center Online Service, provided by the NASA/Goddard Space Flight Center.

¹³ These have been blurred by the Monte-Carlo process used to determine the uncertainties on the distributions.

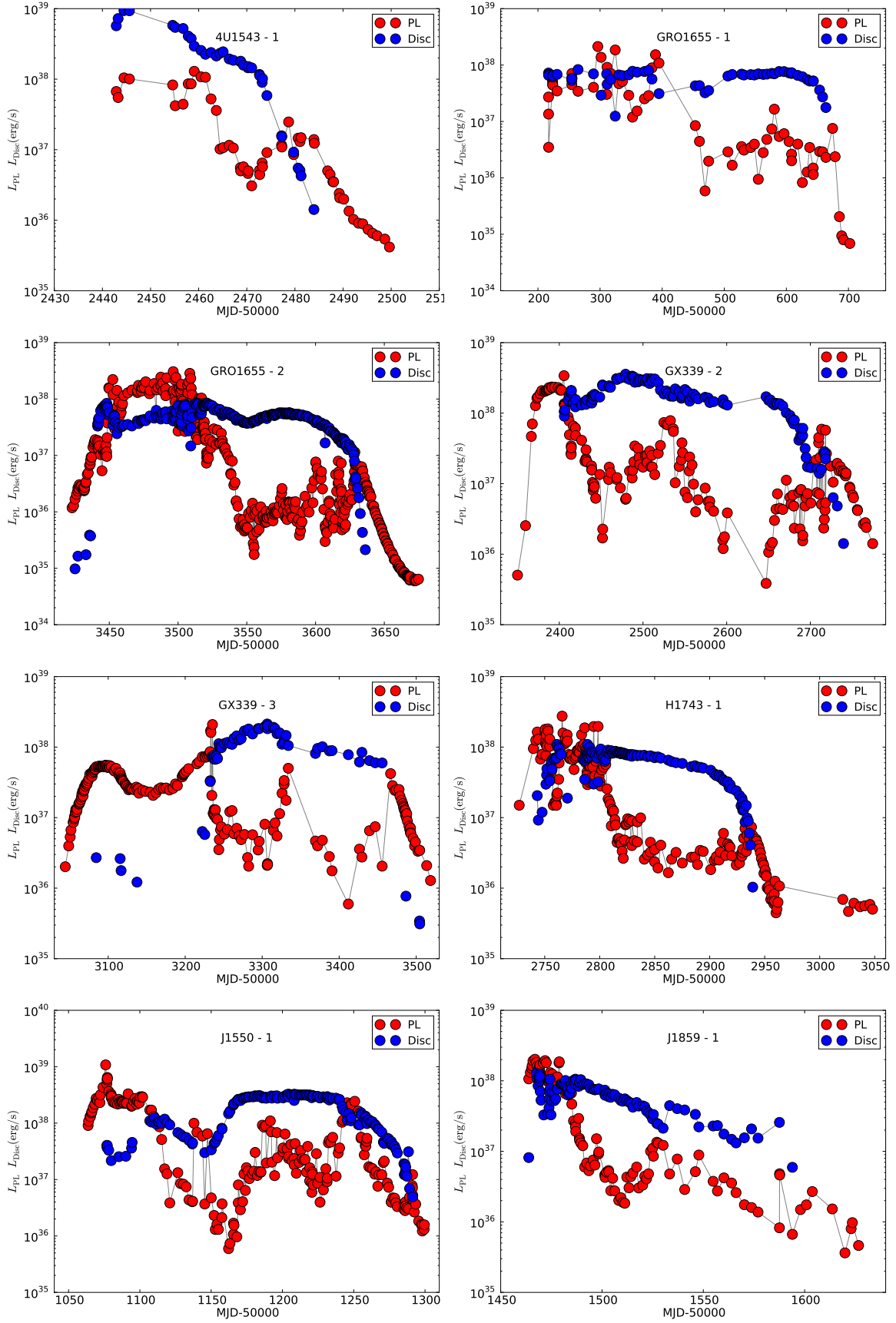


Figure 14. The powerlaw and disc luminosity curves through eight of the outbursts covered in this work.

REFERENCES

- Adelman-McCarthy J. K., Agüeros M. A., Allam S. S., Allende Prieto C., Anderson K. S. J., Anderson S. F., et al., 2008, *ApJS*, 175, 297
- Angelakis E., Kraus A., 2005, *ATel*, 400, 1
- Arnaud K. A., 1996, in *ASP Conf. Ser. 101: Astronomical Data Analysis Software and Systems V*, Jacoby G. H., Barnes J., eds., p. 17
- Augusteijn T., Kuulkers E., van Kerkwijk M. H., 2001, *A&A*, 375, 447
- Belloni T., 2004, *Nuclear Physics B Proceedings Supplements*, 132, 337
- Belloni T., Homan J., Casella P., van der Klis M., Nespoli E., Lewin W. H. G., Miller J. M., Méndez M., 2005, *A&A*, 440, 207
- Belloni T., Parolin I., Del Santo M., Homan J., Casella P., Fender R. P., Lewin W. H. G., Méndez M., Miller J. M., van der Klis M., 2006, *MNRAS*, 367, 1113
- Belloni T. M., 2009, 0909.2474
- Brocksopp C., Bandyopadhyay R. M., Fender R. P., 2004, *New Astronomy*, 9, 249
- Brocksopp C., Corbel S., Fender R. P., Rupen M., Sault R., Tingay S. J., Hannikainen D., O'Brien K., 2005a, *MNRAS*, 356, 125
- , 2005b, *MNRAS*, 356, 125
- Brocksopp C., Corbel S., Rupen M., Sault B., Tzioumis T., Dhawan V., Mioduszewski A., Cimo G., Fender R., 2005c, *ATel*, 612, 1
- Brocksopp C., Fender R. P., McCollough M., Pooley G. G., Rupen M. P., Hjellming R. M., de la Force C. J., Spencer R. E., Muxlow T. W. B., Garrington S. T., Trushkin S., 2002, *MNRAS*, 331, 765
- Brocksopp C., McGowan K. E., Krimm H., Godet O., Roming P., Mason K. O., Gehrels N., Still M., Page K., Moretti A., Shrader C. R., Campana S., Kennea J., 2006, *MNRAS*, 365, 1203
- Brocksopp C., Miller-Jones J. C. A., Fender R. P., Stappers B. W., 2007, *MNRAS*, 378, 1111
- Cabanac C., Fender R. P., Dunn R. J. H., Koerding E. G., 2009, *MNRAS*, 396, 1415
- Cadolle Bel M., Rodriguez J., Sizun P., Farinelli R., Del Santo M., Goldwurm A., Goldoni P., Corbel S., Parmar A. N., Kuulkers E., Ubertini P., Capitanio F., Roques J.-P., Frontera F., Amati L., Westergaard N. J., 2004, *A&A*, 426, 659
- Campana S., Stella L., Belloni T., Israel G. L., Santangelo A., Frontera F., Orlandini M., Dal Fiume D., 2002, *A&A*, 384, 163
- Capitanio F., Belloni T., Del Santo M., Ubertini P., 2009, *MNRAS*, 398, 1194
- Capitanio F., Ubertini P., Bazzano A., Kretschmar P., Zdziarski A. A., Joinet A., Barlow E. J., Bird A. J., Dean A. J., Jourdain E., De Cesare G., Del Santo M., Natalucci L., Cadolle Bel M., Goldwurm A., 2005, *ApJ*, 622, 503
- Casares J., Zurita C., Shahbaz T., Charles P. A., Fender R. P., 2004, *ApJ*, 613, L133
- Casella P., Belloni T., Homan J., Stella L., 2004, *A&A*, 426, 587
- Chaty S., Haswell C. A., Malzac J., Hynes R. I., Shrader C. R., Cui W., 2003, *MNRAS*, 346, 689
- Chen W., Shrader C. R., Livio M., 1997, *ApJ*, 491, 312
- Corbel S., Fender R. P., Tomsick J. A., Tzioumis A. K., Tingay S., 2004, *ApJ*, 617, 1272
- Corbel S., Fender R. P., Tzioumis A. K., Nowak M., McIntyre V., Durouchoux P., Sood R., 2000, *A&A*, 359, 251
- Corbel S., Nowak M. A., Fender R. P., Tzioumis A. K., Markoff S., 2003, *A&A*, 400, 1007
- Corbel S., Tzioumis A., 2008, *ATel*, 1349, 1
- Cowley A. P., Crampton D., Hutchings J. B., Remillard R., Penfold J. E., 1983, *ApJ*, 272, 118
- Cui W., Heindl W. A., Swank J. H., Smith D. M., Morgan E. H., Remillard R., Marshall F. E., 1997, *ApJ*, 487, L73+
- Debnath D., Chakrabarti S. K., Nandi A., Mandal S., 2008, *Bulletin of the Astronomical Society of India*, 36, 151
- di Benedetto G. P., 1997, *ApJ*, 486, 60
- Done C., Gierliński M., 2003, *MNRAS*, 342, 1041
- Done C., Gierliński M., Kubota A., 2007, *The Astronomy and Astrophysics Review*, 15, 1
- Dunn R. J. H., Fender R. P., Körding E. G., Cabanac C., Belloni T., 2008, *MNRAS*, 387, 545
- Falcke H., Körding E., Markoff S., 2004, *A&A*, 414, 895
- Fender R., Corbel S., Tzioumis T., McIntyre V., Campbell-Wilson D., Nowak M., Sood R., Hunstead R., Harmon A., Durouchoux P., Heindl W., 1999, *ApJ*, 519, L165
- Fender R. P., 2009, 0909.2572
- Fender R. P., Belloni T. M., Gallo E., 2004, *MNRAS*, 355, 1105
- Fender R. P., Homan J., Belloni T. M., 2009, 0903.5166
- Foellmi C., 2009, *New Astronomy*, 14, 674
- Gallo E., 2009, 0909.585
- Gallo E., Corbel S., Fender R. P., Maccarone T. J., Tzioumis A. K., 2004, *MNRAS*, 347, L52
- Gallo E., Fender R. P., Pooley G. G., 2003, *MNRAS*, 344, 60
- Gallo E., Tzioumis T., 2007, *ATel*, 1138, 1
- Gelino D. M., Balman Ş., Kızıloğlu Ü., Yılmaz A., Kalemci E., Tomsick J. A., 2006, *ApJ*, 642, 438
- Gierliński M., Done C., 2003, *MNRAS*, 342, 1083
- Gierliński M., Done C., Page K., 2008, *MNRAS*, 388, 753
- Gierliński M., Maciołek-Niedźwiecki A., Ebisawa K., 2001, *MNRAS*, 325, 1253
- Gierliński M., Newton J., 2006, *MNRAS*, 370, 837
- Gilfanov M., 2004, *MNRAS*, 349, 146
- , 2009, 0909.2567
- Greiner J., Dennerl K., Predehl P., 1996, *A&A*, 314, L21
- Grimm H.-J., Gilfanov M., Sunyaev R., 2003, *MNRAS*, 339, 793
- Haardt F., Galli M. R., Treves A., Chiappetti L., Dal Fiume D., Corongiu A., Belloni T., Frontera F., Kuulkers E., Stella L., 2001, *ApJS*, 133, 187
- Heinz S., Grimm H. J., 2005, *ApJ*, 633, 384
- Heinz S., Grimm H. J., Sunyaev R. A., Fender R. P., 2008, *ApJ*, 686, 1145
- Hjellming R. M., 2000, *ATel*, 61, 1
- Hjellming R. M., Rupen M. P., 1995, *Nature*, 375, 464
- Hjellming R. M., Rupen M. P., Ghigo F., Waltman E. B., Mioduszewski A. J., Fender R. P., Stappers B. W., Wieringa M., Wark R., Green D. W. E., 1998a, *IAU Circular*, 6937, 1
- Hjellming R. M., Rupen M. P., Mioduszewski A. J., Kuulkers E., McCollough M., Harmon B. A., Buxton M., Sood R., Tzioumis A., Rayner D., Dieters S., Durouchoux P., 1999, *ApJ*, 514, 383
- Hjellming R. M., Rupen M. P., Mioduszewski A. J., Smith D. A., Harmon B. A., Waltman E. B., Ghigo F. D., Pooley G. G., 1998b, in *Bulletin of the American Astronomical Society*, Vol. 30, *Bulletin of the American Astronomical Society*, pp. 1405—+
- Homan J., Belloni T., 2005, *APSS*, 300, 107
- Homan J., Wijnands R., Kong A., Miller J. M., Rossi S., Belloni T., Lewin W. H. G., 2006, *MNRAS*, 366, 235
- Homan J., Wijnands R., van der Klis M., Belloni T., van Paradijs J., Klein-Wolt M., Fender R., Méndez M., 2001, *ApJS*, 132, 377
- Hunstead R., Campbell-Wilson D., 1996, *IAU Circular*, 6410, 3

- Hutchings J. B., Crampton D., Cowley A. P., Bianchi L., Thompson I. B., 1987, *AJ*, 94, 340
- Hutchings J. B., Winter K., Cowley A. P., Schmidtke P. C., Crampton D., 2003, *AJ*, 126, 2368
- Hynes R. I., Haswell C. A., Chaty S., Shrader C. R., Cui W., 2002, *MNRAS*, 331, 169
- Hynes R. I., Haswell C. A., Shrader C. R., Chen W., Horne K., Harlaftis E. T., O'Brien K., Hellier C., Fender R. P., 1998a, *MNRAS*, 300, 64
- Hynes R. I., Roche P., Walton N., Hjellming R. M., Rupen M. P., Mioduszewski A. J., 1998b, *IAU Circular*, 6932, 2
- Hynes R. I., Steeghs D., Casares J., Charles P. A., O'Brien K., 2003, *ApJ*, 583, L95
- in't Zand J. J. M., Kuulkers E., Bazzano A., Cornelisse R., Cocchi M., Heise J., Muller J. M., Natalucci L., Smith M. J. S., Ubertini P., 2000, *A&A*, 357, 520
- in't Zand J. J. M., Markwardt C. B., Bazzano A., Cocchi M., Cornelisse R., Heise J., Kuulkers E., Natalucci L., Santos-Lleo M., Swank J., Ubertini P., 2002, *A&A*, 390, 597
- Jonker P. G., Nelemans G., 2004, *MNRAS*, 354, 355
- Kalemci E., 2002, PhD thesis, University of California, San Diego
- Kalemci E., Tomsick J. A., Buxton M. M., Rothschild R. E., Pottschmidt K., Corbel S., Brocksopp C., Kaaret P., 2005, *ApJ*, 622, 508
- Kalemci E., Tomsick J. A., Corbel S., Tzioumis T., 2008, *ATel*, 1378, 1
- Kalemci E., Tomsick J. A., Rothschild R. E., Pottschmidt K., Corbel S., Kaaret P., 2006, *ApJ*, 639, 340
- Kalemci E., Tomsick J. A., Rothschild R. E., Pottschmidt K., Kaaret P., 2004, *ApJ*, 603, 231
- King A. R., Ritter H., 1998, *MNRAS*, 293, L42
- Kitamoto S., Tsunemi H., Pedersen H., Ilovaisky S. A., van der Klis M., 1990, *ApJ*, 361, 590
- Körding E. G., Jester S., Fender R., 2006, *MNRAS*, 372, 1366
- , 2008, *MNRAS*, 383, 277
- Kotani T., Kawai N., Nagase F., Namiki M., Sakano M., Takeshima T., Ueda Y., Yamaoka K., Hjellming R. M., 2000, *ApJ*, 543, L133
- Kubota A., Done C., 2004, *MNRAS*, 353, 980
- Lin D., Smith I. A., Liang E. P., Bridgman T., Smith D. M., Martí J., Durouchoux P., Mirabel I. F., Rodríguez L. F., 2000, *ApJ*, 532, 548
- Maccarone T. J., 2003, *A&A*, 409, 697
- Maitra D., Bailyn C. D., 2006, *ApJ*, 637, 992
- Markoff S., 2009, 0909.2574
- McClintock J. E., Haswell C. A., Garcia M. R., Drake J. J., Hynes R. I., Marshall H. L., Muno M. P., Chaty S., Garnavich P. M., Groot P. J., Lewin W. H. G., Mauche C. W., Miller J. M., Pooley G. G., Shrader C. R., Vrtilik S. D., 2001, *ApJ*, 555, 477
- McClintock J. E., Remillard R. A., Rupen M. P., Torres M. A. P., Steeghs D., Levine A. M., Orosz J. A., 2007, 0705.1034
- Merloni A., Heinz S., 2008, *MNRAS*, 388, 1011
- Merloni A., Heinz S., di Matteo T., 2003, *MNRAS*, 345, 1057
- , 2005, *APSS*, 300, 45
- Miller J. M., Fabian A. C., Reynolds C. S., Nowak M. A., Homan J., Freyberg M. J., Ehle M., Belloni T., Wijnands R., van der Klis M., Charles P. A., Lewin W. H. G., 2004, *ApJ*, 606, L131
- Miller J. M., Wijnands R., Homan J., Belloni T., Pooley D., Corbel S., Kouveliotou C., van der Klis M., Lewin W. H. G., 2001, *ApJ*, 563, 928
- Miniutti G., Fabian A. C., Miller J. M., 2004, *MNRAS*, 351, 466
- Nowak M., Juett A., Homan J., Yao Y., Wilms J., Schulz N., Canizares C., 2008, in *AAS-High Energy Astrophysics Division*, Vol. 10, *AAS-High Energy Astrophysics Division*, pp. 14.04–
- Nowak M. A., 1995, *PASP*, 107, 1207
- Nowak M. A., Wilms J., Dove J. B., 2002, *MNRAS*, 332, 856
- Ogley R. N., Ash T. D. C., Fender R. P., 1997, *IAU Circular*, 6726, 2
- Oosterbroek T., van der Klis M., Vaughan B., van Paradijs J., Rutledge R., Lewin W. H. G., Tanaka Y., Nagase F., Dotani T., Mitsuda K., Yoshida K., 1996, *A&A*, 309, 781
- Orosz J. A., Kuulkers E., van der Klis M., McClintock J. E., Garcia M. R., Callanan P. J., Bailyn C. D., Jain R. K., Remillard R. A., 2001, *ApJ*, 555, 489
- Orosz J. A., McClintock J. E., Remillard R. A., Corbel S., 2004, *ApJ*, 616, 376
- Orosz J. A., Polinsky E. J., Bailyn C. D., Tourtellotte S. W., McClintock J. E., Remillard R. A., 2002, in *Bulletin of the American Astronomical Society*, Vol. 34, *Bulletin of the American Astronomical Society*, pp. 1124–+
- Orosz J. A., Steeghs D., McClintock J. E., Torres M. A. P., Bochkov I., Gou L., Narayan R., Blaschak M., Levine A. M., Remillard R. A., Bailyn C. D., Dwyer M. M., Buxton M., 2009, *ApJ*, 697, 573
- Park S. Q., Miller J. M., McClintock J. E., Remillard R. A., Orosz J. A., Shrader C. R., Hunstead R. W., Campbell-Wilson D., Ishwara-Chandra C. H., Rao A. P., Rupen M. P., 2004, *ApJ*, 610, 378
- Pooley G. G., 1998, *IAU Circular*, 6926, 3
- , 2001, *MNRAS*, 324, L23
- , 2005, *ATel*, 385, 1
- Pottschmidt K., Chernyakova M., Zdziarski A. A., Lubiński P., Smith D. M., Bezayiff N., 2006, *A&A*, 452, 285
- Remillard R. A., Levine A. M., Morgan E. H., Smith E., Swank J., 2003, *IAU Circular*, 8050, 1
- Remillard R. A., McClintock J. E., 2006, *ARA&A*, 44, 49
- Revnivtsev M., Gilfanov M., Churazov E., 1998, *A&A*, 339, 483
- Revnivtsev M. G., Trudolyubov S. P., Borozdin K. N., 2000a, *MNRAS*, 315, 655
- , 2000b, *MNRAS*, 312, 151
- Ritter H., Kolb U., 2003, *A&A*, 404, 301
- Rupen M. P., Dhawan V., Mioduszewski A. J., 2003a, *ATel*, 175, 1
- , 2004a, *ATel*, 304, 1
- , 2004b, *ATel*, 303, 1
- , 2005a, *ATel*, 437, 1
- , 2005b, *ATel*, 387, 1
- , 2005c, *ATel*, 420, 1
- , 2005d, *ATel*, 609, 1
- , 2005e, *ATel*, 419, 1
- , 2005f, *ATel*, 489, 1
- , 2005g, *ATel*, 404, 1
- , 2005h, *ATel*, 443, 1
- , 2006a, *ATel*, 721, 1
- , 2006b, *ATel*, 717, 1
- , 2008a, *ATel*, 1352, 1
- , 2008b, *ATel*, 1384, 1
- Rupen M. P., Jonker P. G., Mioduszewski A. J., Dhawan V., Fender R. P., Dubus G., 2004c, *ATel*, 315, 1
- Rupen M. P., Mioduszewski A. J., Dhawan V., 2003b, *ATel*, 172, 1
- , 2003c, *ATel*, 142, 1
- , 2004d, *ATel*, 296, 1
- , 2004e, *ATel*, 314, 1

- , 2005i, ATel, 434, 1
 —, 2005j, ATel, 441, 1
 —, 2005k, ATel, 575, 1
 —, 2005l, ATel, 425, 1
 Russell D., Fender R., Gallo E., Miller-Jones J. C. A., Kaiser C. R., 2006, in VI Microquasar Workshop: Microquasars and Beyond
 Russell D. M., Maccarone T. J., Körding E. G., Homan J., 2007, MNRAS, 379, 1401
 Sala G., Greiner J., Ajello M., Bottacini E., Haberl F., 2007, A&A, 473, 561
 Shahbaz T., Charles P. A., King A. R., 1998, MNRAS, 301, 382
 Shahbaz T., Smale A. P., Naylor T., Charles P. A., van Paradijs J., Hassall B. J. M., Callanan P., 1996, MNRAS, 282, 1437
 Shahbaz T., van der Hooft F., Casares J., Charles P. A., van Paradijs J., 1999, MNRAS, 306, 89
 Smith D. M., Heindl W. A., Swank J. H., 2002, ApJ, 578, L129
 Strohmayer T., Marshall F. E., Hjellming R. M., Rupen M. P., Mioduszewski A. J., 1998, IAU Circular, 6934, 2
 Thorstensen J. R., 1987, ApJ, 312, 739
 Tomsick J. A., Corbel S., Goldwurm A., Kaaret P., 2005, ApJ, 630, 413
 Tomsick J. A., Kaaret P., 2000, ApJ, 537, 448
 Tomsick J. A., Rupen M. P., Corbel S., Dhawan V., Fender R., Kaaret P., Kuulkers E., Miller J. M., Mioduszewski A. J., Orosz J. A., Tzioumis T., Wijnands R., 2002, ATel, 105, 1
 Trudolyubov S. P., Borozdin K. N., Priedhorsky W. C., 2001, MNRAS, 322, 309
 van der Klis M., 2006, Rapid X-ray Variability, Lewin W. H. G., van der Klis M., eds., pp. 39–112
 Wagner R. M., Foltz C. B., Shahbaz T., Casares J., Charles P. A., Starrfield S. G., Hewett P., 2001, ApJ, 556, 42
 Wagner R. M., Starrfield S., Shrader C., Skiff B., Hjellming R. M., Mioduszewski A. J., 1998, IAU Circular, 6924, 1
 Wilson C. A., Patel S. K., Kouveliotou C., Jonker P. G., van der Klis M., Lewin W. H. G., Belloni T., Méndez M., 2003, ApJ, 596, 1220
 Zdziarski A. A., Gierliński M., Mikołajewska J., Wardziński G., Smith D. M., Harmon B. A., Kitamoto S., 2004, MNRAS, 351, 791

APPENDIX

In Fig. A.1 we plot all the HIDs, DFLDs, the X-ray colour and Disc Fraction curves for the outbursts where a transition as determined from the automated routine is detected in either the X-ray colour or Disc Fraction curves. The source 4U 1630-47 shows a complicated outburst structure between MJD 52500 and 53500. We have split this outburst structure into two separate components as the final rise in flux is very similar to stand-alone outbursts from other well known BHXRBs.

The colour schemes are as follows; for the HIDs and DFLDs it shows the time since the beginning of the current outburst, starting at black and ending at white. For the X-ray colour and Disc Fraction curves it shows the flux (3–10 keV)/luminosity ($L_{\text{PL}} + L_{\text{Disc}}$) of the source, white being bright, and black being faint. The normalisation is such to use the full range for each diagram.

In Fig. A.2 we show the HIDs and DFLDs of the remaining BHXRBs which are not shown in Fig. A.1

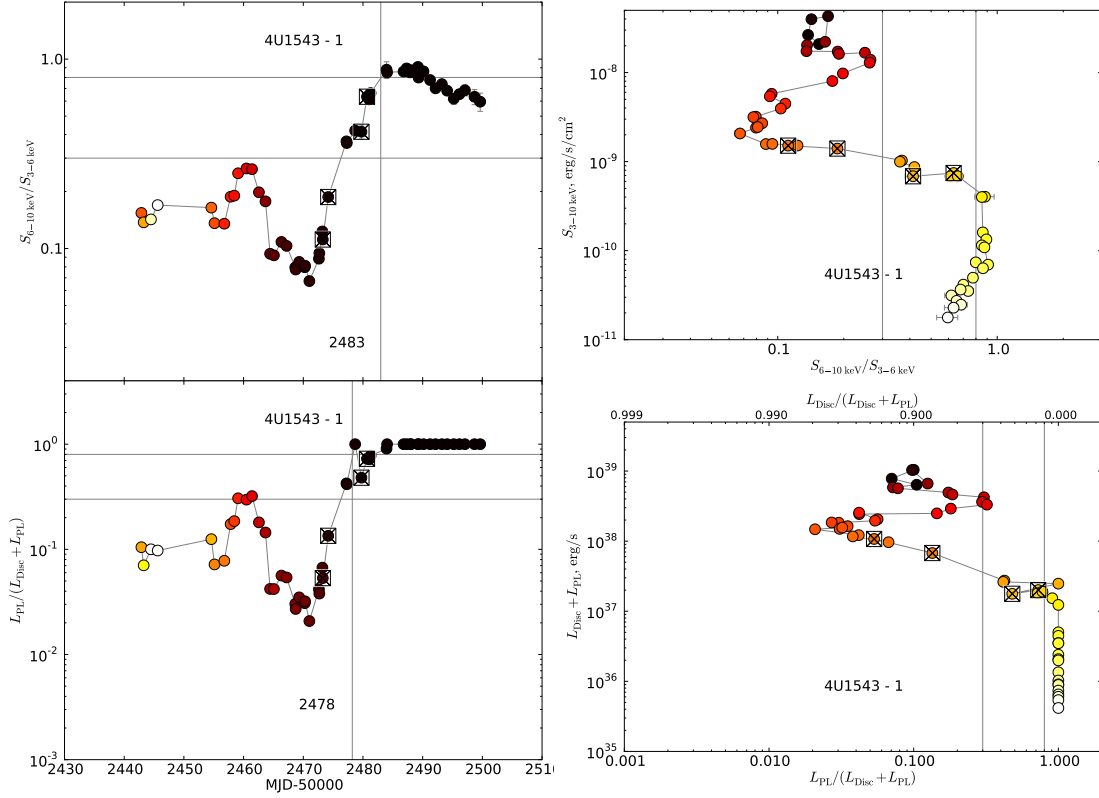


Figure A.1. The curves of X-ray colour (TOP LEFT) and powerlaw fraction (BOTTOM LEFT) against time, and the HID (TOP RIGHT) and DFLD (BOTTOM RIGHT) for 4U 1543-47 Outburst 1. The observations from which the transition dates have been determined from timing properties are shown with the crossed box (see Table 3 for the dates and references). In the HID and DFLD, the two vertical lines are the Powerlaw Fractions and X-ray colours used when calculating the transitions. For the X-ray colour and Powerlaw fraction curves, the two horizontal lines show the values used for calculating the transition. The vertical lines show the dates of the transitions as calculated in Section 7..

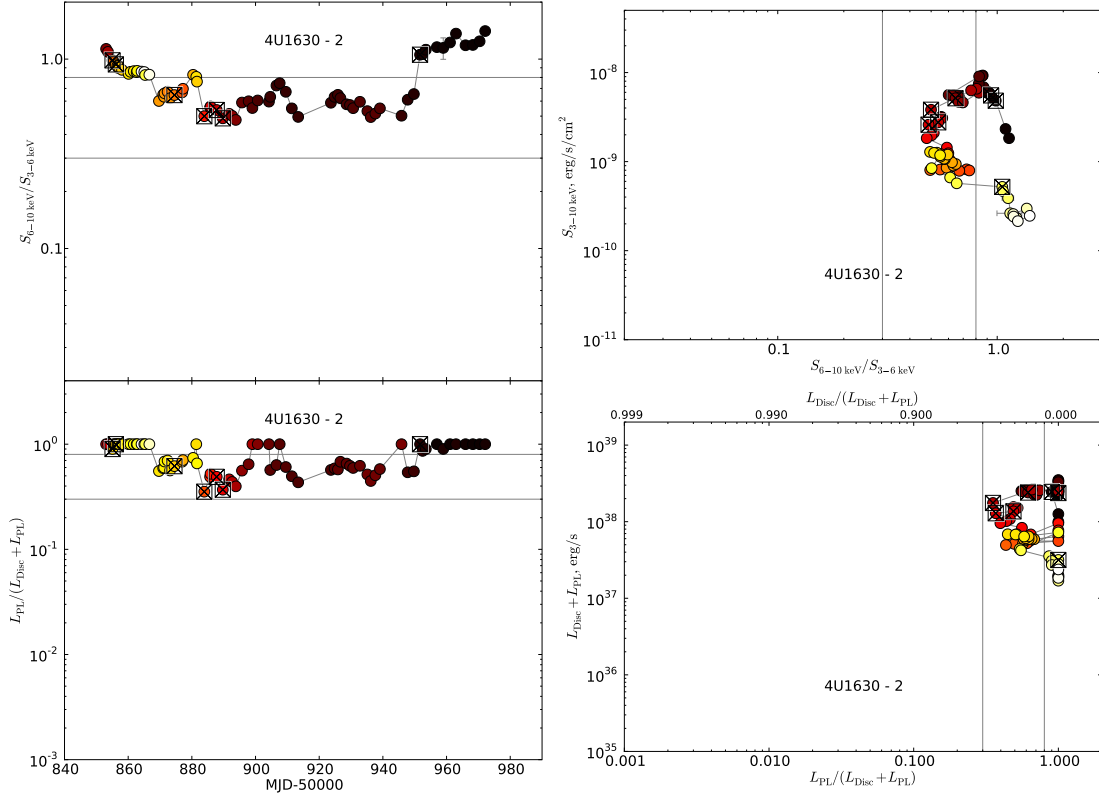


Figure A.1. (cont) X-ray colour curves and diagnostic diagrams for the outbursts observed - 4U 1630-47 Outburst 2.

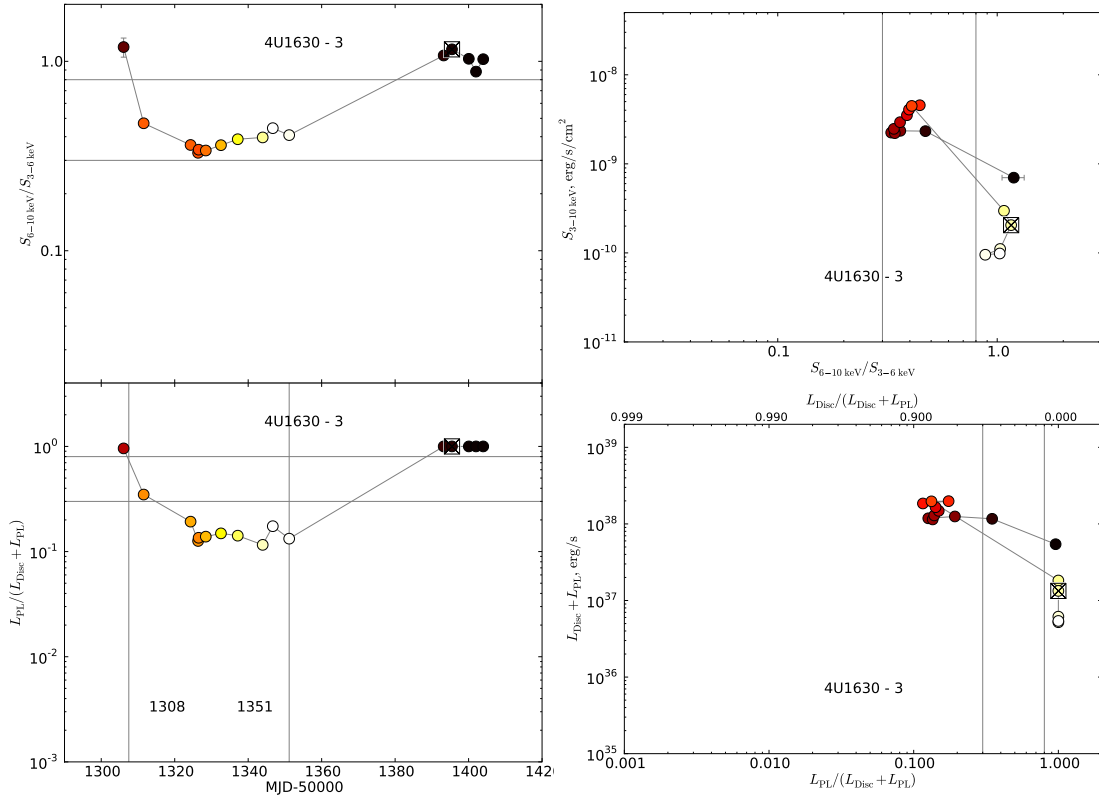


Figure A.1. (cont) X-ray colour curves and diagnostic diagrams for the outbursts observed - 4U 1630-47 Outburst 3.

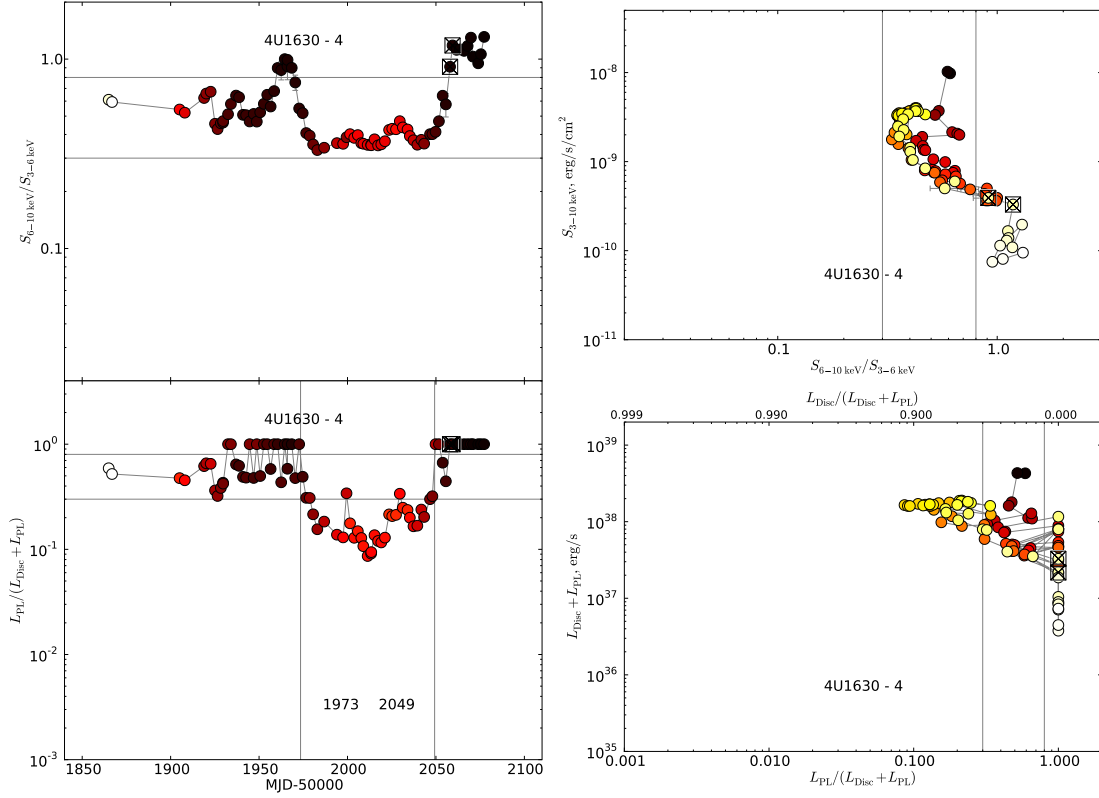


Figure A.1. (cont) X-ray colour curves and diagnostic diagrams for the outbursts observed - 4U 1630-47 Outburst 4.

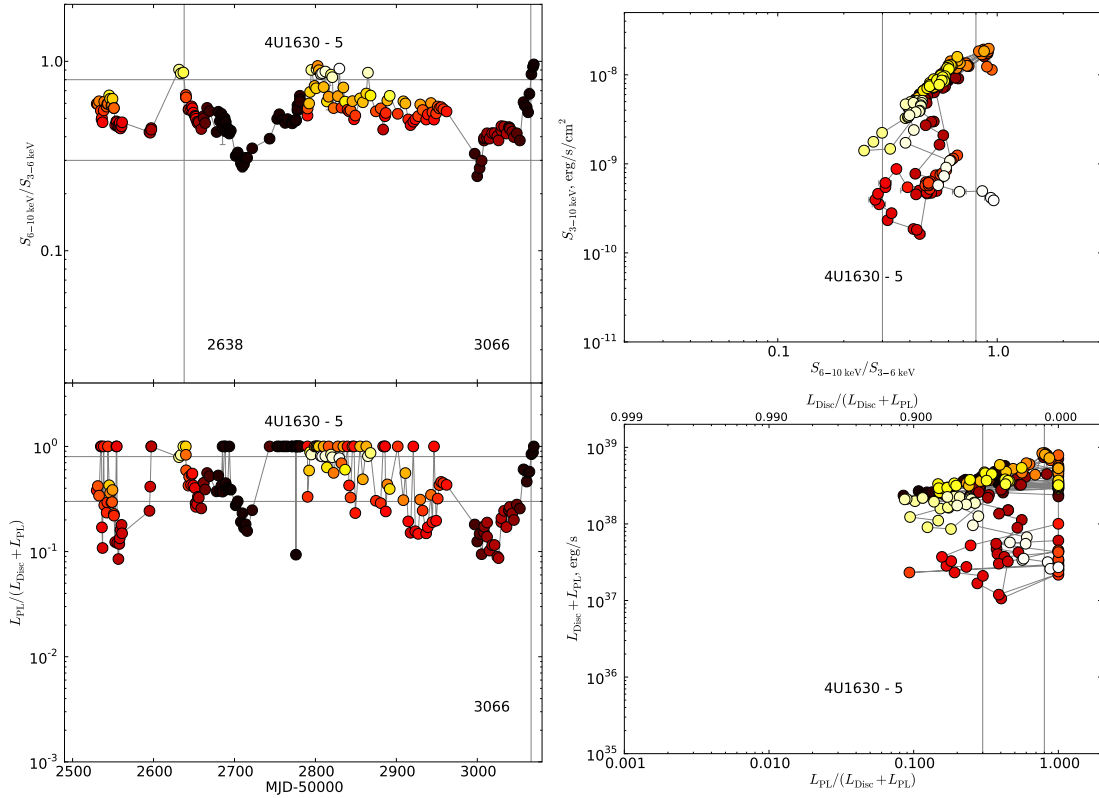


Figure A.1. (cont) X-ray colour curves and diagnostic diagrams for the outbursts observed - 4U 1630-47 Outburst 5.

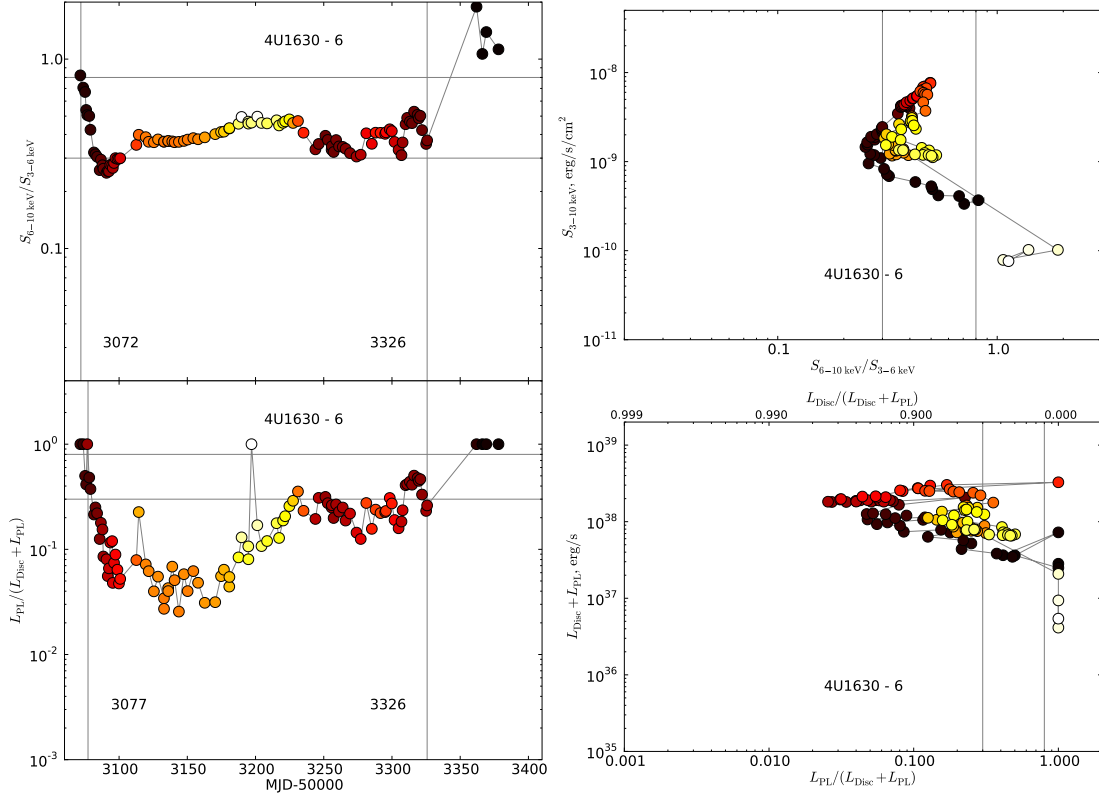


Figure A.1. (cont) X-ray colour curves and diagnostic diagrams for the outbursts observed - 4U 1630-47 Outburst 6.

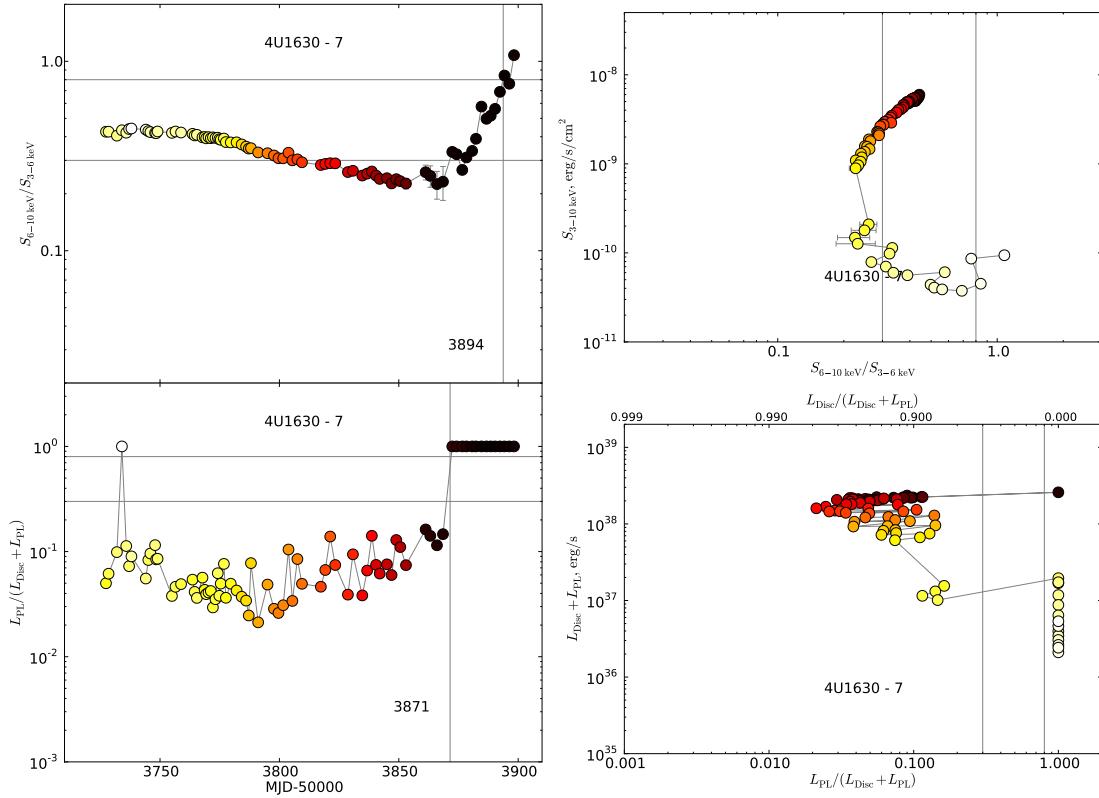


Figure A.1. (cont) X-ray colour curves and diagnostic diagrams for the outbursts observed - 4U 1630-47 Outburst 7.

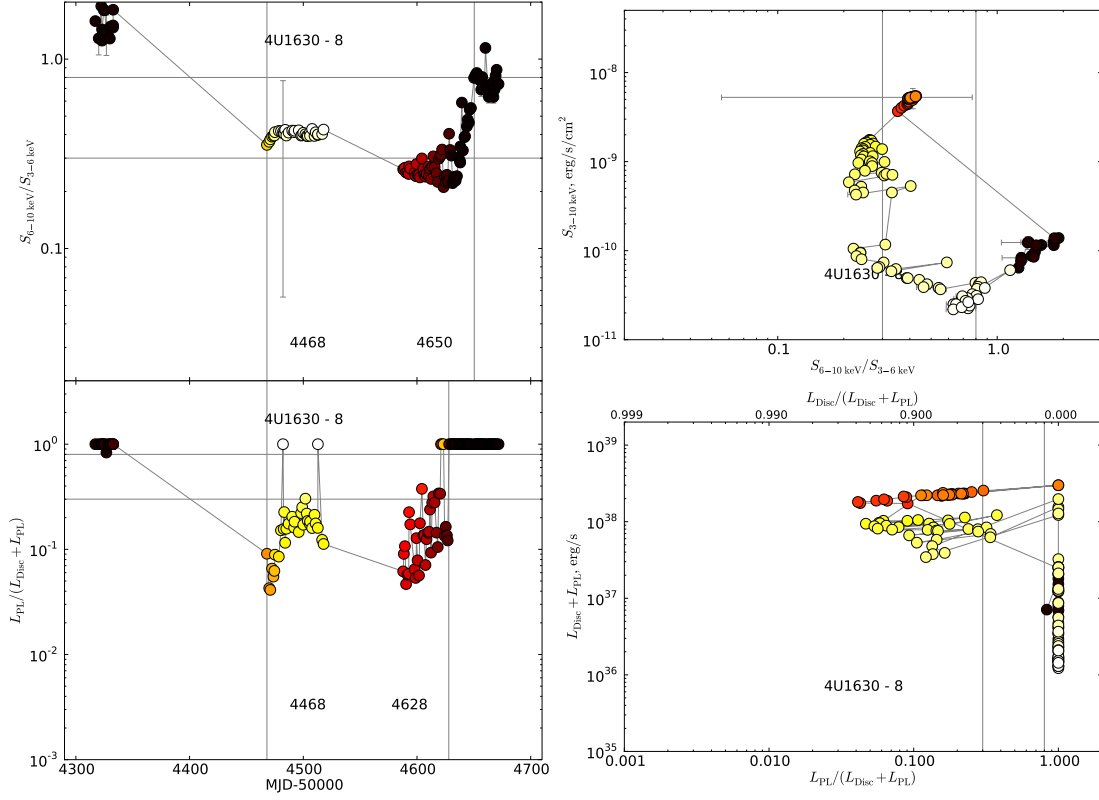


Figure A.1. (cont) X-ray colour curves and diagnostic diagrams for the outbursts observed - 4U 1630-47 Outburst 8.

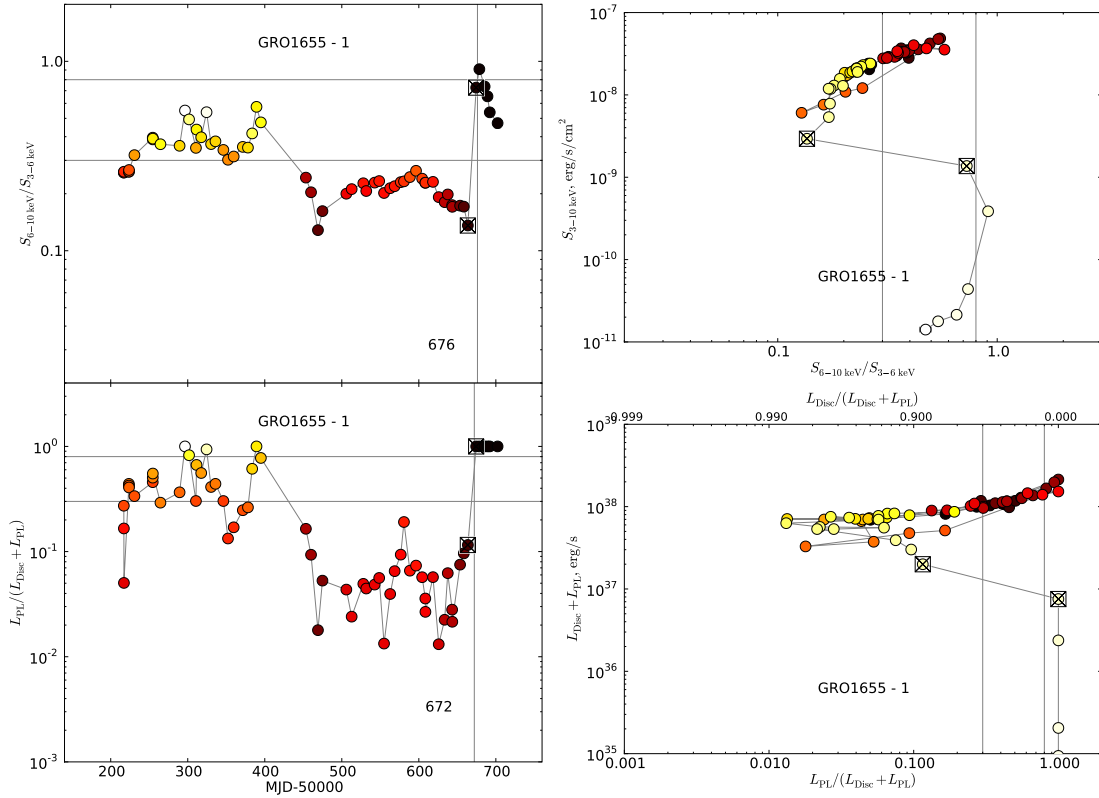


Figure A.1. (cont) X-ray colour curves and diagnostic diagrams for the outbursts observed.

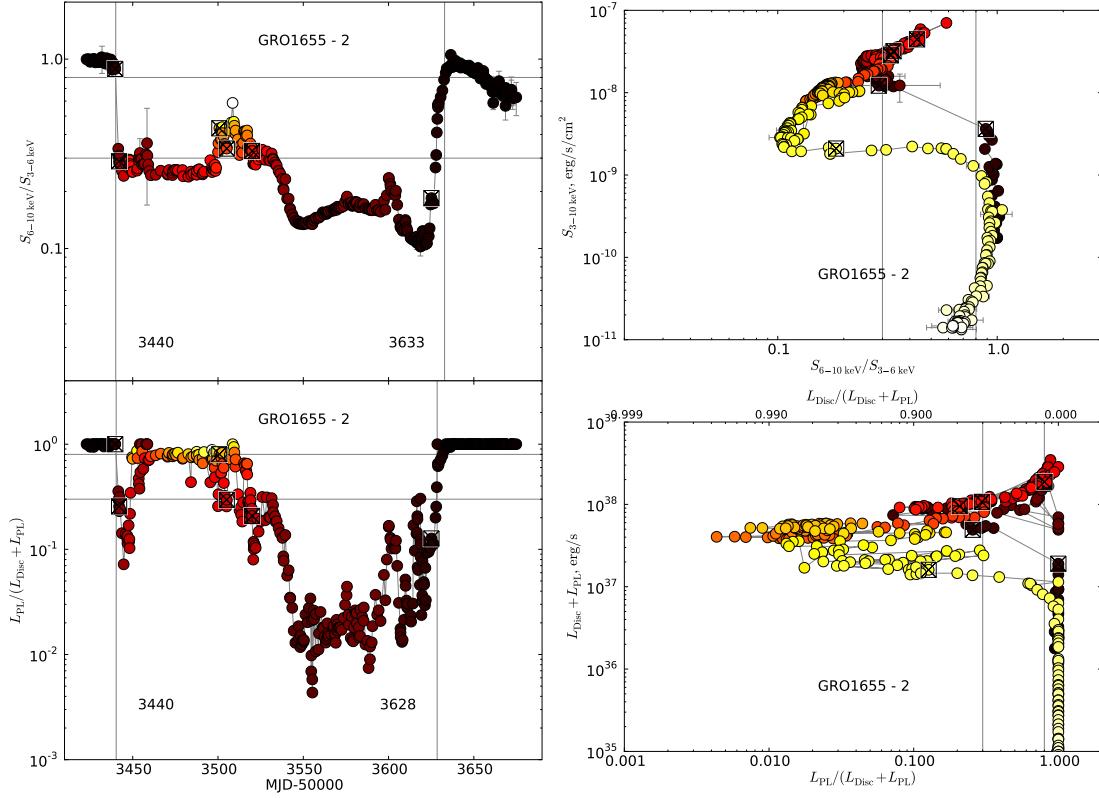


Figure A.1. (cont) X-ray colour curves and diagnostic diagrams for the outbursts observed.

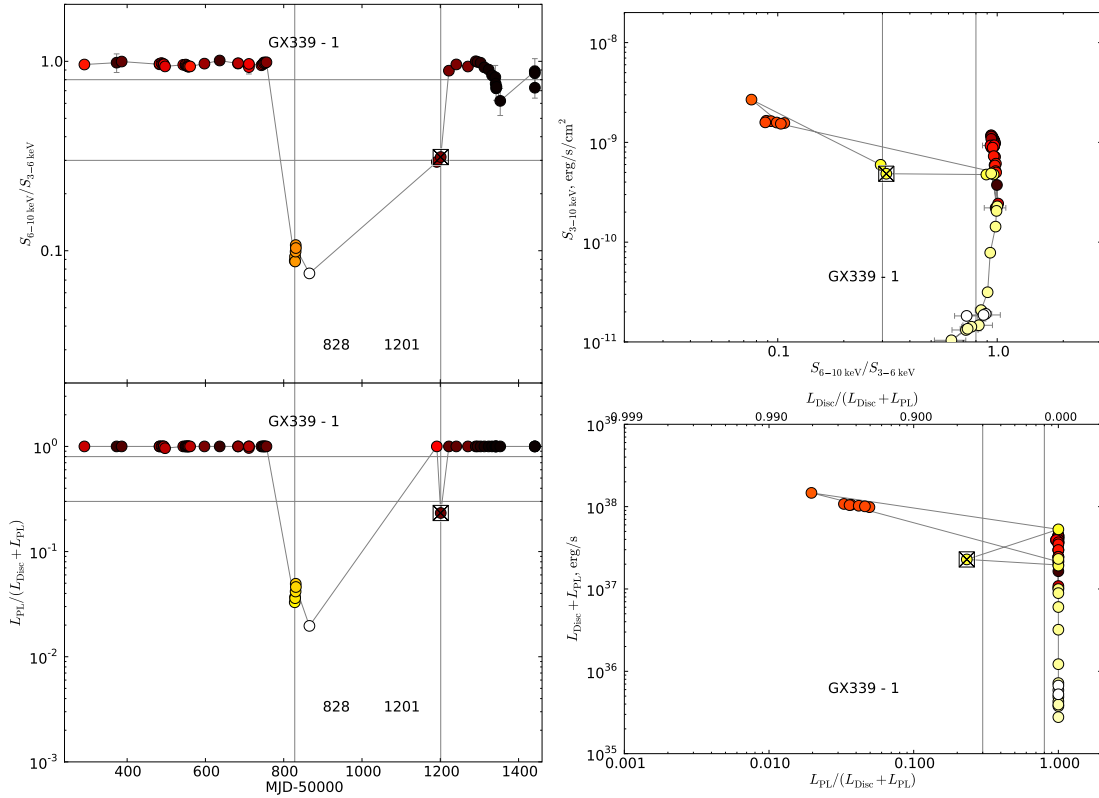


Figure A.1. (cont) X-ray colour curves and diagnostic diagrams for the outbursts observed - GX 339-4 Outburst 1.

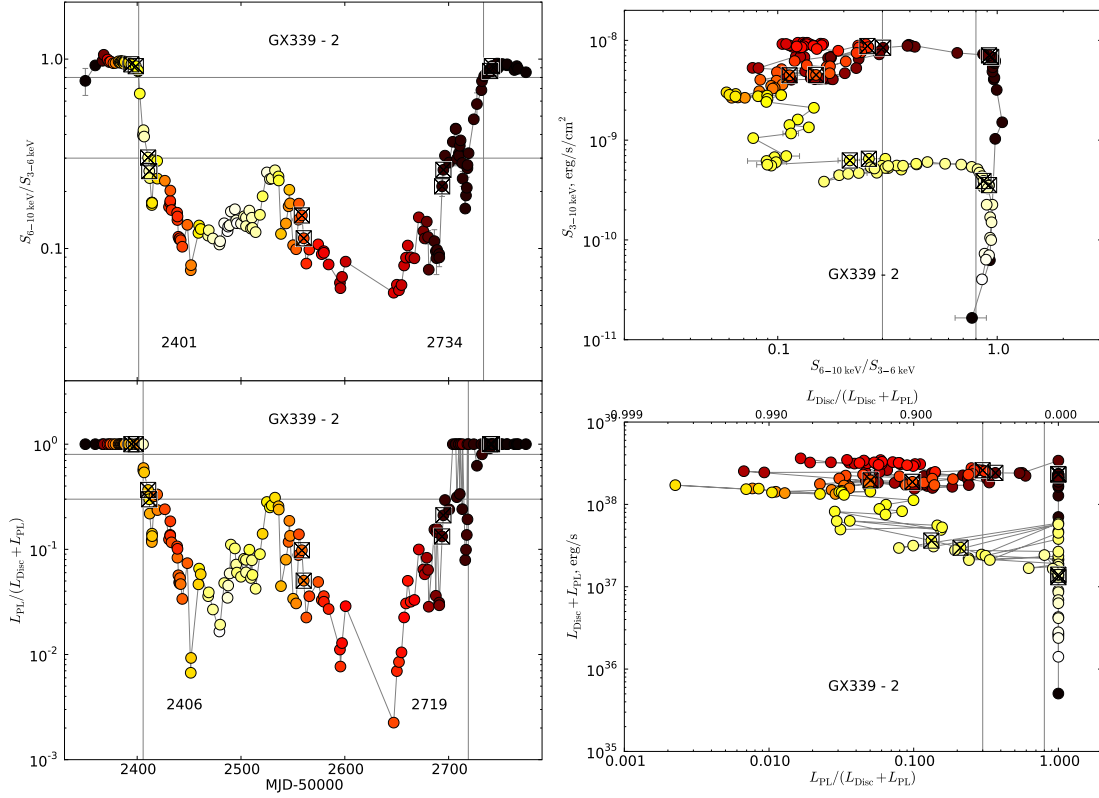


Figure A.1. (cont) X-ray colour curves and diagnostic diagrams for the outbursts observed - GX 339-4 Outburst 2.

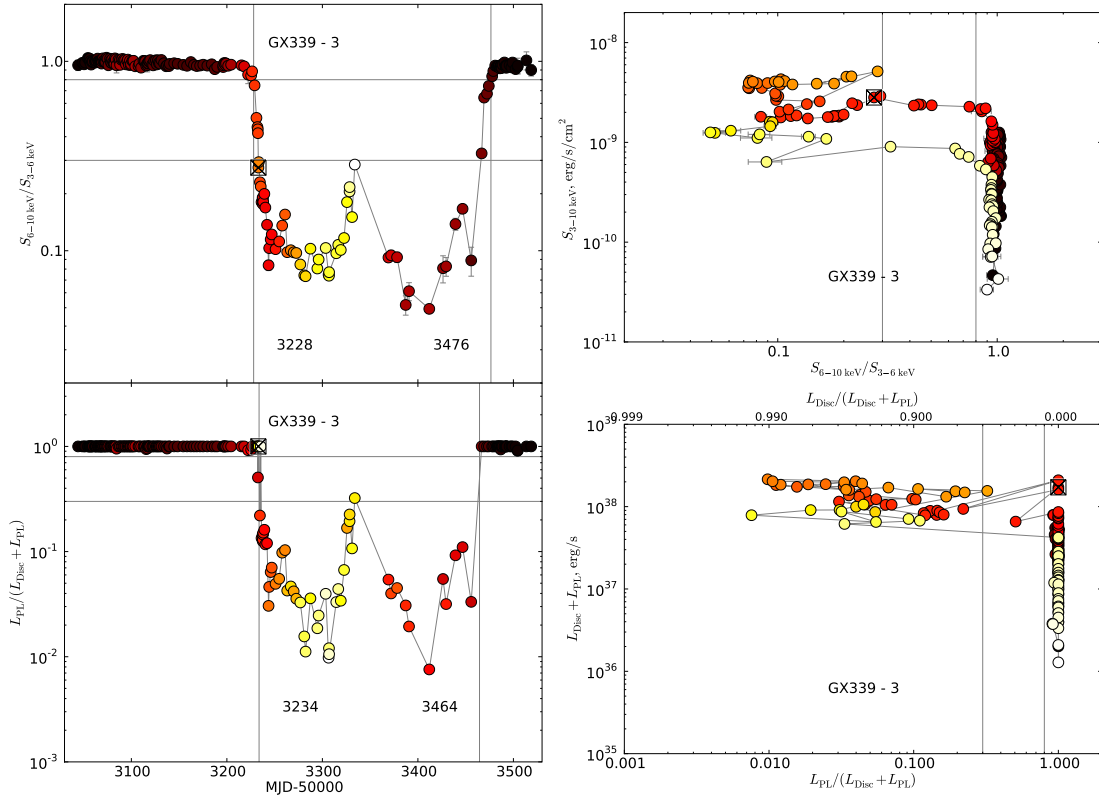


Figure A.1. (cont) X-ray colour curves and diagnostic diagrams for the outbursts observed - GX 339-4 Outburst 3.

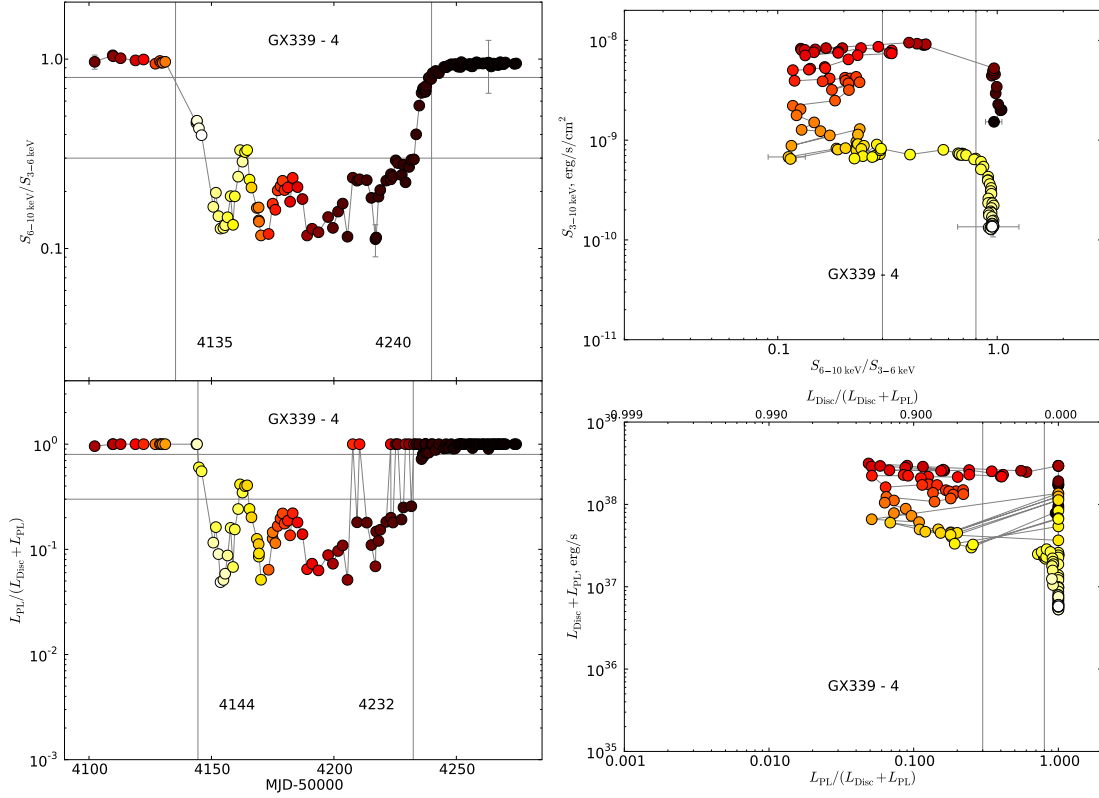


Figure A.1. (cont) X-ray colour curves and diagnostic diagrams for the outbursts observed - GX 339-4 Outburst 4.

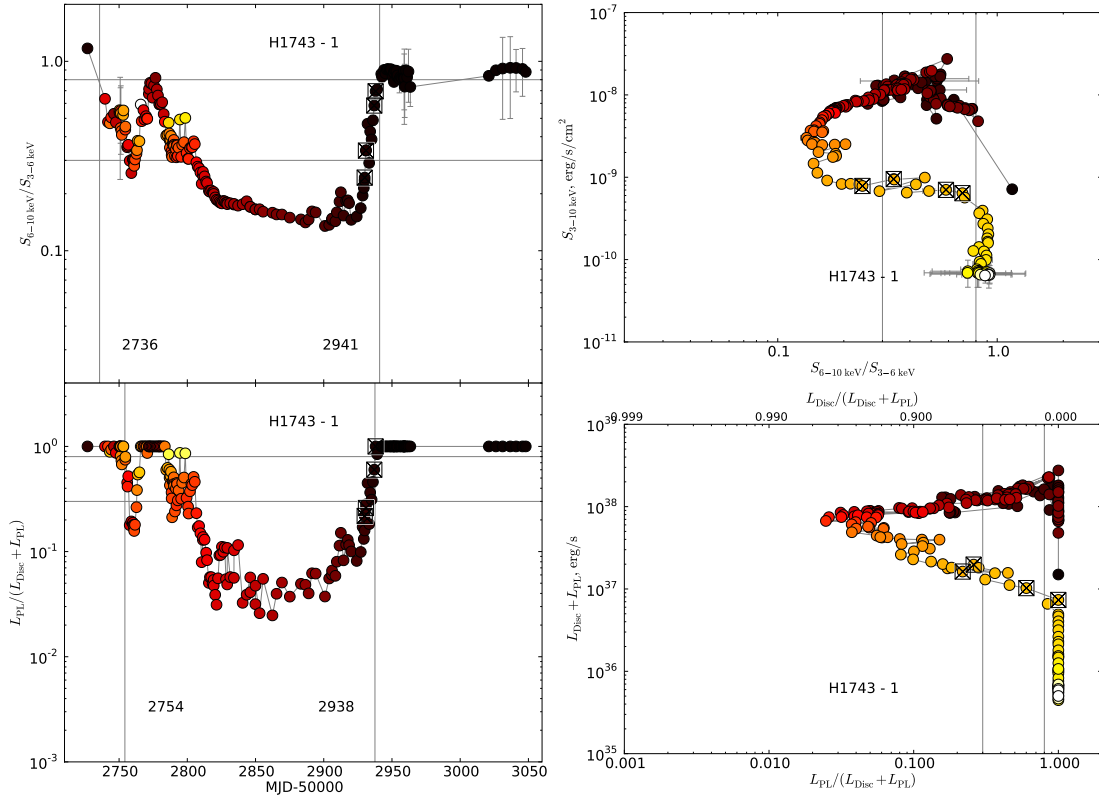


Figure A.1. (cont) X-ray colour curves and diagnostic diagrams for the outbursts observed - H1743-332 Outburst 1.

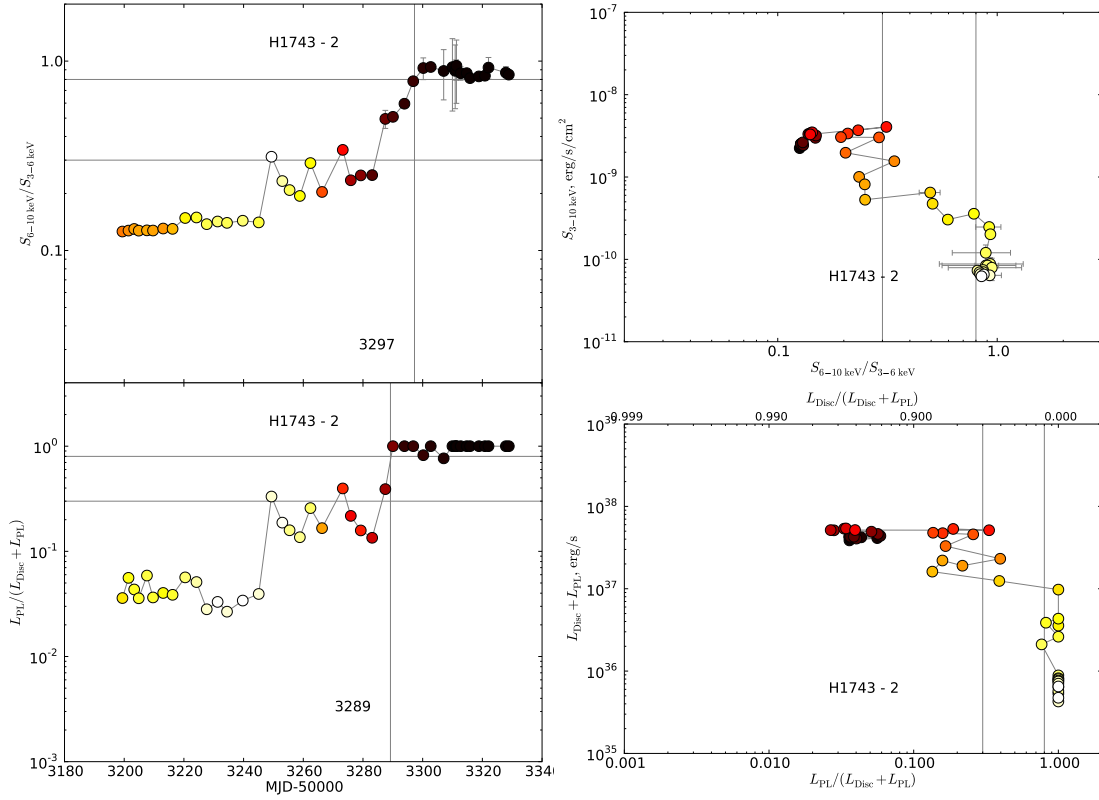


Figure A.1. (cont) X-ray colour curves and diagnostic diagrams for the outbursts observed - H1743-332 Outburst 2.

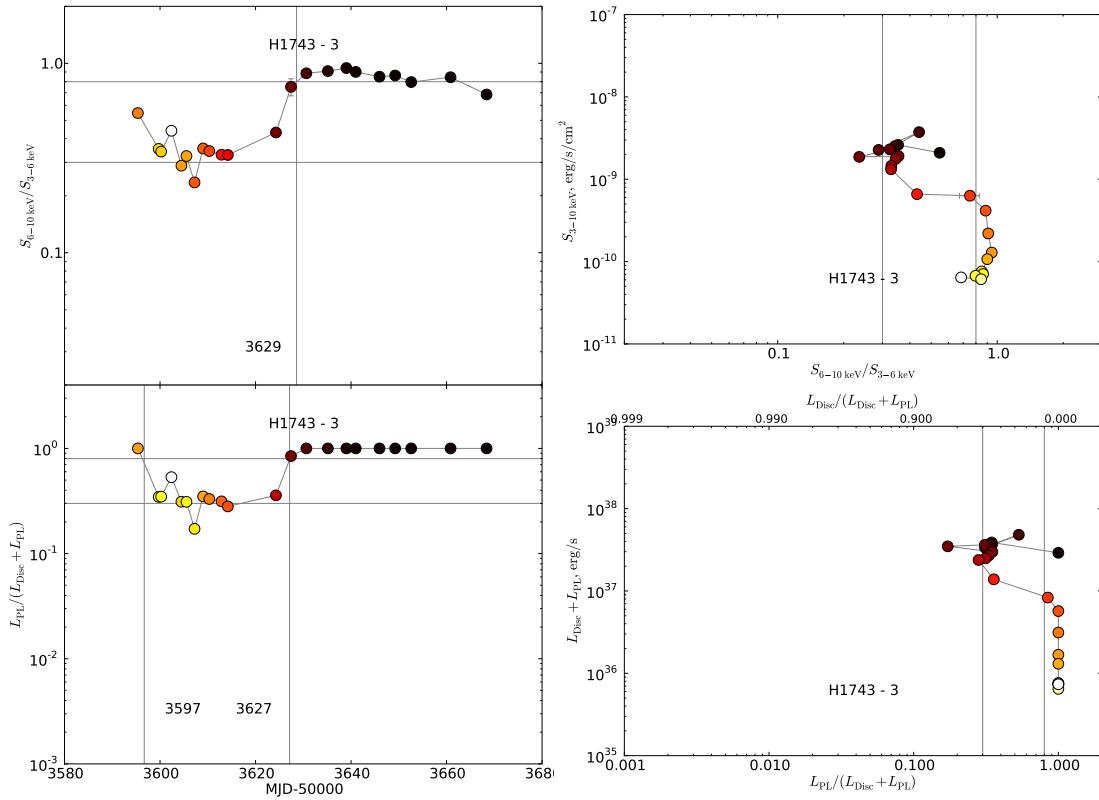


Figure A.1. (cont) X-ray colour curves and diagnostic diagrams for the outbursts observed - H1743-332 Outburst 3.

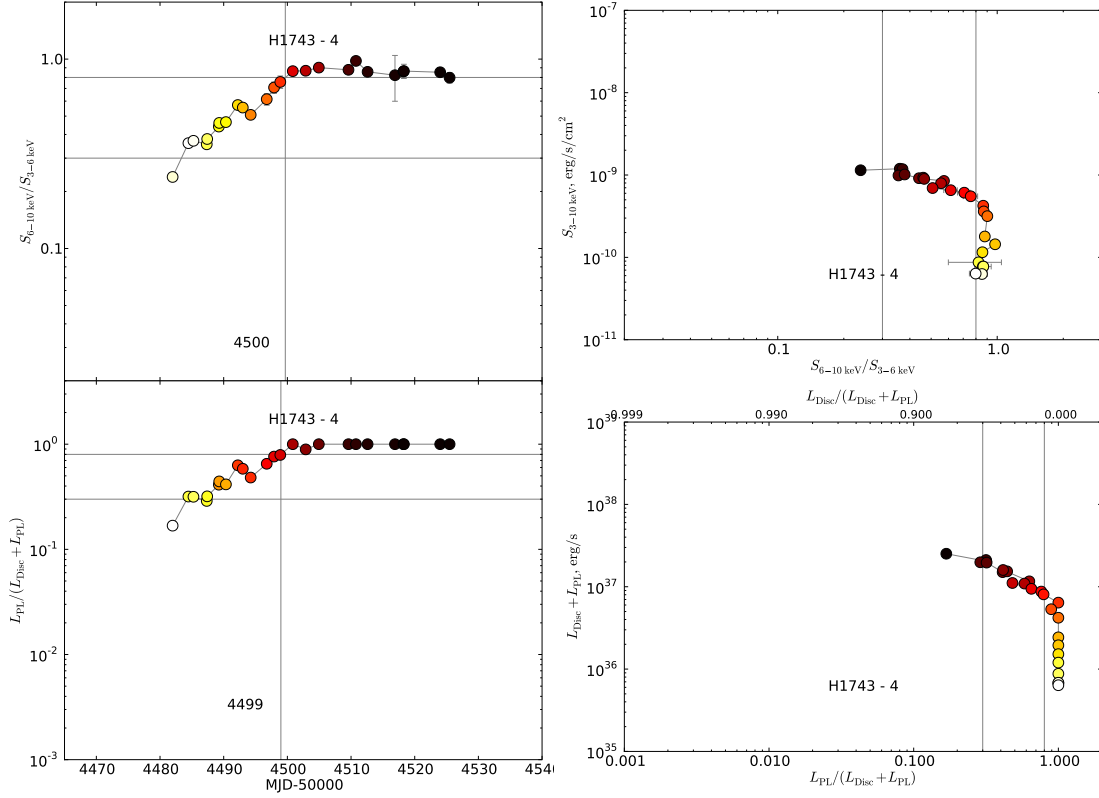


Figure A.1. (cont) X-ray colour curves and diagnostic diagrams for the outbursts observed - H1743-332 Outburst 4.

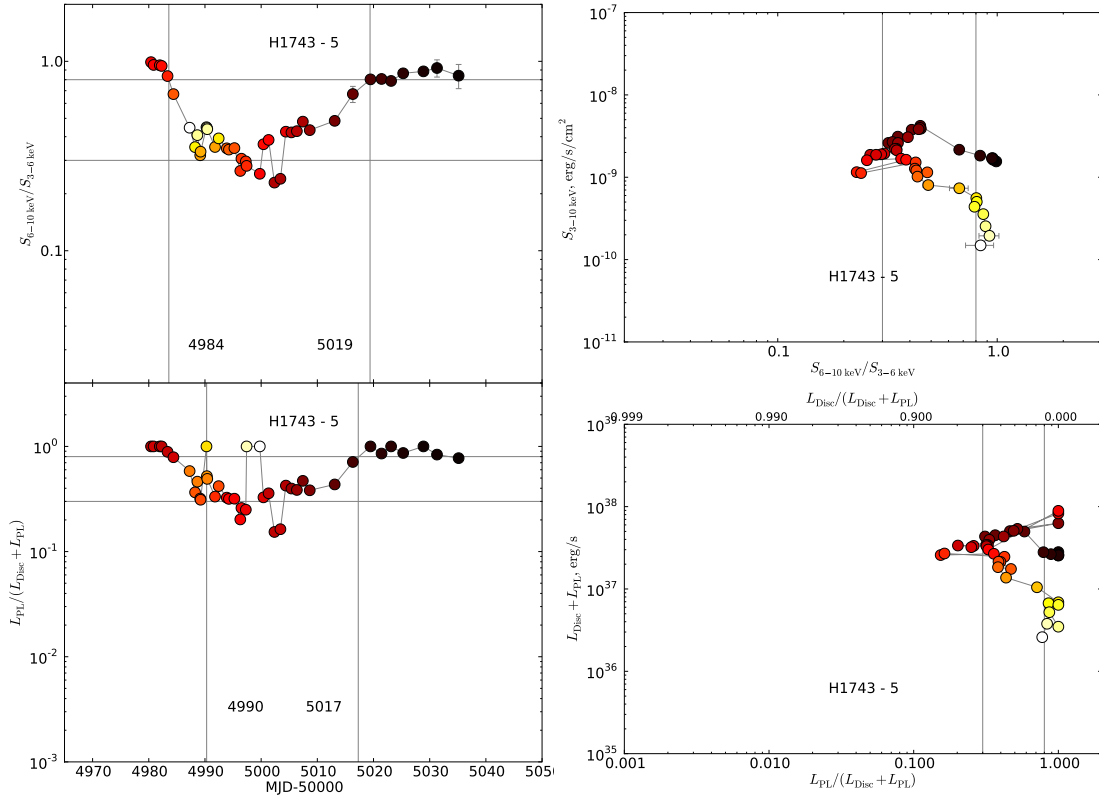


Figure A.1. (cont) X-ray colour curves and diagnostic diagrams for the outbursts observed - H1743-332 Outburst 5.

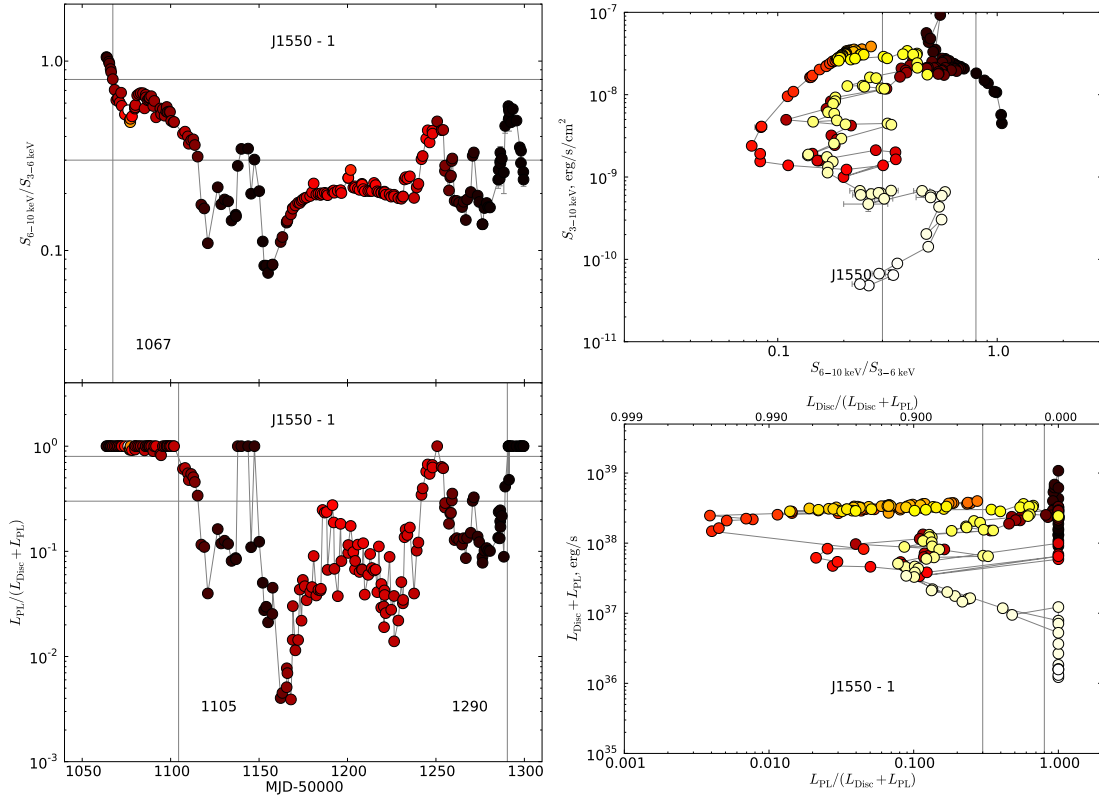


Figure A.1. (cont) X-ray colour curves and diagnostic diagrams for the outbursts observed - XTE J1550-564 Outburst 1.

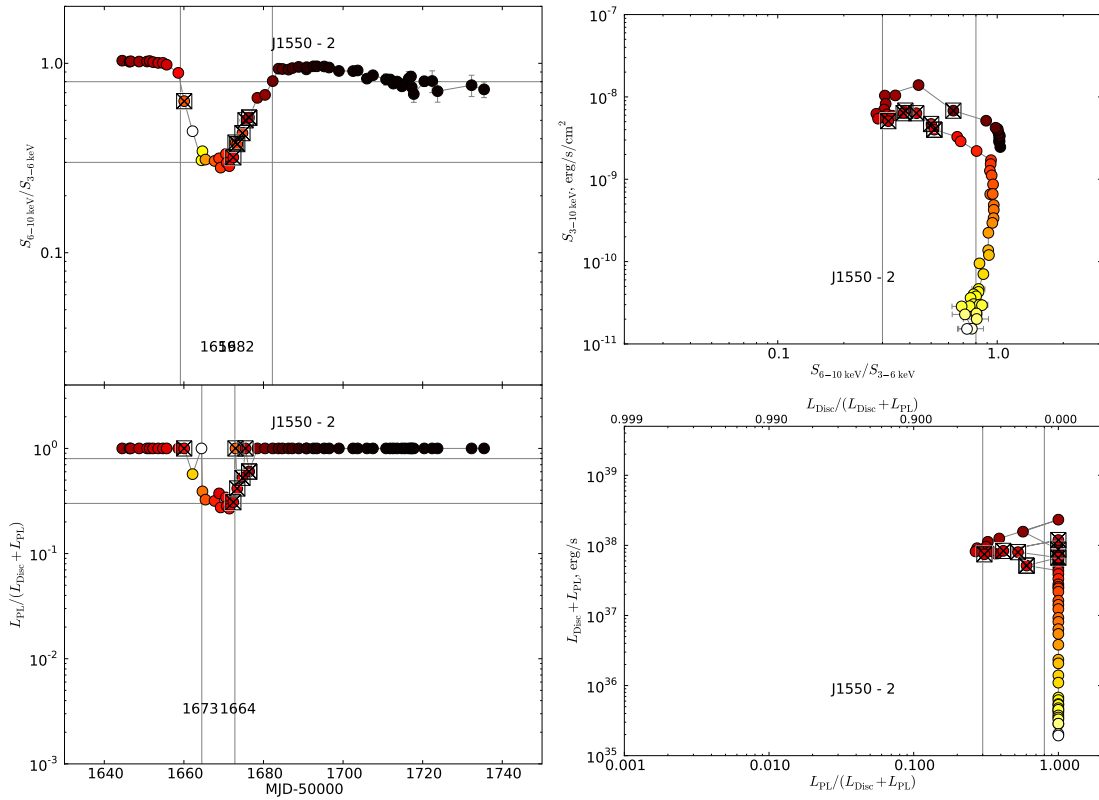


Figure A.1. (cont) X-ray colour curves and diagnostic diagrams for the outbursts observed - XTE J1550-564 Outburst 2.

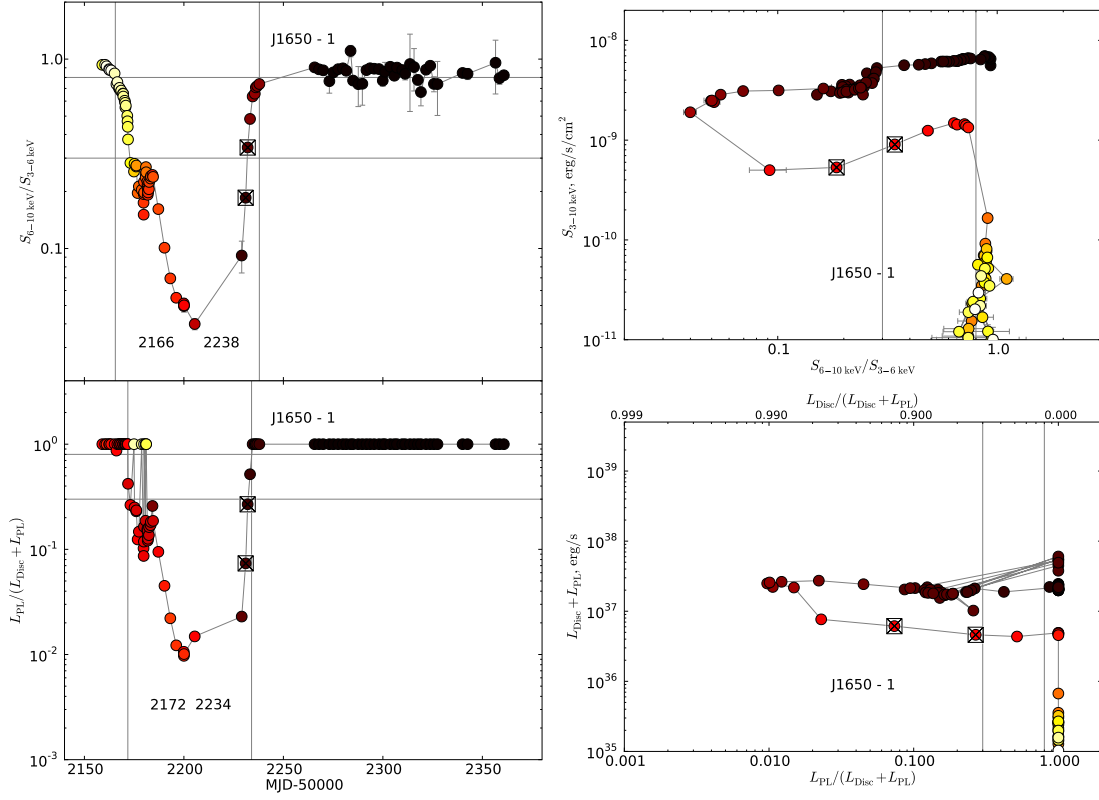


Figure A.1. (cont) X-ray colour curves and diagnostic diagrams for the outbursts observed - XTE J1650-500 Outburst 1.

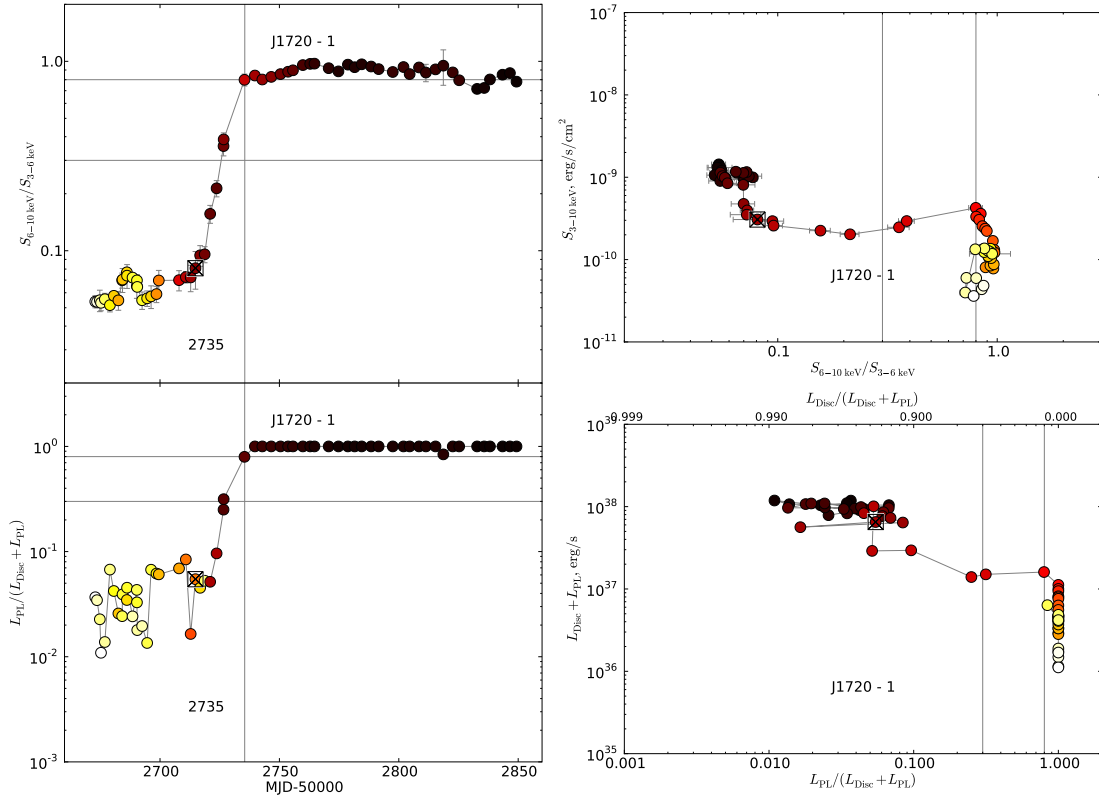


Figure A.1. (cont) X-ray colour curves and diagnostic diagrams for the outbursts observed - XTE J1720-318 Outburst 1.

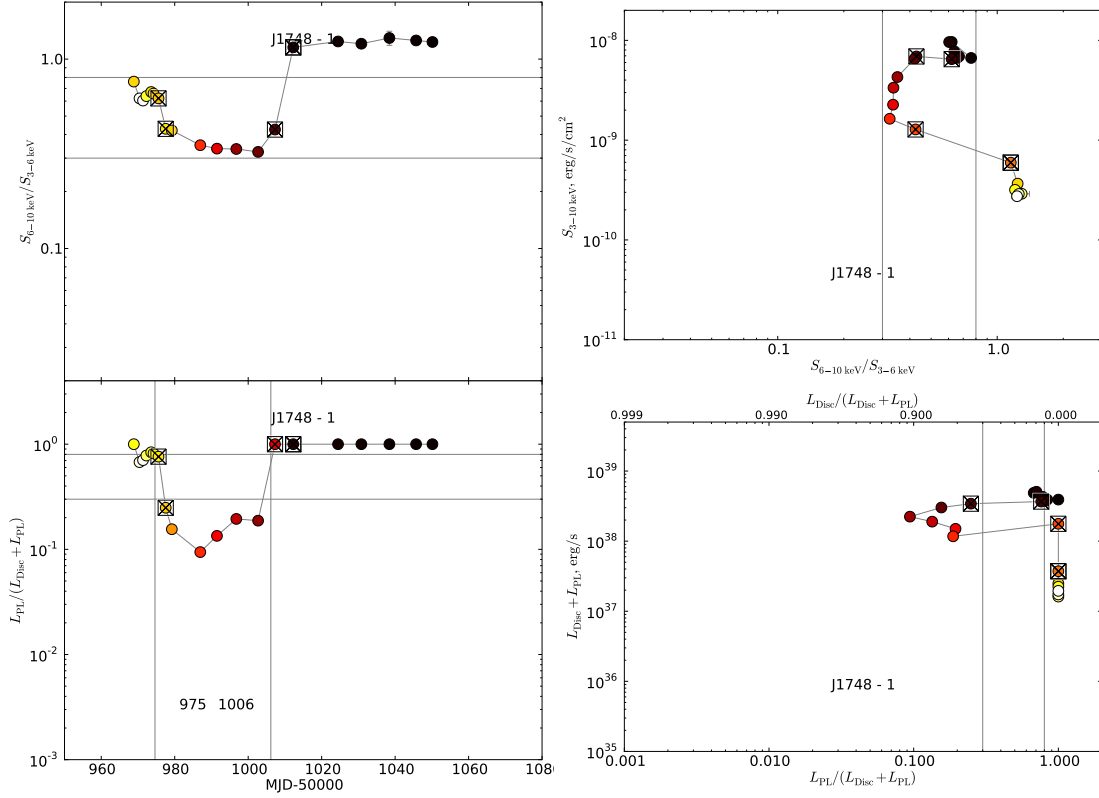


Figure A.1. (cont) X-ray colour curves and diagnostic diagrams for the outbursts observed - XTE J1748-2888 Outburst 1.

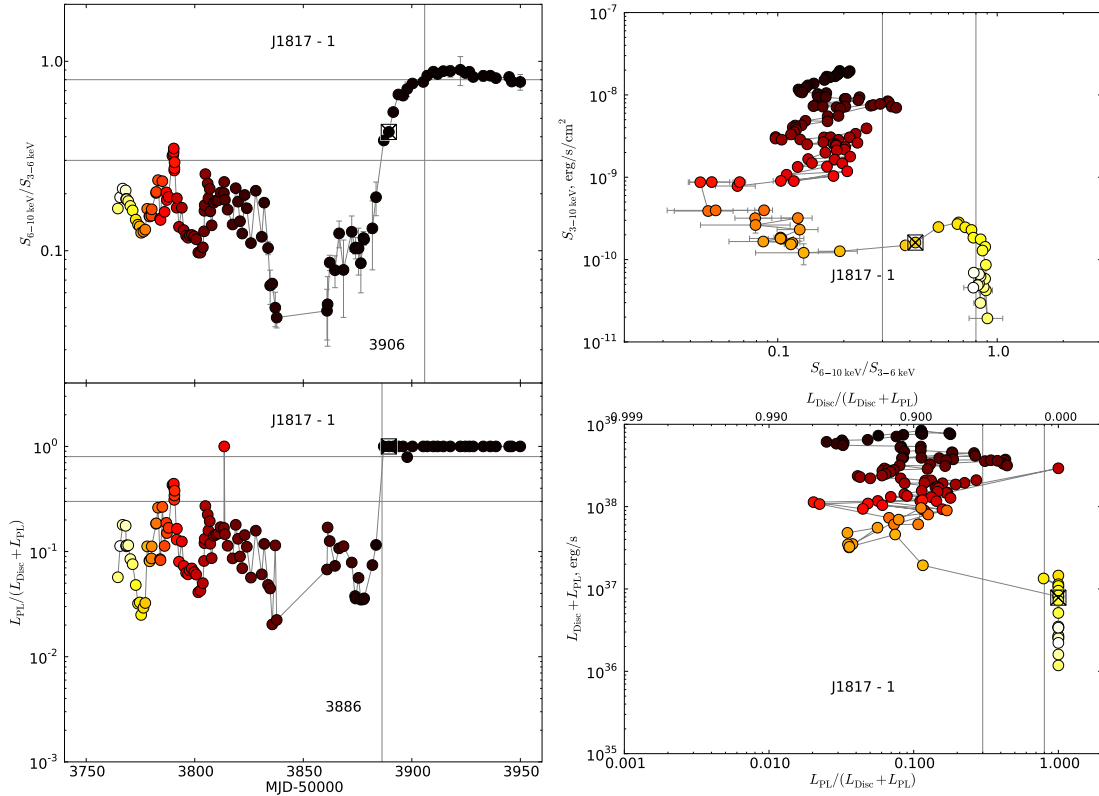


Figure A.1. (cont) X-ray colour curves and diagnostic diagrams for the outbursts observed - XTE J1817-330 Outburst 1.

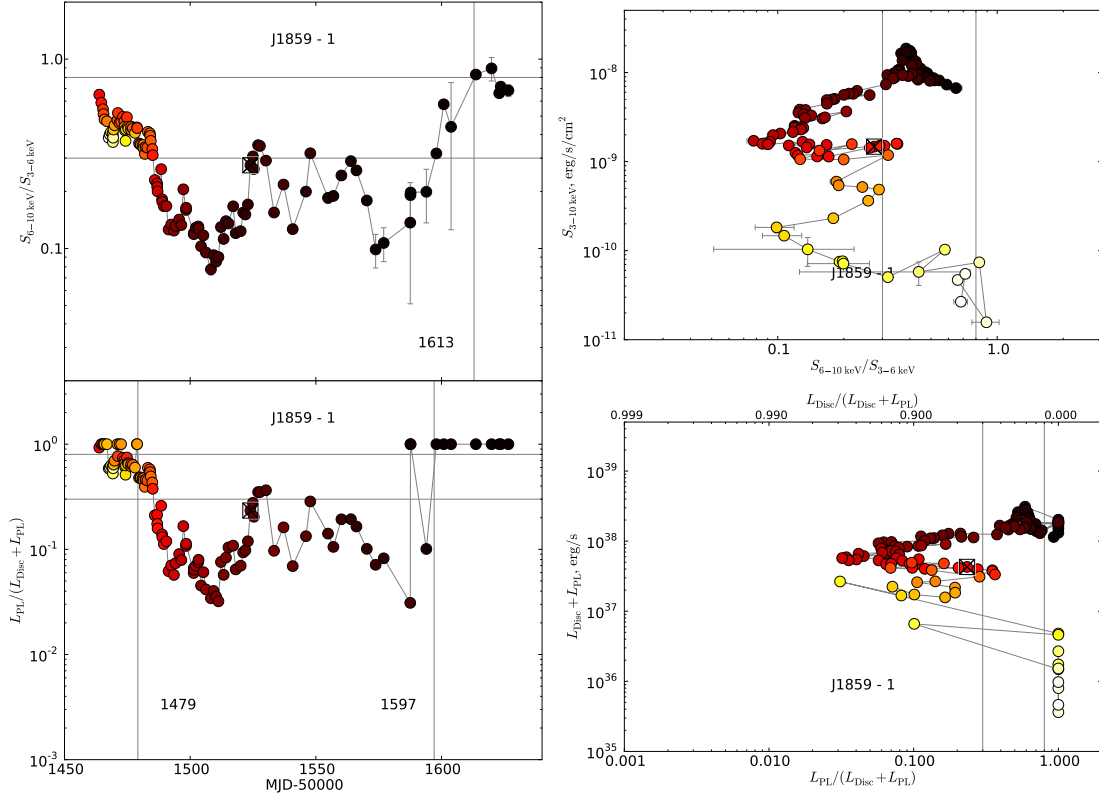


Figure A.1. (cont) X-ray colour curves and diagnostic diagrams for the outbursts observed - XTE J1859-226 Outburst 1.

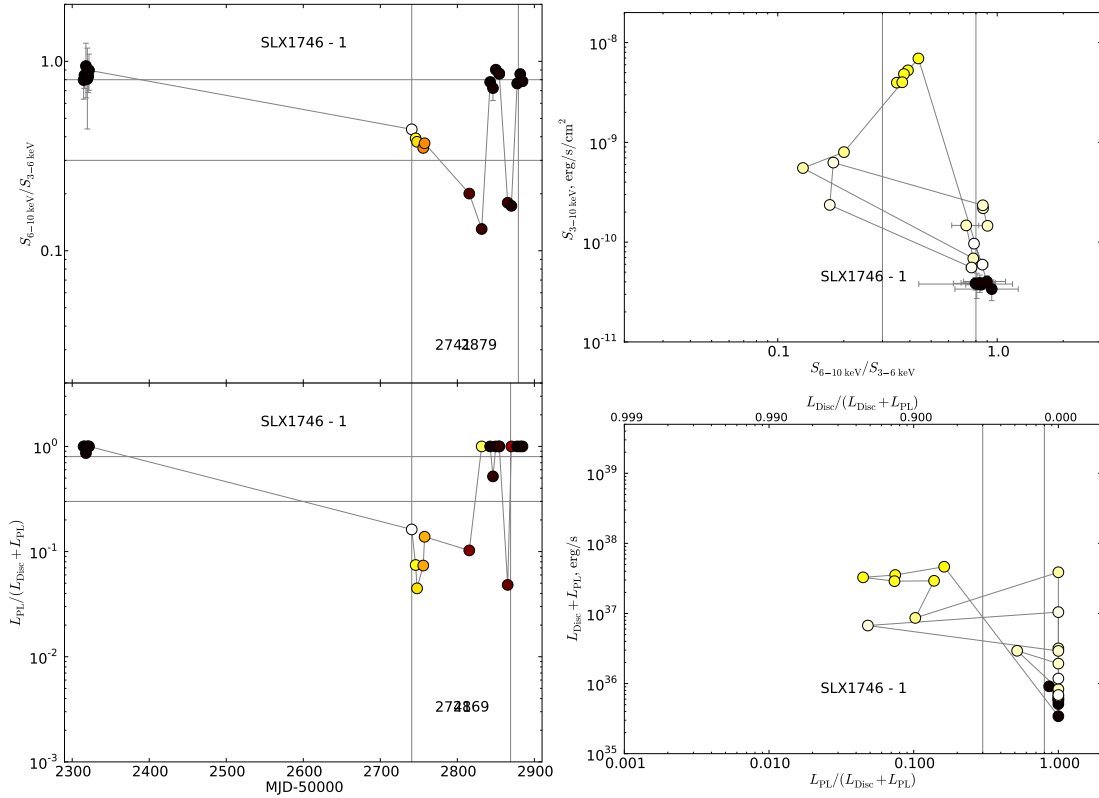


Figure A.1. (cont) X-ray colour curves and diagnostic diagrams for the outbursts observed - SLX 1746-331 Outburst 1.

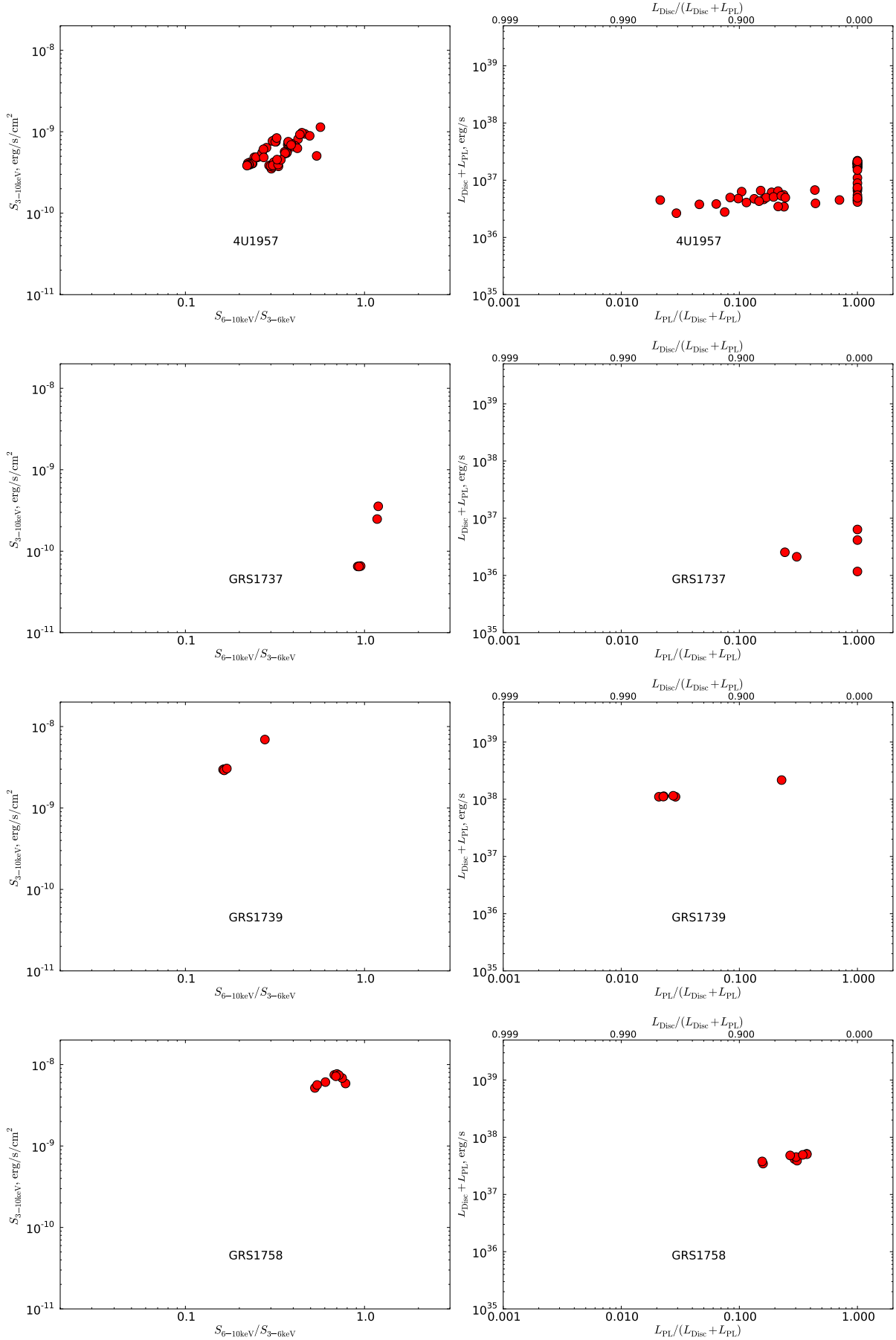


Figure A.2. We show the HID and the DFLD for the remainder of the BHXRBS not shown in Fig. A.1

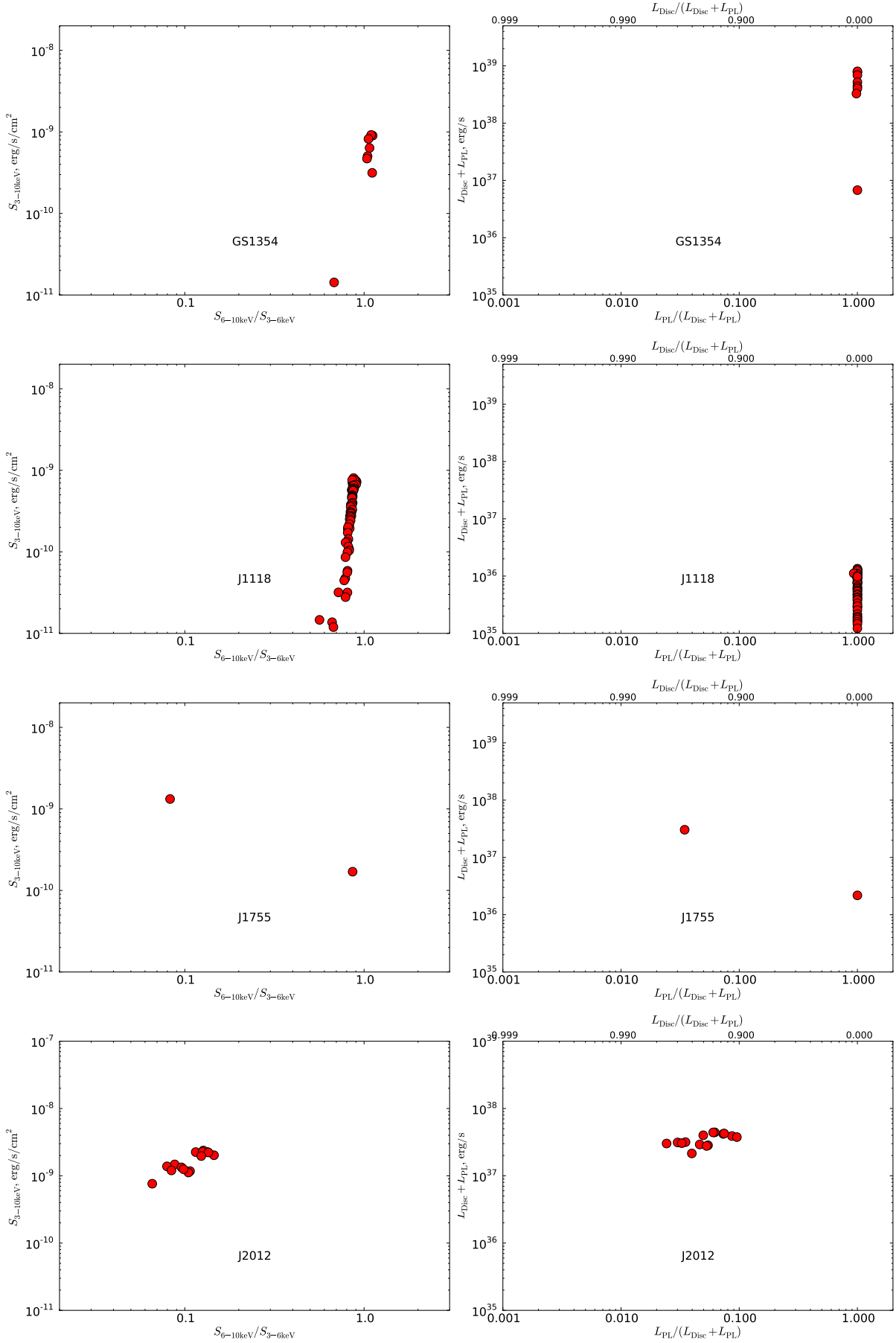


Figure A.2. (cont) HID and DFLDs for the remainder of the BHXBs.

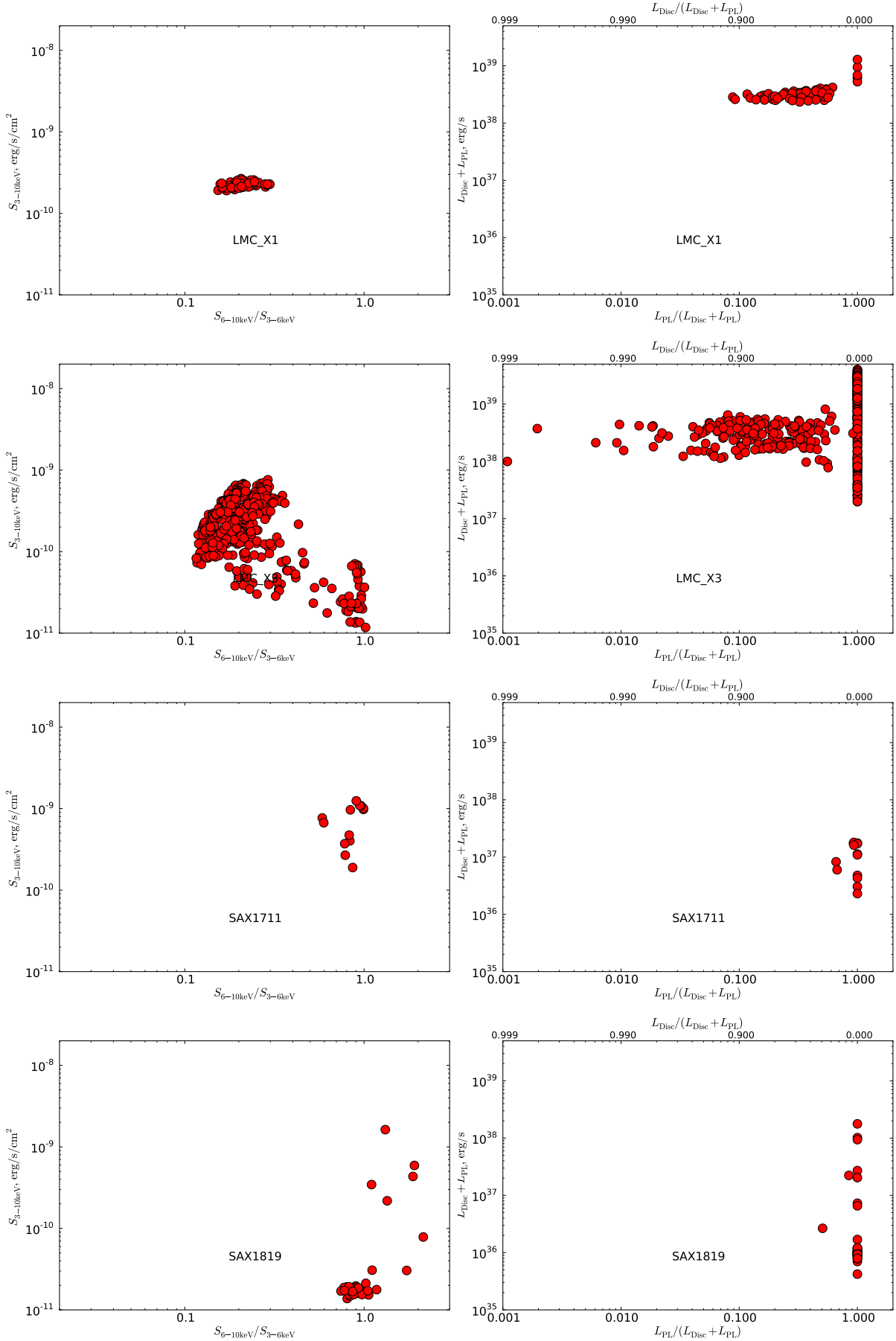


Figure A.2. (cont) HID and DFLDs for the remainder of the BHXRBs.